



저작자표시-비영리-변경금지 2.0 대한민국

이용자는 아래의 조건을 따르는 경우에 한하여 자유롭게

- 이 저작물을 복제, 배포, 전송, 전시, 공연 및 방송할 수 있습니다.

다음과 같은 조건을 따라야 합니다:



저작자표시. 귀하는 원저작자를 표시하여야 합니다.



비영리. 귀하는 이 저작물을 영리 목적으로 이용할 수 없습니다.



변경금지. 귀하는 이 저작물을 개작, 변형 또는 가공할 수 없습니다.

- 귀하는, 이 저작물의 재이용이나 배포의 경우, 이 저작물에 적용된 이용허락조건을 명확하게 나타내어야 합니다.
- 저작권자로부터 별도의 허가를 받으면 이러한 조건들은 적용되지 않습니다.

저작권법에 따른 이용자의 권리는 위의 내용에 의하여 영향을 받지 않습니다.

이것은 [이용허락규약\(Legal Code\)](#)을 이해하기 쉽게 요약한 것입니다.

[Disclaimer](#)

Thesis for a Ph. D. Degree

A study on changes in the vegetation
and land surface dryness
in present and future climate

현재 및 미래기후에서의 식생 및
지면 건조도 변화에 대한 연구

Chang-Eui Park

February 2016

School of Earth and Environmental Sciences
Graduate School
Seoul National University

A study on changes in the vegetation
and land surface dryness
in present and future climate

By
Chang-Eui Park

Dissertation Submitted to the Faculty of the Graduate School of the
Seoul National University in Partial Fulfillment of the Requirement
for the Degree of Doctor of Philosophy

Degree Awarded:
February 2016

Advisory committee:

Professor	Wookap Choi, Chair
Professor	Chang-Hoi Ho,
Professor	Song-You Hong
Professor	Eun-Ju Lee
Professor	Yong-Sang Choi
Doctor	Kwang-Ya Lee

이학박사학위논문

현재 및 미래기후에서의 식생 및
지면 건조도 변화에 대한 연구

A study on changes in the vegetation and land surface
dryness in present and future climate

2016년 2월

서울대학교 대학원

지구환경과학부

박 창 의

Abstract

Historical observations show various responses to global warming over the land surface, one of important elements of Earth's climate system as well as living place of humanity. Among those responses over the land, both changes in vegetation and land surface dryness are regarded as two major phenomena. Vegetation, occupies about 70% of whole land surface, is a key element of both physical and chemical processes over the land surface. Exact understanding of the vegetation change and its feedback influences on climate is essential for both investigating observed climate change and projection of future climate. Changes in land surface dryness are invisible, but important for the hydrological condition over the land, largely influences on agriculture and water management. Thus, researches on changes in both vegetation and land surface dryness contribute to mitigate risks of climate change because of both vegetation and land surface dryness has numerous socio-economic impacts on society. The present dissertation provides remarkable results of three studies about changes in vegetation and land surface dryness.

First, the potential impact of vegetation feedback on land surface dryness in summer season is examined in a condition of doubling of atmospheric CO₂ concentration over the contiguous United States (US) using a set of 100-year-

long climate simulations integrated by global climate model (GCM) interactively coupled with a dynamic vegetation model. The Thornthwaite moisture index (I_m), which quantifies land surface dryness on the basis of atmospheric water supply (i.e. precipitation, P) and atmospheric water demand (i.e., potential evapotranspiration, PET), is used to measure changes in the surface dryness. Warmer atmosphere and drier surface resulting from increased CO₂ concentration increase land surface dryness over most of the contiguous US. This phenomenon is due to larger increments in PET than in P, regardless of the presence or absence of vegetation feedback. Compared to simulation without active dynamic vegetation feedback, the presence of vegetation feedback significantly alleviates the increase in land surface dryness. This vegetation-feedback effects is most notable in the subhumid regions such as southern, Midwestern and northwestern US, primarily by the increasing vegetation greenness. In these regions, the greening in response to warmer temperatures enhances moisture transfer from soil to atmosphere by evapotranspiration (ET). The increased et and subsequent moistening over land areas result in weaker surface warming (1–2 K) and PET (3–10 mm month⁻¹), and greater P (4–10 mm month⁻¹). Collectively, changes in temperature, PET, and P due to vegetation feedback result in moderate increases in I_m , indicating decrease in land surface dryness.

Next, the change in vegetation due to global warming is examined in detail focusing on its speed during twenty-first century using both a definition of plant habitat based on surface temperature and climate scenarios from multiple GCMs. The plant habitat changes are predicted by driving the bioclimate rule in a dynamic global vegetation model using the climate projections from 16 coupled GCMs. The timing of plant habitat change is estimated by the first occurrence of specified fractional changes (10%, 20%, and 30%). All future projections are categorized into three groups by the magnitude of the projected global-mean land surface temperature changes: low (<2.5K), medium (2.5-3.5K), and high (>3.5K) warming. During the course of the twenty-first century, dominant plant habitat changes are projected in ecologically transitional (i.e., from tropical to temperate and temperate to boreal) regions. The timing of plant habitat changes varies substantially according to regions. In the low-warming group, habitat changes of 10% in southern Africa occur in 2028, earlier than in the Americas by more than 70 yrs. Differences in the timing between regions increase with the increase in warming and fractional threshold. In the sub-tropics, fast plant habitat changes are projected for the Asia and Africa regions, where countries of relatively small gross domestic product (GDP) per capita are concentrated. Ecosystems in these regions will be more vulnerable to global warming, because countries of low economic power lack the capability to deal with the warming-induced habitat

changes.

Causes of changes in land surface dryness are not clear due to various attributions of climate variables on dryness changes. For exact understanding on complex spatial variability of land surface dryness changes, relative influences of five climate variables on dryness changes are quantified over continental East Asia, covering diverse hydro-climate regimes from humid to arid regions, by using observations from 189 stations for the period of 1961-2010. For the whole analysis period, the land surface dryness is decreased by both increasing P and decreasing PET, but the increasing trend is not monotonic. Since early 1980s, increasing trend of the land surface dryness is shown over monsoon climate area ($> 100^{\circ}\text{E}$), but different climate variables drive the drying trend in each hydro-climate regimes. Dryness increases over the arid region are mostly explained by decrease in precipitation. In the humid area, increasing saturation vapor pressure following warming primarily contributes to dry surface despite continuous increase in precipitation. These results suggest increased evaporative potential, the secondary impact of atmospheric warming, plays a considerable role in changes in land surface dryness over the humid area even though sufficient atmospheric moisture exists at there.

Conclusions of the present thesis suggest three meaningful implications. 1)

Moistening by enhanced vegetation feedback may prevent aridification under climatic warming especially in areas vulnerable to climate change, with consequent implication for mitigation strategies. 2) The spatial distribution of plant habitat is projected to change quickly over countries of low economic power located on Asia and Africa. It is important to establish international collaboration via which developed countries provide assistance to mitigate the impacts of global warming. 3) The global warming sharply increases atmospheric water demands, inducing the risk of drying out over the land surface. Water management plans should consider the ongoing trend of drying accompanied by warming to mitigate the water scarcity in future.

Keywords: Vegetation Change, Land Surface Dryness, Climate Change, Vegetation Feedback, Aridity Index, Atmospheric Water Demand

Student Number: 2010-30105

Table of Contents

Abstract	i
Table of Contents.....	vii
List of Tables.....	x
List of Figures	xii
1. Introduction	1
1.1 Backgrounds	1
1.2 Motivation and objectives.....	5
1.3 Thesis organization	12
2. Data and Method	13
2.1 Data.....	14
2.2 Method.....	20

3. Vegetation feedback impact on climate aridity.....	33
3.1 Models	33
3.2 Experimental design.....	37
3.3 Changes in climate types	41
3.4 Changes in LAI and surface evapotranspiration.....	46
3.5 Changes in water supply and water demand	51
3.6 Summary and Discussion	58
3.6.1 Comparison of impact of change in ET with change in vegetation physiology and soil moisture.....	58
3.6.2 Importance of vegetation feedback and limitation of potential vegetation and I_m.....	62
4. Understanding of present and future changes in vegetation.....	65
4.1 Temperature and precipitation in present and future climate.....	65
4.2 Projected changes in spatial distribution of potential plant habitat.....	71
4.3 Projected changes in the timing of plant habitat changes..	79
4.3.1 Regional characteristics of timing of plant habitat change	79
4.3.2 Relationship between national wealth and the timing of plant habitat change.....	89
4.4 Summary and Discussion	92

5. Significant drying trend over the humid area in continental East Asia by local warming.....	99
5.1 Trend in land surface dryness over continental East Asia.	99
5.2 Causes of changes in land surface dryness	104
5.3 Summary and Discussion	108
6. Conclusions.....	111
References.....	118

국문 초록

감사의 글

List of Tables

Table 2.1. The gross domestic product (GDP) of nations which total or some part of territory is included in each region (The World Bank, 2012).....	19
Table 2.2. Bio-climate limits for plant habitats: $T_{c,min}$ is the minimum coldest-month temperature for survival; $T_{c,max}$ is the maximum coldest-month temperature for survival.....	23
Table 2.3. Future projection of 16 climate models included in three warming thresholds.....	24
Table 2.4. Climate types defined in terms of the original Thornthwaite moisture index.....	27
Table 3.1. Equilibrium experiments using CAM3-DGVM. Identifiers for each simulation, sea surface temperature (SST), atmospheric CO ₂ concentrations (CO ₂), integration time (Years), number of ensemble (Ensembles), and model horizontal resolution (Resolution).	40
Table 4.1. Annual mean temperature and precipitation (\pm standard deviation) of CRU and 20C3M simulations for present-day.....	67
Table 4.2. Projected changes in annual mean temperature and precipitation (\pm standard deviation) for low, medium, and high warming groups in future (2080-2099).	68
Table 4.3. Area of observed and projected plant habitat (10^6 km ²). The numbers	

are the total area (in 10^6 km^2) covered by each climate type. The numbers of in parentheses are one standard deviation of total area (in 10^6 km^2) projected by 12, 18, and 18 projections in low, medium, and high warming groups. 75

Table 4.4. Estimated year that ensemble mean of projected habitat changes firstly exceed 10%, 20%, and 30% threshold for all warming groups in the three latitudes belts. En-dash means that the ensemble means does not reach the three thresholds until 2099. 84

Table 4.5. Estimated year that 10% and 90% of model simulations of projected habitat changes firstly exceed 10%, 20%, and 30% threshold for all warming groups in the three latitudes belts. En-dash means that the ensemble means does not reach the three thresholds until 2099. 86

List of Figures

Figure 3.1. Spatial distribution of Thornthwaite moisture index over the US in boreal summer for VegOff_1× (a), and 30-year climatology of CPC monthly analysis of global surface air temperature and land precipitation for the period 1980–2009 (b).....	44
Figure 3.2. Spatial distribution of changes in Thornthwaite moisture index by radiative effect (a), radiative and vegetation feedback effect (b), and vegetation feedback only (c). Blue dots and red dots represent regions that the climate type change more humid and arid, respectively.....	45
Figure 3.3. Spatial distribution of leaf area index over the US in boreal summer for VegOff_1× (left) and changes in leaf area index between VegOn_2× and VegOff_1× (right). Black dots represent the regions that changes in leaf area are statistically significant at the 95% confidence level.....	49
Figure 3.4. Spatial distribution of changes in total evaporation, canopy evaporation, canopy transpiration, and soil evaporation due to radiative effect (a–d), radiative and vegetation feedback effect (e–h), and vegetation feedback only (i–l). Black dots represent the regions that changes are statistically significant at the 95% confidence level.....	50
Figure 3.5. Spatial distribution of changes in precipitation, temperature, and PET	

over the US due to radiative effect (a-c), radiative and vegetation feedback effect (d-f), and vegetation feedback only (g-i). Black dots represent the regions that changes are statistically significant at the 95% confidence level. 56

Figure 3.6. Scatter plot of the values of I_m in present climate run (VegOff_1x) with respect to ratio of precipitation to PET. Black, blue, and red dots represent the ratio of VegOff_1x, VegOff_2x, and VegOn_2x, respectively. 57

Figure 3.7. Spatial distribution of changes in vertically integrated volumetric soil water due to radiative effect (a), radiative and vegetation feedback effect (b), and vegetation feedback only (c). 61

Figure 4.1. Spatial distributions of averaged temperature of (a) CRU and (b) ensemble of 20C3M simulations, and precipitation of (c) CRU and (d) ensemble of 203CM simulations for present-day (1980-2009). 69

Figure 4.2. Spatial distribution of changes in averaged temperature (2080-2099 minus 1980-1999) for (a) 12 models in low, (b) 18 models in medium, and (c) 18 models in high warming threshold. (d), (e), and (f) show changes in averaged precipitation for low, medium, and high warming threshold. 70

Figure 4.3. Spatial distribution of averaged plant habitat of present day (1980-1999) for (a) CRU and (b) ensemble of 20C3M simulations. Spatial distribution of averaged plant habitat of future projection (2080-2099) for (c) 12 models in low, (d) 18 models in medium, and (e) 18 models in high warming threshold.

Regions with grey shading represent the desert areas. 77

Figure 4.4. Difference of zonal-mean fractional change in plant habitat between the period of 2080–2099 and 1980–1999 for (a) tropical habitat, (b) temperate habitat, and (c) boreal habitat. Red dashed, green solid, and blue dotted line indicates high, medium, and low warming threshold. 78

Figure 4.5. Regional mean fractional changes in plant habitats for (a) 10°–25°S, (b) 15°–30°N, and (c) 50°–65°N. Each projection from the CMIP3 model simulation included in low-, medium-, and high- warming groups are shown in light blue, light green, and light orange. Blue, green, and red bars represent the range of timing when projected habitat changes might cross the 10%, 20%, and 30% thresholds of low-, medium-, and high- warming groups. 88

Figure 4.6. Timing of averaged plant habitat change reaches (a) 10%, (b) 20%, and (c) 30% threshold for GDP per Capita 2012 of Botswana, China, Mexico, Russia, and Canada. Blue, yellow, and red dots represent low, medium, and high warming threshold, respectively. 91

Figure 5.1. Temporal variations of annual mean PET/P, P, and PET in East Asia. a-c, PET/P (a), P (b), and PET (c). Yellow and blue bars indicate that positive and negative anomalies for PET/P and PET, but negative and positive anomalies for P. Black, blue, and red lines are linear regression lines (% decade⁻¹) for the period of 1961-2010, 1961-1983, 1984-2010, respectively. 102

Figure 5.2. Spatial distributions of trends of PET/P, P, and PET in East Asia. a-c, The spatial distribution of trends in annual mean PET/P (a), P (b), and PET (c) for the period of 1961-1983. d-f, as a-c, but for the period of 1984-2010. The empty square indicates that the trend is significant at 95% level. 103

Figure 5.3. Spatial distributions of contributions of the five climate parameters on the PET/P trends in East Asia. a-e, The spatial distribution of the contribution of changes in P (a), Rn (b), WS (c), Ta (d), and RH (e) for the period of 1961-1983. f-j, as a-e, but for the period of 1984-2010. 106

Figure 5.4. Averaged relative influences of five climate parameters on the PET/P changes. a-c, Relative influences ($\% \text{ decade}^{-1}$) of five climate parameters is averaged for the three hydro-climate regimes: arid (a), semi-arid (b), and humid (c). The averaged influences are computed for the two periods of 1961-1983 and 1984-2010. Blue, pink, beige, orange, and cyan bars represent averaged influence of P, Rn, WS, Ta, and RH, respectively. Error bars represent confidence intervals at 95% significance level. 107

Figure 5.5. Schematic diagram explaining the small and large influence of RH on the PET/P trends in the arid and humid regions. The map shows the spatial distributions of annual mean temperature for the period of 1961-2010 (degree C). Empty squares, cross marks, and filled circles are stations that classified by arid, semi-arid, and humid regions, respectively. The map clearly shows that the arid

and humid region of continental East Asia has the cold and warm climate, respectively. In the arid region, warming magnitude is large, but decrease in RH is small following the Clousius-Clapeyron relationship between the saturation vapor pressure (e_s) and T_a (brown line in the graph). In contrast, the increase in the e_s is relatively large in the humid region despite the small warming magnitude (blue line in the graph). The difference in the increment of e_s between two regions causes much larger decrease in RH, further large influence of RH on PET/P trends in the humid region. 110

1. Introduction

1.1 Backgrounds

As climate changes according to rising concentration of greenhouse gases (GHGs), the land surface experiences enormous changes, bring significant impacts on regional climate through variations of surface temperature, radiation, and cloudiness (Denman et al. 2007). Changes in plant habitats are among the key responses of terrestrial ecosystems to climate change (Sturm et al. 2001; Rosenzweig et al. 2007; Xu et al. 2013). Recent observational studies show that the global warming induced by the emissions of anthropogenic greenhouse gases may have caused notable habitat changes, particularly for shrub- and grasslands in the high latitudes (Parmesan and Yohe 2003; ACIA 2005; Jia et al. 2009; Forbes et al. 2010). Future climate projection studies also suggest that global warming may accelerate the current global habitat changes (Sala et al. 2005; Sitch et al. 2008; Gonzalez et al. 2010). The plant habitat changes can cause various ecological effects such as decline in biodiversity, increased extinction risks, and alterations in biogeochemical cycles (Thomas et al. 2004; Bellard et al. 2012; Hartley et al. 2012), which can further alter local/regional climate through vegetation-climate feedback (Chapin et al. 2005; Bonan 2008; Jeong et al. 2011a; Park et al. 2012). Thus, understanding plant habitat changes due to global

warming is crucial for mitigating and adapting to future climate and ecological changes.

The vegetation change in response to climate change have been projected using dynamic global vegetation models (DGVMs) and bioclimate envelope models either driven by climate model forcing (Cramer et al. 2001; Sitch et al. 2008; Bellard et al. 2012) or equipped with global climate model (Boudena et al. 2010; Jeong et al. 2011a). Previous studies show that future vegetation change is drastic in the northern high-latitudes (Sitch et al. 2003; Scholze et al. 2006; Jia et al. 2012). It is because of the large temperature increase induces profound penetration of the grasses and shrubs into non-vegetation regions in the high-latitudes (Wang et al. 2008; Jeong et al. 2011a). In mid-latitude and tropics, changes in the vegetation are mainly represented by changes in density of forests. With increasing the warming magnitude, more severe vegetation changes are appeared surely.

Altered vegetation influences regional climate through vegetation feedback by changing land-atmosphere interaction (Bonan et al. 2003; Jackson et al. 2008; Jeong et al. 2011a). Changes in the surface albedo and ET are the two main mechanisms involved in vegetation feedback with the surface climate. For example, an increase in vegetation greenness reduces surface albedo to favor

surface warming. This warming effect is countered by the cooling due to enhanced evapotranspiration (ET). The net impact of the two opposite effects determines the surface air temperature changes. Further, changes in vegetation may alter regional precipitation and water cycle. Through diverse regional features of the net effects (i.e., both temperature and moisture effects), vegetation feedback determines the magnitude of the changes in regional temperatures and water cycle (Notaro et al. 2007; Liu et al. 2006; Diffenbaugh 2009).

In warmer climate, water holding capacity of atmosphere is exponentially increased based on the relationship between saturation vapor pressure (e_s) and air temperature following Clausius-Clapeyron equation (Tsonis 2002; Hegerl et al. 2007). The increased capability of water vapor of the atmosphere induces two contrasting impact on land surface dryness. Large amount of water vapor is regarded as a favor condition of cloud formation (Held and Soden 2006; Meehl et al. 2007b). The amount of P is surely increased over the land surface, indicating moistening of the land. However, increased water demand of the atmosphere could dry out the land surface through increasing surface evaporation (Denman et al. 2007; Hegerl et al. 2015). Relative importance of two contrasting impacts is regionally different due to spatial heterogeneity of both characteristics of the land surface and mean climate condition (Greve et al. 2014).

Changes in land surface dryness have substantial socio-economic influences on human society. Projected increase in surface dryness with increasing GHGs may increase in natural disaster and social problems related to water availability such as drought (Meehl et al. 2007b; Sheffield and Wood 2008), desertification (Le Houerou 1996), vegetation die-out (van Mantgem et al. 2009), famine (Wang 2005; Edmonds and Rosenberg 2005), water management (Kundzewicz et al. 2007; Yohe et al. 2007), and energy production (Filed et al. 2007; Hightower and Pierce 2008). Among those problems, drought is one of significant extreme event because of it can induce a severe socio-economic impact by extremely large water stress (Bruke and Brown 2008; Seager et al. 2009). Over the 20th century, risk of drought occurrence is increased over Sahel, Mediterranean, and Asia where decreasing trend of Palmer Drought Severity Index (PDSI) is shown (Trenberth et al. 2007). In addition, analysis of GCM projections in IPCC AR4 consistently shows that occurrence and duration of drought will be increased with GHGs induced warming (Wang 2005; Meehl et al. 2007; Bruke and Brown 2008).

1.2 Motivation and objectives

Projected changes in land surface dryness shows large uncertainties related to land surface conditions and its feedback (Notaro et al. 2007; Meehl et al. 2007a; Christensen et al. 2007). Surely, the land surface dryness is influenced by vegetation feedback, playing considerable roles on surface hydrology (Bonan 2008; Jeong et al. 2011a). The first objective of present thesis is to examine the feedback impact of vegetation change on climate aridity, representing the degree of land surface dryness. Projections of several global climate models (GCM) in IPCC Fourth Assessment Report (IPCC AR4) show increasing trend of surface air temperature during 2000-2099, particularly over continental mid- and high-latitude in northern hemisphere (Meehl et al. 2007b). This warming lead to increase in moisture transport from surface to atmosphere due to increased atmospheric water-holding capacity (Hegerl et al. 2007). Hence, water stress will increase due to larger water demand associated with warmer temperature. Precipitation regarded as a water supply, however, is generally decreased over the subtropics in the future warmer climate (Meehl et al. 2007b). Thus, climate of continental subtropics is getting more arid due to increasing atmospheric water demand and decrease in water supply.

The potential impact of vegetation feedback on the climate aridity in warmer climate condition is examined using the results of atmosphere-land-vegetation coupled model. As mentioned above, the vegetation feedback is considered as one of important modulator of regional climate in future climate projection by changing surface energy budget and hydrological cycle (Bonan et al. 2003; Diffenbaugh 2009; Jeong et al. 2009; Jeong et al. 2011a). However, previous studies are not sufficient to explain the impact of vegetation change on climate aridity. Hence, it is valuable work that evaluating the impact of vegetation feedback on drought potential and projecting potential impact of vegetation change on climate aridity.

Next target of present thesis is changes in vegetation in future focusing on changing speed. Projections of ecosystem-level plant habitat changes in response to climate change have been made using dynamic global vegetation models (DGVMs) and bio-climate envelope models either driven by climate model forcing (Cramer et al. 2001; Sitch et al. 2008; Bellard et al. 2012) or coupled with global climate models (GCMs) (Bounoua et al. 2010; Jeong et al. 2011a). Plant habitat changes are investigated by contrasting the time-mean geographical distributions of plant habitats in a future period against that in a present-day period, in general (e.g., 2071–2100 minus 1961–1990 in Scholze et al. (2006)). This method is useful for measuring the amount of habitat change in targeted

regions and periods (Lucht et al. 2006; Alo and Wang 2008), but is not suitable for obtaining the point of time (i.e., timing) at which a specified amount of habitat change will occur. The timing of plant habitat change can tell us which parts of the world will experience faster changes, indicating higher risks from habitat change. This also allows us to estimate the amount of time required for the occurrence of a specific amount of habitat change for a specific level of climate change. Information on the timing to exceed a particular threshold value is useful for the development and timely implementation of management plans to adapt to and mitigate the impact of plant habitat changes (IPCC 2007; Joshi et al. 2011).

The second objective of this study is to evaluate the regional variations in the timing of plant habitat changes corresponding to a specified level of global warming in terms of the surface air temperature. Forest management plans have been generally developed at regional or national levels (Adger et al. 2007). Thus regional variations in the timing of plant habitat changes are directly useful in forest management practices. We also examine the relationship between the gross domestic product (GDP) per capita and the projected timing of plant habitat changes to help individual nations in developing ecosystem management plans. Ecosystem management policy needs sufficient economic capability. Adaptation policies and actions cannot be implemented if the associated cost is

too large for a nation to afford (Naidoo et al. 2006; IPCC 2007; Chan et al. 2011). Nations with weaker economic capability will experience difficulties in implementing mitigation plans, thus are more vulnerable to the same amount of habitat changes than wealthier nations.

To obtain future global plant habitat changes, this study projects the spatial and temporal variations in the changes of woody plant habitats in the 21st century using the bio-climate rule and multiple global warming scenarios from multiple atmosphere-ocean coupled GCMs. Because the bio-climate rule describes the plant habitat changes only in terms of the surface air temperature, the biotic factors such as the physiological impacts of CO₂ fertilization on plant habitat and competition among plant species under given climate change are not included in the projections. This may be an over-simplification in projecting plant habitat changes, however, a hierarchical framework in Turner et al. (2001) showed that climate is the highest environmental constrain for distribution of plant habitat in the global scale. This hierarchy of environmental variables is supported by limited impacts of the biotic factors when the climate change is less severe (Brown and Lomolino 1998; Pearson and Dawson 2003). Thus, global plant habitat changes in response to climate change obtained using the bio-climate rule is reliable although it does not include the effects of other factors such as CO₂ fertilization. This study have utilized all available climate model

outputs from the Intergovernmental Panel on Climate Change (IPCC) Fourth Assessment Report (AR4) archives to calculate the response of plant habitats to climate change (Meehl et al. 2007a). Ensemble of various projected habitat changes could cope with a wide range of inter-GCM variations in climate sensitivity (Meehl et al. 2007b).

The third topic is about examining exact mechanisms of changes in land surface dryness induced by present climate changes. Recent studies reveal that complex spatial variability of dryness changes over the land that contrasts to the “dry gets drier, wet gets wetter” paradigm (Greve et al. 2014; Hegerl et al. 2015). However, causes of changes in land surface dryness are not clear due to various attributions of climate variables on dryness changes (Estes et al. 2014; Christensen et al. 2007; Greve et al. 2014). The mechanism of changes in surface dryness over the land fundamentally differs from that over the ocean due to limited surface moisture availability (Feng and Fu 2013; Sherwood and Fu 2014). In many assessments, variation of precipitation (P), representing the amount of moisture supply, is regarded as a key variable for historical changes in land surface dryness, particularly over monsoon climate zones (Piao et al. 2010; Estes et al. 2014). For example, land surface dryness changes over East Asia are generally summarized by “Dry western region ($< 100^{\circ}\text{E}$) is getting wetter, dry northern region ($> 100^{\circ}\text{E}$, $35^{\circ}\text{-}45^{\circ}\text{N}$) drier, and wet southern region ($> 100^{\circ}\text{E}$,

25°-35°N) wetter” based on changes in annual mean P (Wang and Ding 2006; Piao et al. 2010). However, climate changes lead to significant changes in pan evaporation and potential evapotranspiration (PET), measurement of the amount of atmospheric moisture demand (Liu et al. 2010; Han et al. 2012). PET changes show large influence on the dryness trend over many regions according to changes in absorbed radiation, surface wind, and air temperature (Westerling et al. 2006; Estes et al. 2014). Thus, it is necessary to quantify impacts of each climate parameters on land surface dryness over various hydro-climate regimes for comprehensive understanding of complicated dryness changes over the land.

To investigate exact causes of changes in land surface dryness over continental East Asia, relative influences of five climate parameters on dryness changes are compared. Relative influences are computed using climate records at 179 and 10 meteorological stations of China and South Korea during the period of 1961-2010. Continental East Asia may be appropriate target region for examining the impact of climate variables on changes in land surface dryness due to both observed abrupt climate change and widespread of various hydro-climate regimes. An aridity index, defined as PET based on Penman-Monteith equation divided by P (PET/P), is used to determine changes in land surface dryness (Penmen 1948; Allen et al. 1998). If PET/P is decreased, it means that the land surface gets wetter; if it rises, the land surface is getting drier. In addition, the

analysis domain is divided into three hydro-climate regimes using 50-year climatology of PET/P: arid ($PET/P > 2$), semi-arid ($1 < PET/P < 2$), and humid ($PET/P < 1$). This classification is essential considering the spatial variability of changes in land surface dryness. Through using this method, we estimate influence of changes in P, net radiation (R_n), wind speed (WS), surface air temperature (T_a), and relative humidity (RH) on the changes in PET/P over three hydro-climate regimes of continental East Asia to present exact causes of changes in land surface dryness.

1.3 Thesis organization

The present thesis is organized as the following.

The data and analysis methods are mentioned in chapter 2. The data section includes descriptions of station based climate record, reanalysis field, model outputs from CMIP3, and satellite-observed vegetation. The method section explains the calculation of PET based on both Thornthwaite's equation and Penman-Monteith equation, and the land surface dryness (Thornthwaite aridity index and aridity index). Also the definition of plant habitats based on surface temperature is described in the method section. In chapter 3, influences of vegetation feedback on the climate aridity are investigated using several set of coupled GCM outputs in a condition of doubled CO₂ concentration. Chapter 4 deals with when the timing of plant habitat changes is occurred for multiple warming scenarios and regions. Chapter 5 reveals the exact causes of changes in land surface dryness over continental East Asia by comparing relative influences of five climate parameters using observational record of 1961-2010. Overall conclusions of the present thesis and possible future works are proposed in chapter 6.

2. Data and Method

The employed data sets are consists of the observed climate records from ground stations, satellite-retrieved observations, reanalysis data, and future projections of fully coupled GCM. The ground observation consists of 179 and 10 stations of China and South Korea for the period of 1961-2010. The satellite observations of NDVI are regarded as vegetation greenness and used as observation. Land surface temperature and precipitation of Climate Research Unit Time Series v3.0 (CRU TS3.0) is used as environmental climate of present-day. In addition, long-term integrations of 16 fully coupled GCMs in the third phase of the Coupled Model Intercomparison Project (CMIP3: Meehl et al. 2007a) are used as hindcast and future projections of climate.

Present-day and future plant habitat of woody plant species are examined using the bio-climate rule of plant functional types (PFTs) in the Lund-Potsdam-Jena dynamic global vegetation model (LPJ-DGVM) (Sitch et al. 2003). The timing of plant habitat change is estimated based on the computed plant habitat. In addition, Thornthwaite moisture index is used as a quantifier of climate aridity on the basis of atmospheric water supply (i.e., precipitation) and atmospheric water demand (i.e., potential evapotranspiration: PET). Climate observations of

ground stations are used to compute PET following FAO Penman-Monteith method.

2.1 Data

2.1.1 Station based climate records

The climate data for the period of 1961-2010 are come from selected 179 and 10 meteorological sites of China and South Korea, respectively. Data includes daily mean air temperature, precipitation, wind speed, relative humidity, sunshine duration, and several other variables. The quality of this data is controlled by National Meteorological Center of China Meteorological Administration and Korea Meteorological Administration. Selection of meteorological sites is carried out by two two conditions: 1) existence of all climate parameters of the year 2010, 2) continuous records of at least 10-year for both analysis periods.

2.1.2 Normalized Difference Vegetation Index (NDVI)

To determine the area of vegetation and soil, satellite-derived NDVI data is used in this study. The NDVI is the contrast between red and near-infrared reflectance of vegetation. This contrast is indicative of the abundance of pigments such as chlorophyll, or simply, leaf area. It is calculated from reflectances in channel 1 (0.58-0.68 μm) and channel 2 (0.73-1.1 μm) and is defined as

$$\text{NDVI} = (\text{Channel 2} - \text{Channel 1}) / (\text{Channel 2} + \text{Channel 1}).$$

The NDVI is expressed on a scale between -1 to +1, and ranges between -2 and 0.1 for snow, inland water bodies, deserts, and 85 exposed soils, and increases from about 0.1 to 0.7 for increasing amounts of vegetation, but saturates in the case of dense leaf canopies, e.g., the humid tropical forests. The primary data source are measurements from the Advanced Very High Resolution Radiometers (AVHRR) on board the afternoon-viewing NOAA series satellites (NOAA 7, 9, 11 and 14), which were processed to NDVI by the Global Inventory Monitoring and Modeling Systems (GIMMS) group. The important data processing features contained improved navigation, sensor calibration, and atmospheric correction for stratospheric aerosols. Details on development of the GIMMS NDVI data set and its quality can be found in *Zhou et al. (2001)*. Residual problems from lack of an explicit atmospheric correction for

tropospheric aerosols, water vapor absorption, surface anisotropy, etc. can be identified in this data set (Zhou et al. 2001). To minimize such effects, Los et al. (2000) developed a four-step procedure, which involved a Fourier Adjustment of outliers in the time series, Solar zenith angle correction, Interpolation for missing data, and Reconstruction of NDVI values over tropical rain forests. This data set overcomes most problems noted in previous generation of NDVI data sets. In this study, we used $0.5^\circ \times 0.5^\circ$ and monthly temporal resolution for the period 1982-2007.

2.1.3 Climate Research Unit Time Series v3 (CRU TS3.0)

CRU TS3.0 dataset is high-resolution gridded datasets presented by Climate Research Unit (Harris et al. 2013). The CRU TS3.0 is constructed by composing land surface observations of > 4000 stations. In the CRU TS3.0 datasets, 9 kinds of meteorological variables are provided for land surface: mean temperature, minimum temperature, maximum temperature, precipitation, daily temperature range, vapor pressure, cloud cover, wet day frequency, and frost day frequency. The CRU TS3.0 has $0.5^\circ \times 0.5^\circ$ horizontal resolution and monthly temporal resolution for the period from 1901 to 2005. In this thesis, land surface

temperature and precipitation data are used to determine the plant habitat for the present-day (1980-1999).

2.1.4 CMIP3 multi-model dataset

The third phase of Coupled Model Intercomparison Project (CMIP3) is huge project, which provides simulations of many atmosphere-ocean global climate models for assessment of climate variability and climate change (Meehl et al. 2007a). Long-term simulation of 16 fully coupled GCMs is obtained from CMIP3. Surface temperature and precipitation of multi-model dataset is used to identify present and future distribution of plant habitat. All GCM outputs are first statistically downscaled onto a $0.5^\circ \times 0.5^\circ$ latitude-longitude grid for the period 1950–1999 using the bias-corrected spatial downscaling (BCSD) scheme of Wood et al. (2004) in conjunction with the gridded observations of Adam and Lettenmaier (2003). We analyzed a total of 64 sets of downscaled GCM simulations: 16 present-day simulations following the Special Report on Emissions Scenarios (SRES) 20C3M for 1950–1999 and 48 (= 16×3) future projections corresponding to the SRES B1, A1b, and A2 emissions scenarios for 2000–2099.

2.1.5 Gross Domestic Product

The Gross Domestic Product (GDP) is the market value of all officially recognized final goods and services produced within a nation in a year. The GDP could represent the total economic size of each nation, thus the GDP is adopted to evaluate the relationship between the timing of plant habitat change and regional economic power. Table 2.1 shows the 2011 GDP values of all nations that have some or all of their territory located in the latitude bands 10°S–25°S, 15°N–30°N, and 50°N–65°N (World Bank 2012). Notice that these three latitude bands are found to have significant plant habitat changes (see results section later). The six selected nations (Angola, Brazil, China, Mexico, Russia, and Canada) have the largest GDP values in each region, representing the upper limits of regional economic power. The United States is excluded from the representative nations because only a small part of its territory is located within the latitudes 15°N–30°N and 50°N–65°N.

Table 2.1. The gross domestic product (GDP) of nations which total or some part of territory is included in each region (The World Bank, 2012).

Latitudinal belt	Region	Nation	GDP (billion US dollar)
10°S–25°S	southern Africa	Angola	104.3
		Zambia	19.2
		Namibia	12.3
		Botswana	17.3
		Zimbabwe	9.7
		Mozambique	12.8
		Madagascar	9.9
		central South America	Brazil
	Bolivia	23.9	
	Paraguay	23.8	
15°N–30°N	East Asia	Pakistan	210.2
		India	1848.0
		Bangladesh	111.9
		Lao PDR	8.3
		Thailand	345.7
		Vietnam	123.6
		Philippine	224.8
		Nepal	18.9
		Bhutan	1.7
		China	7318.5
		southern North America	Mexico
	Cuba	-	
	United States	14991.3	
50°N–65°N	northern Eurasia	Russia	1857.8
		Kazakhstan	188.1
	northern North America	Canada	1736.1
		United States	14991.3

2.2 Method

2.2.1 The bio-climate rule and plant habitats

Habitat changes of woody plant species in response to global warming are assessed using the bio-climate rule of plant functional types (PFTs) in the Lund-Potsdam-Jena dynamic global vegetation model (LPJ-DGVM) (see Table 2 in Sitch et al. 2003) where the bio-climate rule for woody PFTs is defined by temperature-based bio-climatic limitation of survival and establishment. The climatic limitation is represented by range of the coldest-month temperature in the 20-year running mean (T_c). For example, in regions where T_c ranges between 3°C and 15.5°C, temperate needleleaf evergreen, temperate broadleaf evergreen, temperate broadleaf summergreen, and temperate herbaceous plants can coexist. The bio-climate rule has been used in a number of previous studies on future vegetation changes using LPJ-DGVM based models (Lucht et al. 2006; Alo and Wang 2008; Scholze et al. 2008; Jiang et al. 2012). On the basis of the bio-climate rule, eight plant habitats are defined according to dominant PFTs (Table 2.2); tropical (Tr-type: Tr1 and Tr2), temperate (Te-type: Te1, Te2, Te3, and Te4), and boreal (Bo-type: Bo1 and Bo2). For every year in the analysis period, the spatial distribution of T_c is transformed into the spatial distribution of plant habitats following the T_c ranges in table 2.2. Thus, the distribution of plant

habitats is calculated at annual time steps with the horizontal resolution same as T_c . To remove remaining non-vegetative regions, i.e., deserts, the tropical and temperate regions with annual precipitation totals < 200 mm (UNEP 2009; Jeong et al. 2011b) are excluded. Polar deserts in the arctic region are defined as the areas of annual precipitation totals < 250 mm with the warmest-month temperatures $< 10^\circ\text{C}$ (UNEP 2009). In addition, the land cover product from MODIS retrievals is used to verify the present-day distributions of the eight plant habitats and deserts (Friedl et al. 2002).

2.2.2 Temperature-based approach for plant habitat change

Instead of the SRES emission scenarios, the global-mean warming thresholds are used to calculate habitat changes corresponding to specified amounts of increased global mean surface temperature. The global-mean surface temperature is conventionally used to represent the degree of climate change (Scholze et al. 2006; Solomon et al. 2007) because different degrees of global-mean temperatures are reflected by combined impacts of land-use and greenhouse gas changes (Joshi et al., 2011). In addition, the global-mean temperature change is relevant to planning mitigation policies about the impact of climate change (Meinshausen et al. 2009; UNFCCC 2009). Thus, assessing the climate change impact as a function of the global-mean temperature change is a rational way to

quantify the climate change impacts (Scholze et al. 2006; Joshi et al. 2011). The 48 sets of GCM projections are grouped into three categories following the projected global-mean land surface temperature differences (ΔT) between the late 21st century period (2080–2099) and the present-day period (1980–1999): $\Delta T < 2.5^\circ\text{K}$ as low warming, $2.5^\circ\text{K} < \Delta T < 3.5^\circ\text{K}$ as medium warming, and $\Delta T > 3.5^\circ\text{K}$ as high warming. These warming thresholds are larger than in Scholze et al. (2006) by 0.5°K because the warming signal is generally larger over lands than ocean surfaces (Meehl et al. 2007b). Using these threshold values, 12, 18, and 18 sets of GCM projections are categorized into the low, medium, and high warming groups, respectively. (Table 2.3). For all warming thresholds, the timing at which a plant habitat changes by 10%, 20%, and 30% is estimated. In a specific analysis domain, the fractional change is computed by a ratio of the area where plant habitat change occurs to the total area in that region. A year at which the ratio first exceeds 10%, 20%, or 30% indicate the timing of 10%, 20%, or 30% habitat change, respectively. The timing is computed based not only on the ensemble mean, but on 10% and 90% of model projections to deal with the uncertainty in model simulations. Because previous studies showed that the regional-mean fraction of wood species is likely to be $< 20\%$ over the globe, these three habitat-change thresholds must be sufficiently large to capture meaningful habitat changes (Scholze et al. 2006; Sitch et al. 2008).

Table 2.2. Bio-climate limits for plant habitats: $T_{c,min}$ is the minimum coldest-month temperature for survival; $T_{c,max}$ is the maximum coldest-month temperature for survival.

	Plant habitat	$T_{c,min}$ (°C)	$T_{c,max}$ (°C)
Tropical PFTs dominated habitat (Tr-type)	Tr1 tropical broadleaf green tropical herbaceous	22	-
	Tr2 tropical broadleaf green temperate needleleaf evergreen tropical herbaceous	18.8	22
Temperate PFTs dominated habitat (Te-type)	Te1 tropical broadleaf green temperate needleleaf evergreen temperate broadleaf evergreen tropical herbaceous	15.5	18.8
	Te2 temperate needleleaf evergreen temperate broadleaf summergreen temperate herbaceous	3	15.5
	Te3 temperate needleleaf evergreen temperate broadleaf summergreen temperate herbaceous	-2	3
	Te4 temperate broadleaf summergreen boreal summergreen boreal needleleaf evergreen temperate herbaceous	-17	-2
Boreal PFTs dominated habitat (Bo-type)	Bo1 boreal summergreen boreal needleleaf evergreen temperate herbaceous	-32.5	-17
	Bo2 temperate herbaceous	-	-32.5

Table 2.3. Future projection of 16 climate models included in three warming thresholds.

	Low warming ($\Delta T < 2.5^\circ\text{C}$)	Medium warming ($2.5^\circ\text{C} < \Delta T < 3.5^\circ\text{C}$)	High warming ($\Delta T > 3.5^\circ\text{C}$)
BCCR-BCM2.0	B1	A1b, A2	
CGCM3.1 (T63)	B1	A1b	A2
CCSM3	B1	A1b	A2
CNRM-CM3	B1	A1b	A2
CSIRO-MK3.0	B1, A1b	A2	
ECHAM5/MPI-OM		B1	A1b, A2
ECHO-G		B1	A1b, A2
GFDL-CM2.0		B1	A1b, A2
GFDL-CM2.1	B1		A1b, A2
GISS-ER	B1	A1b, A2	
INMCM3.0	B1	A1b	A2
IPSL-CM4		B1	A1b, A2
MIROC3.2(M)		B1	A1b, A2
MRI-CGCM2.3.2	B1	A1b, A2	
PCM	B1, A1b	A2	
UKMO-HadCM3		B1	A1b, A2

2.2.3 Thornthwaite moisture index

The Thornthwaite moisture index (Thornthwaite 1948; hereafter I_m) is used as a measure of climate aridity in this study as in changes in climate aridity (e.g., Mather and Feddema 1986; McCabe et al. 1990; McCabe and Wolock 1992). I_m is defined in terms of the atmospheric water supply and demand represented by precipitation (P) and potential evapotranspiration (PET), respectively. The moisture index consists of two indices: I_a that represents the potential aridity and I_h the potential humidity. These two indices are separately calculated based on moisture surplus and deficit from the water budget as

$$I_a = 100 \frac{D}{N} \quad (2.2.1)$$

$$I_h = 100 \frac{S}{N} \quad (2.2.2)$$

where D is water deficit defined as the sum of monthly PET minus P for $PET > P$, S is water surplus defined as the sum of monthly P minus PET for $P > PET$, and N is water need defined as the sum of monthly PET. The moisture index I_m is represented by combining of these two indices as

$$I_m = I_h - 0.6I_a. \quad (2.2.3)$$

Negative values of I_m imply arid climate where atmospheric water demand exceeds atmospheric water supply, and vice versa. The factor of 0.6 accounts for the assumption that water can infiltrate into soil more easily than it is extracted (Thornthwaite 1948). Monthly PET is calculated using an empirical formula as a function of mean surface air temperature (Thornthwaite 1948). In addition, I_m is used to separate climate type based on regional moisture condition. Table 2.4 provides that 9 climate types based on I_m .

Table 2.4. Climate types defined in terms of the original Thornthwaite moisture index.

Climate Type	Minimum	Maximum
A Perhumid	100	Infinite
B₄ Humid	80	100
B₃ Humid	60	80
B₂ Humid	40	60
B₁ Humid	20	40
C₂ Moist Subhumid	0	20
C₁ Dry Subhumid	-20	0
D Semiarid	-40	-20
E Arid	-60	-40

2.2.4 FAO Penman-Monteith method

In the FAO Penman-Monteith method, daily PET values are estimated for a reference crop defined as a hypothetical crop assumed by a height of 0.12 m, surface resistance of 70 s m^{-1} , and an albedo of 0.23. The computed daily PET closely resembles the evaporation of an extension surface of green grass of uniform height, actively growing and adequately watered. The formulation of daily PET following FAO Penman-Monteith method is written as:

$$\text{PET} = \frac{0.408\Delta(R_n - G) + \gamma\left(\frac{900}{T + 273}\right)U_2(e_s - e_a)}{\Delta + \gamma(1 + 0.34U_2)} \quad (2.2.4)$$

where R_n is the net radiation at the crop surface ($\text{MJ m}^{-2} \text{ day}^{-1}$), G the soil heat flux density ($\text{MJ m}^{-2} \text{ day}^{-1}$), T the air temperature at 2 m height, U_2 the wind speed at 2m height, e_s the saturation vapor pressure of the air (kPa), e_a the actual vapor pressure (kPa), Δ the slope of the vapor pressure curve ($\text{kPa } ^\circ\text{C}^{-1}$) at T , and γ the psychrometric constant ($\text{kPa } ^\circ\text{C}^{-1}$). The complete equation set for all variables is described in the FAO56 report (Allen et al. 1998).

2.2.5 Change-point method

Two methods are used to find change-point of temporal variation of PET/P.

One method defines the change-point when cumulative sum of PET/P variation for t th year (C_t) is the largest (Pettitt 1980). The cumulative sum C_t is provided as following:

$$C_0 = 0$$

$$C_t = C_{t-1} + (X_t - \bar{X}) \quad (2.2.5)$$

where X_t is PET/P in year t , and \bar{X} the averaged PET/P for whole analysis period.

In the other change-point model, X_t is same, PET/P of t th year and Y_t is defined as $\log_{10}(X_t + 1)$. The step variable S_t is defined for an integer l that changes from 2 to $m = N - 1$ as following:

$$S_t(l) = \begin{cases} 0, & t < l \\ 1, & t \geq l \end{cases} \quad (2.2.6)$$

where N is the total years of analysis period 1961-2010. Using the step variable S_t , a simple linear first-order regression model is suggested for an integer l as following:

$$Y_t = \beta_0(l) + \beta_1(l)S_t(l) + \epsilon_t(l) \quad (2.2.7)$$

where $\beta_0(l)$ is the intercept, $\beta_1(l)$ the slope and $\epsilon_t(l)$ the error of residual at Y_t for a fixed l . In addition, the value of $L(l)$ is computed by

$$L(l) = \hat{\beta}_1(l) / \text{se}[\hat{\beta}_1(l)] \quad (2.2.8)$$

where $se[\beta_1(t)]$ is the standard error of $\beta_1(t)$.

Let $L(l_1) = \max\{|L(2)|, |L(3)|, \dots, |L(m)|\}$. The l_1 can be a change-point if the $L(l_1)$ is statistically significant (Chu 2002).

2.2.6 Computing relative influences of climate parameters on PET/P trends

The relative influences of the five climate parameters on the PET/P changes are estimated by applying stepwise regression method to 189 meteorological stations¹⁹. In the regression, annual mean PET/P is derived by annual P, Rn, WS, Ta, and RH as shown in the following equation:

$$\frac{PET}{P} = a_1P + a_2R_n + a_3WS + a_4T_a + a_5RH + b \quad (2.2.9)$$

where a_1 - a_5 are the regression coefficients of the climate parameters and b is the intercept.

The product of the regression coefficient and annual trends of each climate parameters (P, Rn, WS, Ta, and RH) are regarded as the relative influence of the climate parameter on the PET/P trends as follows:

$$\Delta\left(\frac{PET}{P}\right) = a_1\Delta P + a_2\Delta R_n + a_3\Delta WS + a_4\Delta T_a + a_5\Delta RH \quad (2.2.10)$$

where ΔP , ΔR_n , ΔWS , ΔT_a , and ΔRH are the trend slope of annual P,

Rn, WS, Ta, and RH, respectively. $\Delta\left(\frac{PST}{\rho}\right)$ is the computed trend slope based on sum of influences of five climate parameters.

3. Vegetation feedback impact on climate aridity

The change in temperature and precipitation leads to the climate aridity change by modulating regional balance between water deficit or water surplus. As mentioned in section 1, change in vegetation in response to climate change has feedback impact on climate through changes in albedo and ET (Bonan et al. 2008). Future changes in vegetation and its feedback impact on climate aridity is examined in this section using CAM-DGVM simulations.

3.1 Models

The global climate model (GCM) used in this study is the National Center for Atmospheric Research (NCAR) Community Atmospheric Model version 3 (CAM3) configured with a T42 horizontal resolution and 26 hybrid-sigma vertical layers. Climate Land Model version 3 (CLM3) is used for Land Surface Model to calculate land surface processes. CLM3 contains the dynamic global vegetation model (DGVM), a modified version of the Lund-Potsdam-Jena (LPJ) DGVM (Levis et al. 2004), to compute vegetation dynamics as a function of climate variables. The CLM-DGVM and CAM3-DGVM models have been widely used in many previous climate studies (e.g., Bonan and Levis 2006).

3.1.1 CAM3

The CAM3 is the fifth version of atmospheric general circulation model (AGCM) developed by the National Center for Atmospheric Research (NCAR). The standard NCAR CAM3 is described in *Collins et al.* (2004).

The CAM3 can be run either as an independent AGCM or as a component of the Community Climate System Model version 3 (CCSM3; *Collins et al.* 2006). As a stand-alone AGCM, CAM3 is integrated together with the Community Land Model (CLM; *Bonan et al.* 2002), a thermodynamic sea ice model, and a data ocean or optional slab ocean model. CAM3 includes Eulerian spectral and semi-Lagrangian and finite volume (FV) dynamical core. This dynamical core is perfectly separated from the physical part and can be coupled to the physics in a time-split or process-split approximation (Williamson 2002). Parameters are configured for the Eulerian dynamical core at T31, T42, and T85 spectral truncation and for FV core at $2^\circ \times 2.5^\circ$ horizontal resolution. Zonal resolutions of the Eulerian truncations are from 3.87° for the T31 configuration to 1.41° for the T85 configuration.

The code, documentation, input datasets, and model simulations for CAM3 are freely available from the CAM Web site (www.cesm.ucar.edu/models/atm-cam).

3.1.2 CLM3

The CLM3 has significantly improved over its earlier versions as a result of algorithmic improvements, better input from its parent atmosphere, and use of a higher spatial resolution by its parent model. In the CLM3, land region comprises 3799 gridcells, each of which can have a difference number of landunits as subgrid representation. The landunit includes physically distinct surface types (glacier, lake, wetland, urban, vegetation areas). To capture variability in the soil and snow state variables within a single landunit, the landunit is divided into 10 soil columns and 5 snow columns. As final subgrid, the vegetated subgrid is composed of up to 4 different plant functional types (PFTs) from a total 15 types. In the CLM3, ecological and physical characteristics of vegetation is either prescribed by satellite-derived values or interactively calculated by DGVM.

3.1.3 DGVM

The DGVM were introduced as a practical and ecologically realistic means of simulation vegetation changes in global climate models (Sitch et al. 2003, Bonan et al. 2003). DGVMs coupled to climate models have been used to

simulate vegetation for past, present, and future climates to assess the interactions among climate, CO₂, and vegetation (Levis et al. 2004; Cowling et al. 2009). In this study, we used the CLM-DGVM, which is a modified version from the LPJ DGVM (Levis et al. 2004) to the CLM following the IBIS approach (Foley et al. 1996). The CLM-DGVM consists of CLM3 plus a set of routines that allow vegetation cover and structure to be simulated instead of prescribed from data. The model represents spatial heterogeneity in land cover by dividing each grid cell into four land cover types: glacier, lake, wetland, and vegetation (Bonan et al., 2002). The vegetated portion of the grid cell is further divided into several patches of plant functional types (PFTs). The PFTs consist of 10 different types depending on the climate of grid cell. Two tropical trees, three temperate trees, and two boreal trees are differentiated by bioclimatology, leaf form (broadleaf, needleleaf), phenology (evergreen, summergreen, raingreen), physiology, and response to disturbance. Three grasses are distinguished by bioclimatology and photosynthetic pathway (C3, C4). The plant functional types are similar to those used in versions of LPJ and are a subset of those used in LSM.

The vegetation dynamics of LPJ can be readily incorporated into CLM. LPJ couples fast hydrological and physiological processes with slower ecosystem processes using time-scales of daily (soil water, soil temperature, snow canopy

physiology, phenology), monthly (soil microbial processes), and yearly (vegetation dynamics). In coupling CLM and LPJ, we omitted fast LPJ processes already present in CLM, altered LPJ algorithms to meet the requirements of a climate model, and scaled LPJ's daily and monthly respiration to fit CLM's 20 min coupling with the atmosphere. We retained LPJ's daily time step for leaf phenology and LPJ's annual time step for changes in community composition and ecosystem structure.

3.2 Experimental design

Using the CAM3-DGVM model, three sets of model experiments have been performed. The first one is under the present-day CO₂ concentration ($1 \times \text{CO}_2 = 355$ ppmv, parts per million in volume) with monthly vegetation specified from the climatological mean vegetation state (CMVS) defined below for the simulation period (hereafter VegOff_1×). The other two experiments are under $2 \times \text{CO}_2$ (=710 ppmv) conditions with interactive vegetation feedback (hereafter VegOn_2×) and specified monthly vegetation from CMVS (hereafter VegOff_2×), that is active and inactive DGVM for VegOn_2× and VegOff_2×, respectively. Prior to all model integrations, the CAM3-DGVM model was spun

up for 500 years to obtain the potential vegetation under the present-day climate. Starting from the bare ground, the CAM3-DGVM vegetation achieved an equilibrium climate-vegetation state after about 400 years. CMVS that is defined as the mean state over the last 30 years of the 500-year spin up run is used as the initial or perpetual vegetation fields for all three experiments above. Table 3.1 provides that summary these three experiments.

Each experiment consists of five ensemble members with varying atmospheric initial conditions randomly selected in the last 5 years of the 500-year spin-up run. To include the impacts of the CO₂ increase on oceanic state, sea surface temperatures (SSTs) and sea ice covers (SICs) derived from the 1990 control run and the 2 × CO₂ run of Community Climate System Model version 3 (CCSM3; Collins et al. 2006) are prescribed in the present-day and 2 × CO₂ simulations. Thus the feedback between vegetation effects and oceanic circulation is not included in this experiment. From the three sets of ensemble simulations, we separate the effect of elevated CO₂ from the vegetation feedback as follows: VegOff_2× minus VegOff_1× indicates the effect of elevated CO₂ only, defined as the radiative effect; VegOn_2× minus VegOff_1× includes both the radiative and the vegetation feedback effect; VegOn_2× minus VegOff_2×

isolates the vegetation feedback only. More detailed descriptions on these experiments are documented in *Jeong et al. (2011a)*.

Table 3.1. Equilibrium experiments using CAM3-DGVM. Identifiers for each simulation, sea surface temperature (SST), atmospheric CO₂ concentrations (CO₂), integration time (Years), number of ensemble (Ensembles), and model horizontal resolution (Resolution).

	Identifier	SST	CO₂	Vegetation	Years	Ensembles	Resolution
Spin-up	Spin-up	Present climatology	Present climatology	Dynamic	500	1	T42
Equilibrium	VegOff_1×	CCSM Present	335 ppmv	Fixed	100	5	T42
	VegOff_2×	CCSM CO ₂ doubling	710 ppmv	Fixed	100	5	T42
	VegOn_2×	CCSM CO ₂ doubling	710 ppmv	Dynamic	100	5	T42

3.3 Changes in climate types

Climate types over the contiguous US region is classified in terms of I_m vary in a wide range from -60 to infinity (Table 2.4). Note that aridity increases as I_m decreases (Thornthwaite 1948). Figure 3.1 presents the climate types determined on the basis of I_m calculated using climatology for the last 30 years of present-day CO₂ concentration run (i.e., VegOff_1×). It also shows climatology from the 0.5° Climate Prediction Center's (CPC) monthly analysis of global surface air temperature and land precipitation for a 30-year period (1980–2009) (Chen et al. 2002; Fan and van den Dool 2008). The climate types computed with the CPC data shows that three climate types dominate most of the contiguous US region: the arid type to the west of the Rocky Mountains, the semiarid type over the western Great Plains and Rocky Mountain States, and dry subhumid type over the eastern Great Plains and East Coast (Fig. 3.1b). The VegOff_1× run reproduces well the arid climate found to the west of the Rocky Mountains and the dry subhumid type found over the eastern Great Plains and East Coast (Fig. 3.1a). The relatively wetter climates in the eastern half and drier climates in the western half of the contiguous US region also agree with previous observation-based studies (Thornthwaite 1948; Feddema 2005a). The most notable model errors are the wet biases over the Rocky Mountains and the western Great Plains,

especially Colorado, Nebraska, and Kansas (Fig. 3.1a). This wet bias is also evident in previous modeling studies using CAM3 (e.g., Meehl et al. 2006, Feng et al. 2008). Overall, the simulated present-day regional climate types are largely consistent with the observation-based climate type.

Figure 3.2 shows the changes in I_m and the subsequent climate types over the US by; (a) the radiative effect due to doubling of CO₂ concentration only (VegOff_2× minus VegOff_1×), (b) the combination of the radiative and vegetation-feedback effects (VegOn_2× minus VegOff_1×), and (c) vegetation-feedback effects only (VegOn_2× minus VegOff_2×). Blue (red) dots indicate that the regions shift to a more humid (arid) climate type due to the increase in CO₂ and/or vegetation feedback. In the 2 × CO₂ climate, I_m decreases by the radiative effect suggesting increases in aridity in most (> 75%) of the contiguous US region, (Fig. 3.2a). The most noticeable decrease in I_m appears in Texas, Arkansas, and Louisiana. By contrast, a notable increase in I_m appears in the northern part of the Mountainous regions, especially around Wyoming. The changes in I_m and subsequently the climate types, induced by the radiative effect are generally consistent with the previous studies of Meehl et al. (2007) and Christensen et al. (2007).

Vegetation feedback appears to strongly modify the changes in I_m calculated in the radiative effects only case (Fig. 3.2b). The most noticeable features are the increase in I_m (i.e., decreased aridity) over the Midwest, the East South Central division, and the Northwest. The impacts of vegetation feedback on I_m and subsequent climate types are clearly shown in Fig. 3.2c. Positive I_m anomalies occur in over 75% of the contiguous US region. Due to the large increase in I_m in these regions, climate types in Montana, Wyoming, South Dakota, Illinois, and northern Texas become more humid. In particular, significant drying in the northern Texas region due to the radiative effect (Fig. 3.2a) is reversed into a wetter type due to the inclusion of vegetation feedback (Fig. 3.2c). On the other hand, only small changes in I_m are found over the Northeast and Southwest. I_m even decreases due to vegetation feedback over the southeastern US. Despite those regional differences, Fig. 3.2 shows that the increase in aridity by the radiative effects is generally suppressed by vegetation feedback. The mechanisms by which vegetation feedback alleviates the increasing aridity by the radiative effects are investigated in the next two sections.

Present Climate Type

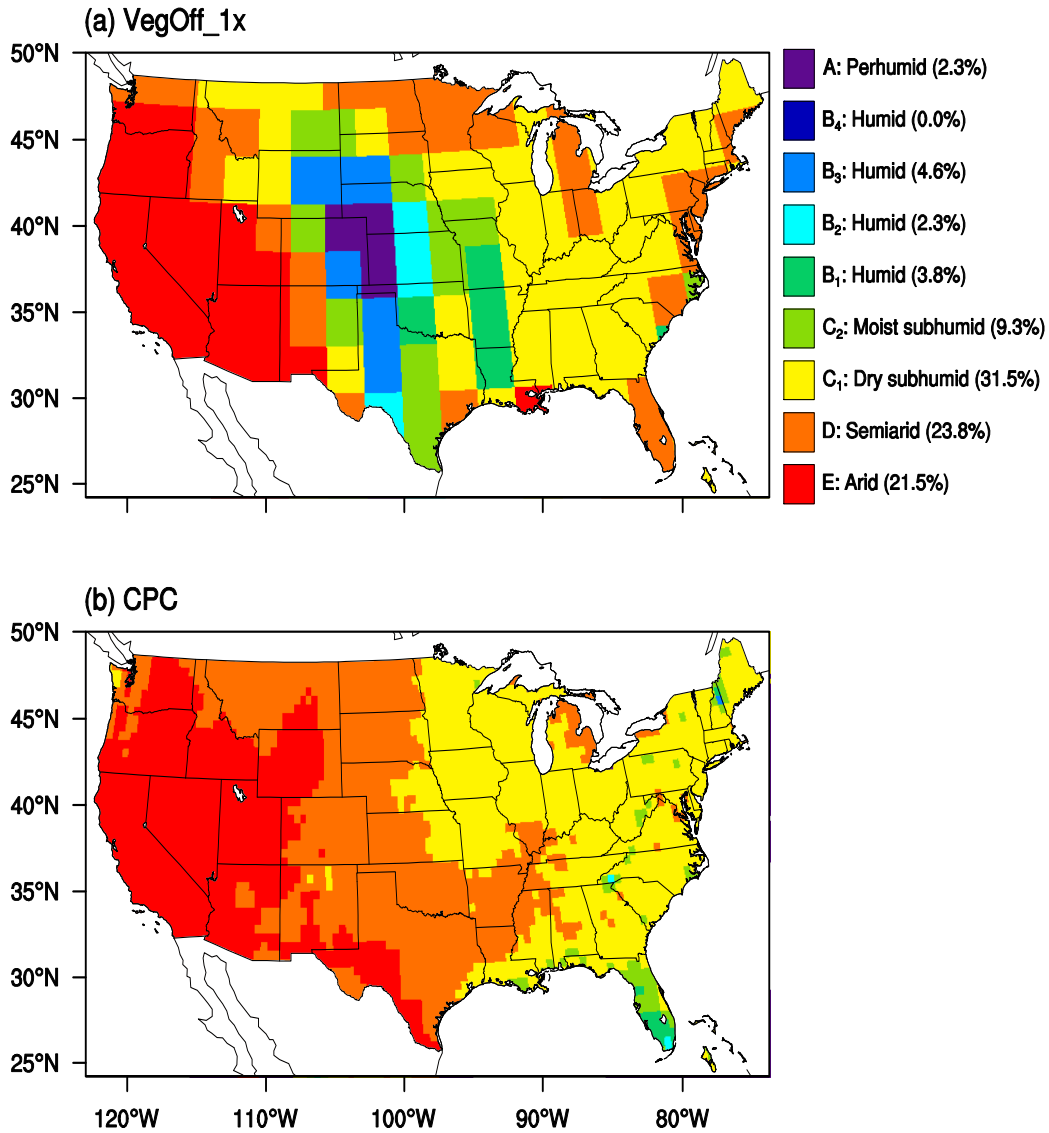


Figure 3.1. Spatial distribution of Thornthwaite moisture index over the US in boreal summer for VegOff_1x (a), and 30-year climatology of CPC monthly analysis of global surface air temperature and land precipitation for the period 1980–2009 (b).

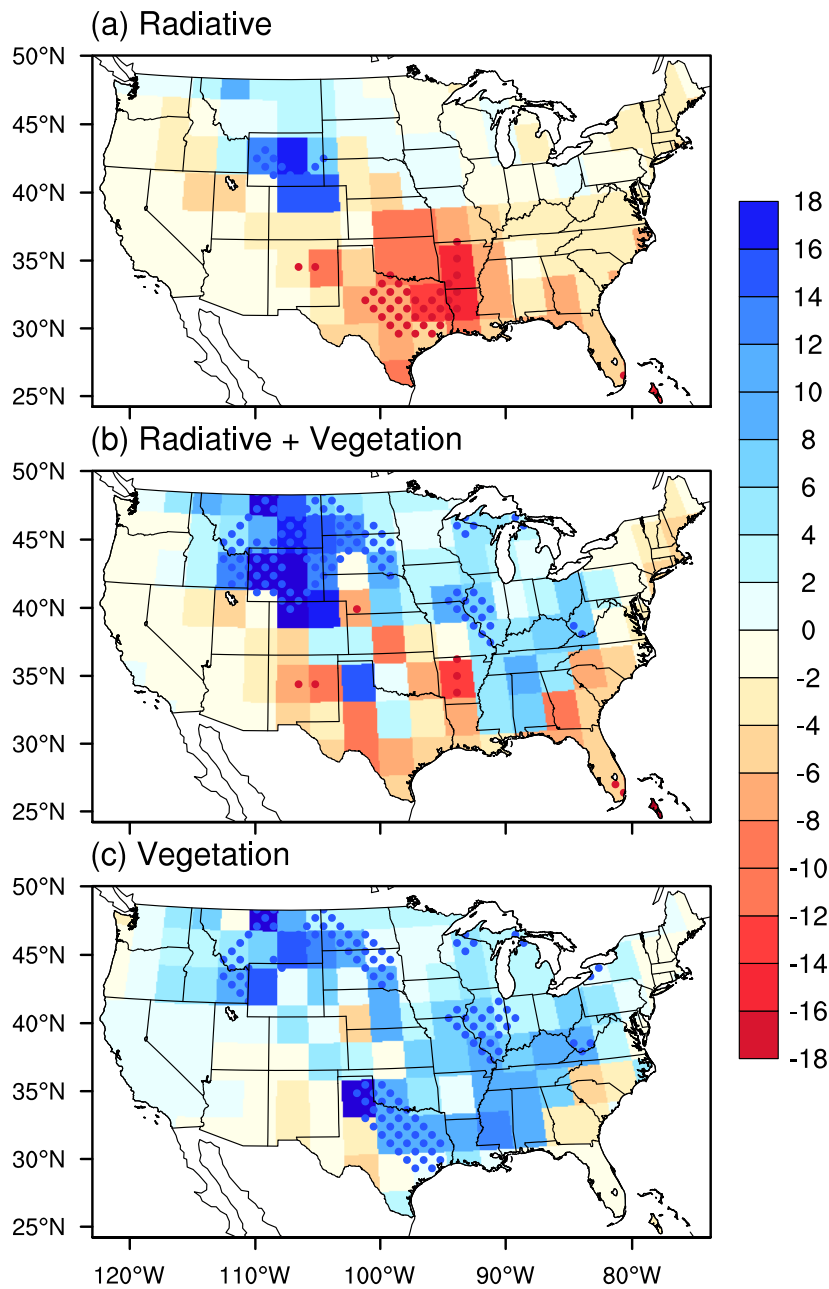


Figure 3.2. Spatial distribution of changes in Thornthwaite moisture index by radiative effect (a), radiative and vegetation feedback effect (b), and vegetation feedback only (c). Blue dots and red dots represent regions that the climate type change more humid and arid, respectively.

3.4 Changes in LAI and surface evapotranspiration

Vegetation feedback in climate model occurs mostly through the changes in PFTs or LAI or both (Bonan et al. 2003; Jeong et al. 2011a). These two variables combined represent vegetation “greenness”. There are two types of vegetation feedback through changes in vegetation greenness (combined effects of PFTs and LAI): 1) vegetation–albedo feedback acting to alter land surface albedo and hence the amount of shortwave absorption, and 2) vegetation–evaporation feedback resulted from changes in ET. Changes in PFTs are minimal in the analysis region, suggesting it plays only a minor role in affecting I_m . A previous study (Jeong et al. 2010) suggested that the impact of vegetation–evaporation feedback through the increase in LAI dominates in the mid-latitude regions, especially Europe and North America. Thus we will focus on the effects through LAI in the following.

Figure 3.3 shows the LAI simulated with the present-day CO₂ concentration and the changes in LAI due to increasing CO₂ concentration. In the present-day climate condition, large LAI values occur in the East Coast region, southern US, western Great Plains, and the Pacific Northwest coastal regions (Fig. 3.3a). Small LAI values can be found in the arid southwestern US region. These spatial distributions and magnitudes of the present-day LAI are generally consistent

with satellite observations, except the unrealistically large values over parts of the southern Great Plains region (approximately 30-40°N, 97-105°W) (Bonan et al. 2003). With $2 \times \text{CO}_2$ concentration, the simulated LAI values increase significantly in most of the contiguous US region (Fig. 3.3b). The greening may be explained by enhanced vegetation productivity and water-use efficiency in the warmer climate under the higher CO_2 concentration (Levis et al. 2000; Jeong et al. 2011a). Noticeable greening is also observed over the Midwest, East South Central division, and northern part of Mountain division. These regions are mostly classified as dry subhumid climate types in the present climate (see Fig. 3.3a). In addition, these greening regions are similar to regions where an increase in I_m is shown on Fig. 3.2c. The consistent increases in I_m and LAI indicate that the enhanced vegetation growth is a key factor in reducing aridity in the VegOn_2× simulation.

Changes in LAI can significantly modulate the magnitude and composition of surface ET, thereby alter the surface water cycle and energy budget (Jeong et al. 2011a). Figure 3.4 illustrates the spatial distribution of the projected changes in the total evaporation, canopy evaporation, canopy transpiration, and bare-soil evaporation by the radiative effect only (Figs. 3.4a–3.4d), the combined radiative and vegetation-feedback effects (Figs. 3.4e–3.4h), and the vegetation-feedback effect only (Figs. 3.4i–3.4l). The total evaporation increases over most of the

contiguous US due to the CO₂-induced radiative effect by as much as 15 mm month⁻¹. The increase in total evaporation is likely to be caused by increased atmospheric water-holding capacity due to CO₂-induced warming (Hegerl et al. 2007). Spatial distribution of the changes in canopy evaporation, canopy transpiration, and bare-soil evaporation are similar to the changes in the total evaporation (Figs. 3.4b–3.4d) indicating evaporation from soil and vegetation responds to the radiative effects in a similar way.

With the inclusion of vegetation feedback (VegOn_2× minus VegOff_1×), the total evaporation increases further (Fig. 3.4e). The increase in evapotranspiration and the decrease in bare-soil evaporation appear clearly over the Midwest, South, and Northwest (Figs. 3.4f–3.4h) where LAI increases significantly (see Fig. 3.3b), especially in western Montana where the canopy and soil evaporation changes by as much as 50 mm month⁻¹. The vegetation-feedback effect increases the total evaporation by as much as 15 mm month⁻¹ in the Midwest, Northwest, and the East South Central division (Figs. 3.4i–3.4l). In addition, significant increase in the total evaporation appears in Idaho, Montana, North Dakota, Tennessee, Mississippi, and Alabama because the sum of the increase in the canopy evaporation and canopy transpiration is larger than the decrease in the bare-soil evaporation.

JJA Leaf Area Index

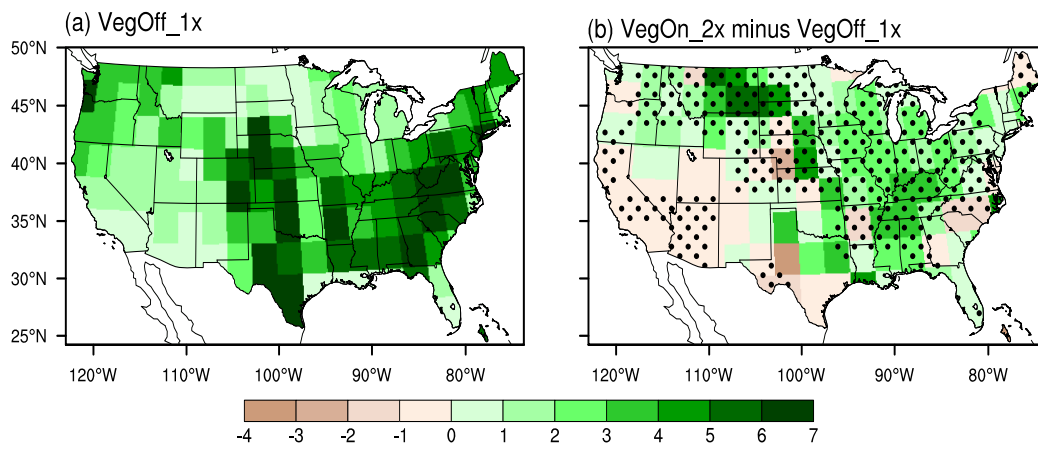


Figure 3.3. Spatial distribution of leaf area index over the US in boreal summer for VegOff_1x (left) and changes in leaf area index between VegOn_2x and VegOff_1x (right). Black dots represent the regions that changes in leaf area are statistically significant at the 95% confidence level.

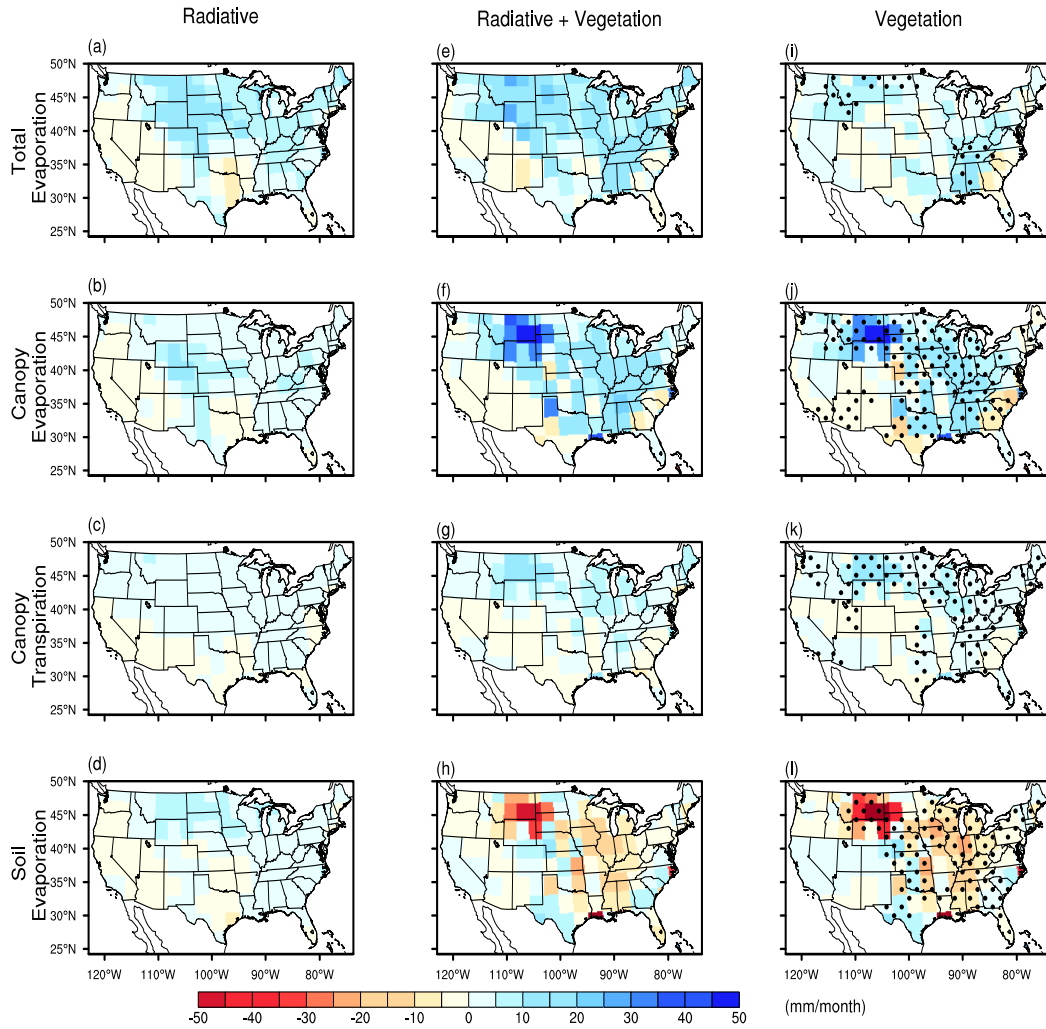


Figure 3.4. Spatial distribution of changes in total evaporation, canopy evaporation, canopy transpiration, and soil evaporation due to radiative effect (a–d), radiative and vegetation feedback effect (e–h), and vegetation feedback only (i–l). Black dots represent the regions that changes are statistically significant at the 95% confidence level.

3.5 Changes in water supply and water demand

In the simulation with active vegetation feedback, LAI is positively correlated with ET over most of the contiguous US region. The CO₂-induced changes in precipitation and surface temperatures are modified by the increase in surface evaporation and evaporative cooling, respectively, through enhanced surface latent heat flux. Those changes indicate that the water supply and demand (precipitation and PET, respectively) are influenced by the increase in evaporation combined with the presence of vegetation feedback. These changes in water supply and demand terms are directly linked with the changes in I_m and subsequent climate types. Figure 3.5 illustrates changes in precipitation, temperature, and PET caused by the radiative effects of the CO₂ increase, the combined radiative and vegetation-feedback effects, and vegetation-feedback effects alone. The radiative effects increase precipitation in the northeastern, midwestern, and some part of southern US regions, and decrease precipitation in the western states except northern Washington, Idaho, and the West South Central division (Fig. 3.5a). These changes in precipitation are consistent with projections made by the climate models included in the IPCC fourth assessment report, at least qualitatively (Karl et al., 2009). With active vegetation feedback, precipitation increases in most contiguous US regions except the southwestern inland region including the Nevada, Arizona, western New Mexico, and

southwestern Utah (Fig. 3.5d) with largest precipitation increases of up to 30 mm month⁻¹ in the Rocky Mountains region (Montana, Wyoming, and Colorado). The results from vegetation feedback only clearly show that this factor increases precipitation (Fig. 3.5g) especially in Idaho, Alabama, Georgia, Tennessee, and Kentucky. Further analysis shows that vegetation feedback increases convective precipitation but slightly reduces large-scale precipitation (not shown) suggesting that the positive feedback between the changes in local precipitation and LAI is mainly through the increase in local convection caused by enhanced ET rather than changes in the large scale circulation.

Spatial distributions of the surface temperature changes due to radiative effects are shown in Fig. 3.5b. In most of the contiguous US, the warming exceeds 2 K, except in regions along the Gulf of Mexico. The CO₂-induced warming is substantially reduced in the Midwest, East South Central division, and northern part of Mountain division when both radiative and vegetation-feedback effects are included (Fig. 3.5e). Vegetation feedback (Fig. 3.5h) alleviates surface warming caused by radiative effects by as much as 2 K over 80% of the total analysis area. Significant cooling effects were observed in wide regions over the Midwest, Northwest, and East South Central division via the enhancement of surface latent heat fluxes by the increase in ET and the decrease in solar radiation resulting from increased cloud cover (Jeong et al. 2011a).

According to the definition used in this study (Thornthwaite 1948), PET is directly influenced by the changes in surface temperatures. Figure 3.5c shows the PET changes due to CO₂-induced surface warming. In general, the increase in PET is largely shown occurring over the southern part of the US, including the South and Southwest whereas a relatively small increase occurs in the Northwest. Due to additional evaporative cooling induced by vegetation feedback, the increment in PET is largely suppressed over the analysis domain (Fig. 3.5f). In particular, strong negative anomalies of PET occur over the eastern US (Fig. 3.5i). Compared to the changes in surface temperatures, changes in PET are generally concentrated in the southern US region, probably because there are nonlinear empirical relationships between surface temperature and PET (Thornthwaite 1948).

Changes in water supply (precipitation) and demand (PET) lead to changes in I_m as inferred from Eqs. 2.2.1 and 2.2.2. The radiative effect increases aridity in most of the contiguous US through the increase in D (water deficit in Eq. 2.2.1) or the decrease in S (water surplus in Eq. 2.2.2) because PET increases are larger than precipitation increases. The increase in aridity is particularly strong in the southwestern US and the West South Central division, where PET increases and precipitation decreases. In the northern part of Mountain division, on the contrary, a large increase in precipitation leads to an increase in S , resulting in

increased I_m . When vegetation feedback is introduced, the changes in water balance induced by the radiative effect are greatly modified. Increases in precipitation and weakened PET increases lead to the decrease in aridity over the Midwest, East South Central division, and the northern part of Mountain division. When the impact of the radiative effect is removed, a decrease in aridity induced by vegetation feedback is clearly shown through enhanced precipitation and reduced PET over most of the contiguous US.

Overall, the changes in atmospheric water supply and demand are consistent with the changes in I_m and the subsequent climate type shown in Fig. 3.6. Decreases (increases) in I_m corresponding to the increase (decrease) in climate aridity occur in the regions where the increase in water demand exceeds the increase in water supply. In addition, changes in climate type appear in regions with notably large changes in both water supply and demand. These changes in water supply and demand, and I_m levels resulting from the radiative effect and vegetation feedback are summarized in Fig. 3.6. The vertical axis indicates I_m in the present-day climate run (VegOff_1×) and the horizontal axis indicates the ratio of precipitation (water supply) and PET (water demand) that is clearly proportional to I_m . The black dots depict the P/PET ratio in the present-day climate simulation. Orange cross markers and green open circles indicate the changes in the P/PET ratio when the radiative effect alone and

radiative/vegetation feedback effects are included, respectively. In general, orange cross markers appear to the left of black dots implying decreases in the P/PET ratio and a shift to a drier climate than the present-day climate. Green open circles, on the contrary, are generally located to the right of black dots implying an increase in the P/PET ratio. This clearly shows that vegetation feedback leads to a more humid climate in the CO₂ doubling condition compared to the radiation effects only case. Additionally, noticeable changes in the P/PET ratio, denoted by the orange cross markers and green open circles, are mainly observed in the subhumid climate type ($-20 < I_m < 20$) represented by the two dashed lines in Fig. 6. Because the subhumid climate type occurs in a large portion (> 40%) of the US, our results would suggest that vegetation feedback could have a considerable influence over changes in aridity induced by the increase in atmospheric CO₂ concentration.

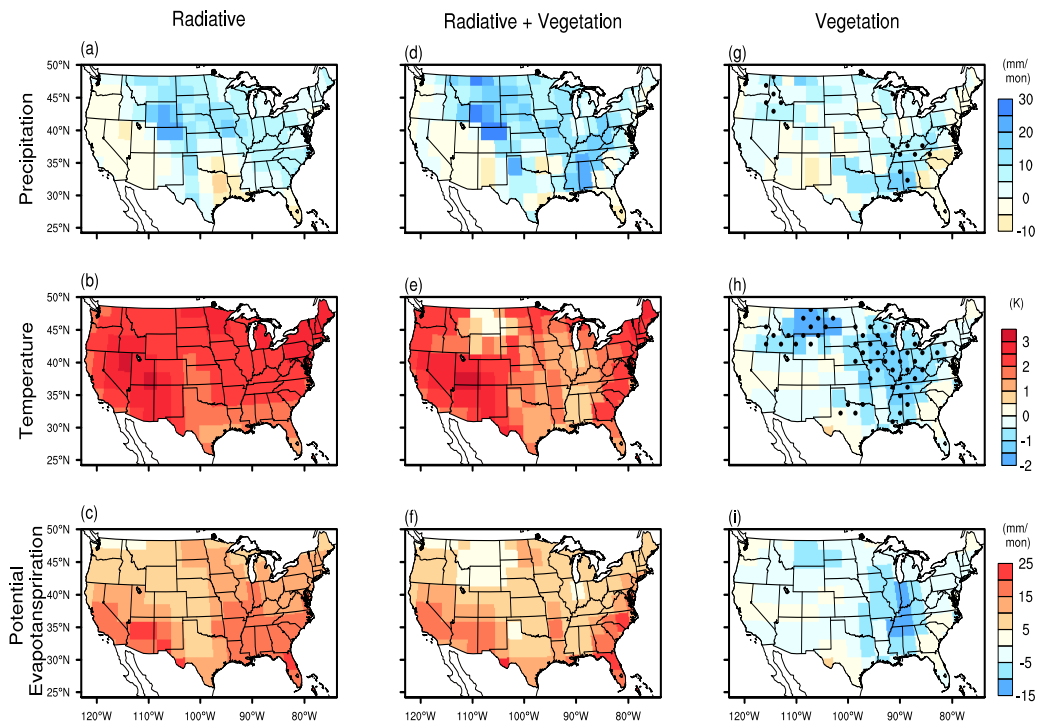


Figure 3.5. Spatial distribution of changes in precipitation, temperature, and PET over the US due to radiative effect (a–c), radiative and vegetation feedback effect (d–f), and vegetation feedback only (g–i). Black dots represent the regions that changes are statistically significant at the 95% confidence level.

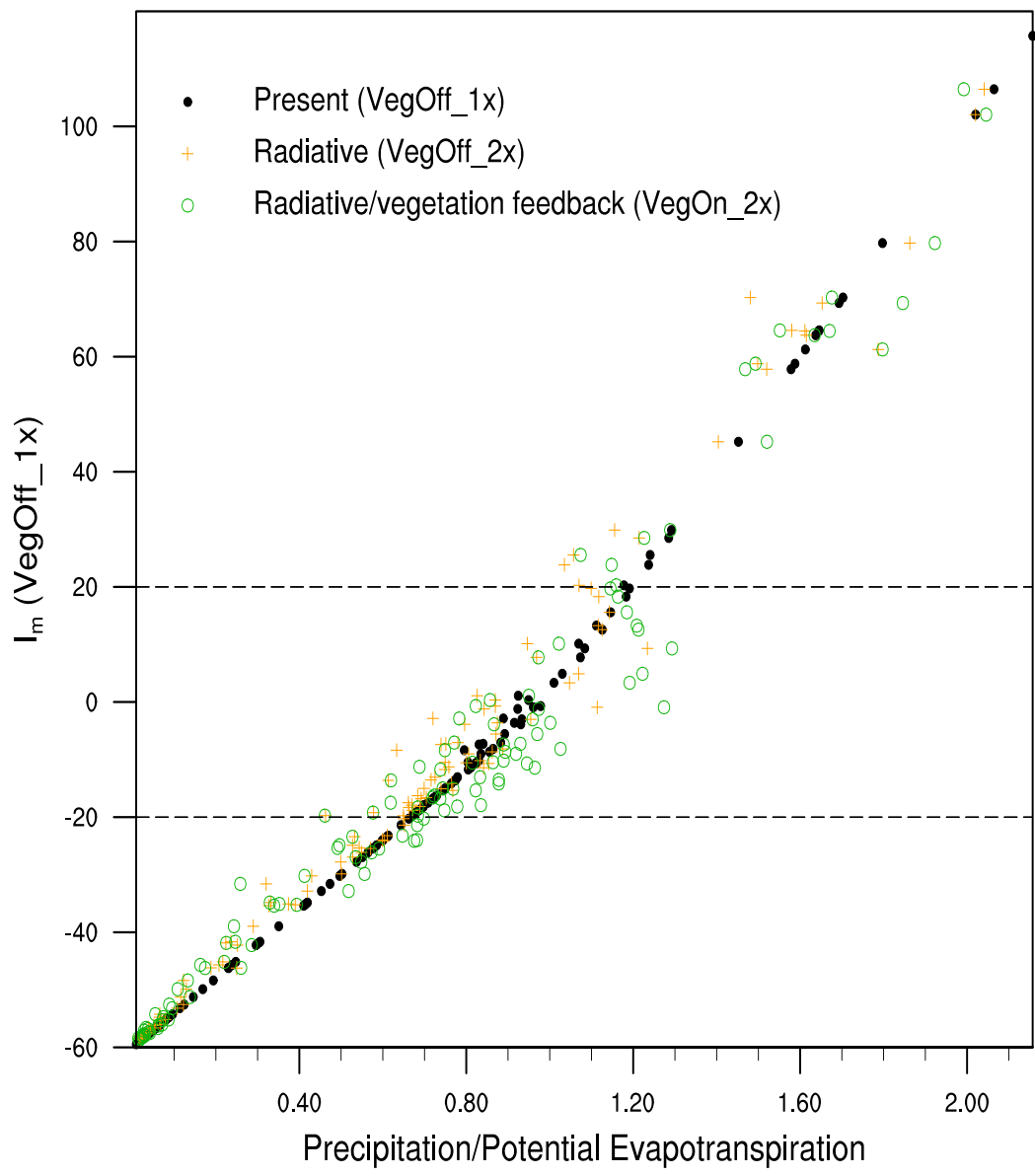


Figure 3.6. Scatter plot of the values of I_m in present climate run (VegOff_1x) with respect to ratio of precipitation to PET. Black, blue, and red dots represent the ratio of VegOff_1x, VegOff_2x, and VegOn_2x, respectively.

3.6 Summary and Discussion

3.6.1 Comparison of impact of change in ET with change in vegetation physiology and soil moisture

As examined in earlier studies (Notaro et al. 2006; Sitch et al 2008; Jeong et al. 2010), the coupled GCM experiments are focused on the combined impact of CO₂ doubling and the associated structural changes in vegetation such as PFTs and LAI. The results show that the increase in LAI, which is contributed by combined effect of direct CO₂ fertilization and indirect climatic warming, is notable structural change and main reason for vegetation feedback effect. But the impact of warming and CO₂ fertilization cannot be separately measured because of our experimental design. The relative contribution between direct CO₂ fertilization and indirect CO₂ induced climatic warming on LAI increases depends on region and climatic conditions. For instance, *Piao et al. (2006)* showed increase in LAI in moisture limited region is mostly explained by CO₂ fertilization over the regions where exhibited sufficient soil moisture. In contrast, increase in LAI in boreal region dominantly explained by temperature increases rather than CO₂ fertilization (Levis et al. 2000, Jeong et al 2011a).

The physiological responses of vegetation to carbon dioxide also cannot be isolated by the CAM3-DGVM model. Under increased CO₂ condition,

physiological effects may enhance the CO₂ induced warming and increase the surface runoff through suppression of plant stomata and transpiration (Seller et al. 1996; Betts et al. 2007; Cao et al. 2010). When structural changes in vegetation exist, however, the changes in surface albedo and ET are the two main mechanisms involved in vegetation feedback with the surface climate (Betts et al. 1997; Notaro et al 2007; Bonan 2008). For example, positive feedback between vegetation cover and surface temperature has been observed in the northern US during spring (March–May) via negative anomalies in surface albedo (Notaro et al. 2006). Potentially, replacing mixed crop land and urban built-up areas with vegetation could cause strong cooling in the Great Plains and the Midwest by increasing evaporation and surface albedo, respectively (Diffenbaugh 2009). Additionally, as a response to increasing GHGs, negative anomalies in surface albedo can induce positive anomalies in surface temperature and extreme warm events in the western US (Diffenbaugh 2005a, and b). Further, increase in vegetation greenness brings dominant vegetation–evaporative cooling over mid-latitudes and warming over high latitudes through a decrease in surface albedo (Jeong et al. 2010).

Soil moisture is another key variable in land-atmosphere interaction and climate aridity (Manabe et al. 2004; Seneviratne et al. 2010), further vegetation feedback (Hoffman and Jackson 2000; Kim and Wang 2007; Mendez-barroso et

al. 2009). Following the method used to calculate I_m , the impact of soil moisture on climate aridity may be ignored in our analysis. However, changes in I_m are connected with soil moisture through precipitation and temperature. Increase in precipitation naturally induces higher soil moisture except few cases (Seneviratne et al. 2010). Surface cooling, which leads to reduction of PET and increase in I_m , also produces higher soil moisture through negative correlation between temperature and soil moisture (Koster et al. 2006; Seneviratne et al. 2006). Additional analysis shows that changes in soil moisture due to radiative and vegetation-feedback-effects are consistent with the changes in precipitation and temperature in the eastern US, but inconsistent in western US (Fig. 3.7).

Volumetric Soil Water

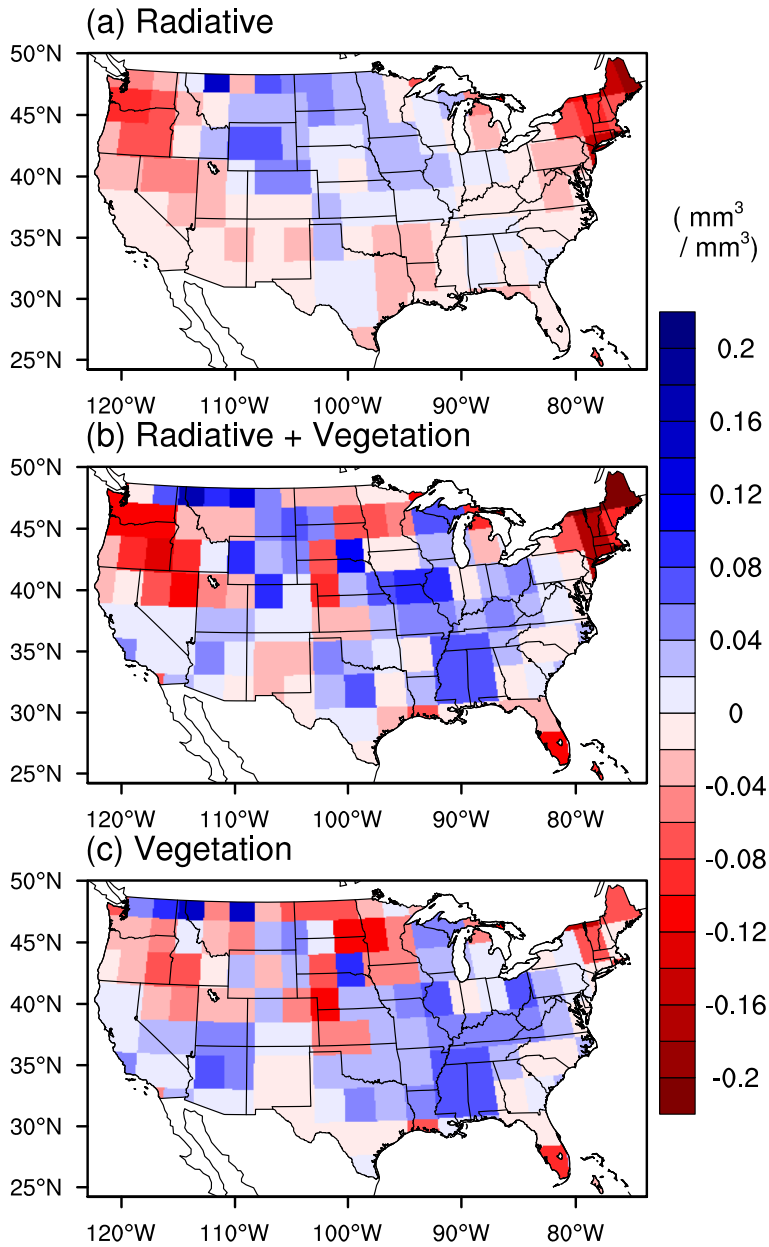


Figure 3.7. Spatial distribution of changes in vertically integrated volumetric soil water due to radiative effect (a), radiative and vegetation feedback effect (b), and vegetation feedback only (c).

3.6.2 Importance of vegetation feedback and limitation of potential vegetation and I_m

If the vegetation feedback is not considered, previous climate model projections with increasing GHGs suggested that increasing aridity may elevate natural disaster and social problems linked with water availability. For example, increasing aridity leads to longer periods of drought (Wang 2005; Sheffield and Wood 2008), greater water demands for irrigation (Edmonds and Rosenberg 2005), more difficult water management (Kundzewicz et al. 2007; Yohe et al. 2007), and difficulties in energy production resulting from limited water supplies (Filed et al. 2007; Hightower and Pierce 2008). *Bonan* (2008) and *Jackson et al.* (2008) reported that vegetation feedback is important to mitigate the impact of climate change and reduce the social and economic costs required to manage those problems. A key result of the present study points to decreases in summer dryness through vegetation feedback, providing additional evidence that vegetation can alleviate climate change. Further, vegetation feedback exerts favorable influences on subhumid climate types that are vulnerable to climate change. Thus, the impact of vegetation feedback is an important component for projection and mitigation of climate change, especially for climate hot spots.

In this thesis, the I_m and related climate types is used to visualize and interpret the impact of radiative and vegetation feedback on climate aridity

because of I_m is known for a reliable index for water balance (Feddema 2005a). The key advantage of I_m is that it is simple, being only defined by monthly temperature and precipitation. Thus, the results are easy to interpret and understand. Though the advantage, formulation of I_m has two limitations. One is the empirical algorithm used to estimate the monthly PET (Thornthwaite 1948). The simple formula used merely monthly air temperature to estimate PET may cause some bias because the effects of wind speed, humidity, and net radiation are not included in the calculation of PET (Allen et al., 1998). This bias, however, has little impact on our result because of diverse validation tests showed that the PET estimated by Thornthwaite method is comparable to PETs calculated from various complex methods in the US (Hulme et al. (1992); Mintz and Walker (1993)).

In the present study, we only focused on potential vegetation which is only modulated by climate, but anthropogenic land cover change can also influence changes in climate regime. Previous studies reported (Zhao and Pitman 2002; Feddema et al. 2005b) that changes in land use/cover, such as for agriculture and urbanization, can potentially influence regional climate over developed regions. Though CAM3-DGVM simulates reliable low-level circulation and spatial distribution of precipitation, in addition, the T42 horizontal resolution may be too coarse to represent complex local topography, particularly over the western

US (Diffenbaugh et al. 2005b). The impact of local topography on regional circulation cannot be well simulated by this coarse spatial resolution model, which likely explains the wet biases in Rocky Mountains and western Great Plains regions (Meehl et al. 2006). Despite these limitations, the CAM3-DGVM has been widely and successfully used to evaluate the impact of land use change and vegetation feedback on North America (Oleson et al. 2004). In addition, positive temperature anomalies in the western US obtained in our simulations are consistent with those obtained by RCM simulation with fine spatial resolution (Diffenbaugh 2005b). Therefore, the CAM3-DGVM model used in this study is sufficient, though certainly not perfect, for estimating the potential impact of vegetation feedback on broader scale summer aridity across the US.

4. Understanding of present and future changes in vegetation

4.1 Temperature and precipitation in present and future climate

Figure 4.1 shows that the 20C3M runs reasonably simulate the present-day (1980-1999) climatology of temperature and precipitation depicted by CRU with the Pearson correlation coefficients of spatial patterns of 0.99 and 0.95 for the temperature and precipitation, respectively. The differences in the global means are also small: 0.44°C for temperature and $-1.83 \text{ mm mon}^{-1}$ for precipitation, respectively (Table 4.1). Also the regional mean of the simulated temperature and precipitation is similar to CRU for each continent (Table 4.1). Figure 4.2 shows the temperature and precipitation changes for the low, medium, and high warming groups in the period 2080–2099. For all these groups, surface temperature increases for all of land surfaces (Figs. 4.2a, 4.2b, and 4.2c) with the global-mean changes of 2.10°C , 3.01°C , and 4.10°C in the low, medium, and high warming groups, respectively (Table 4.2). For each continent, the increase in surface temperatures is proportional to the amount of global warming (Table 4.2). Precipitation changes are generally positive but precipitation changes are small or negative for the central Asia, Mediterranean, southern Africa, and

central America regions (Figs. 4.2d, 4.2e, and 4.2f). The global-mean precipitation increases by 3.45, 4.76, 4.35 mm mon⁻¹ in the low, medium, and high warming groups, respectively (Table 4.2). In contrast to the temperature change, the continental change in precipitation is largest in the medium warming group except for North America and Asia (Table 4.2) due to large decrease in precipitation on South America, southern Africa, and Mediterranean in the high warming group (Fig. 4.2f).

Table 4.1. Annual mean temperature and precipitation (\pm standard deviation) of CRU and 20C3M simulations for present-day.

Continent	Temperature ($^{\circ}\text{C}$)		Precipitation (mm mon^{-1})	
	CRU	20C3M	CRU	20C3M
Globe	13.45	13.01 (± 0.09)	68.89	70.72 (± 1.26)
Africa	23.54	23.30 (± 0.06)	48.72	56.59 (± 1.05)
Asia	9.15	8.37 (± 0.11)	53.19	52.71 (± 1.05)
Australia	21.96	21.69 (± 0.07)	44.72	40.63 (± 1.25)
Europe	10.60	10.09 (± 0.10)	52.60	55.84 (± 1.01)
North America	6.01	5.23 (± 0.12)	62.76	65.30 (± 1.20)
South America	21.80	21.81 (± 0.06)	128.69	137.10 (± 2.03)

Table 4.2. Projected changes in annual mean temperature and precipitation (\pm standard deviation) for low, medium, and high warming groups in future (2080-2099).

Continent	Temperature			Precipitation		
	Low	Medium	High	Low	Medium	High
Globe	2.10 (\pm 0.48)	3.01 (\pm 0.50)	4.10 (\pm 0.57)	3.45 (\pm 5.15)	4.76 (\pm 7.17)	4.34 (\pm 8.91)
Africa	2.02 (\pm 0.43)	2.87 (\pm 0.45)	3.82 (\pm 0.45)	1.20 (\pm 4.51)	1.64 (\pm 5.91)	1.04 (\pm 7.19)
Asia	2.25 (\pm 0.52)	3.26 (\pm 0.53)	4.47 (\pm 0.59)	3.82 (\pm 3.76)	5.45 (\pm 4.97)	6.36 (\pm 6.20)
Australia	1.85 (\pm 0.31)	2.58 (\pm 0.43)	3.31 (\pm 0.45)	1.48 (\pm 4.26)	2.31 (\pm 4.74)	2.02 (\pm 7.37)
Europe	2.06 (\pm 0.44)	3.05 (\pm 0.54)	4.00 (\pm 0.60)	1.04 (\pm 3.56)	0.77 (\pm 4.58)	-0.97 (\pm .29)
North America	2.26 (\pm 0.50)	3.19 (\pm 0.55)	4.39 (\pm 0.66)	4.25 (\pm 4.77)	5.18 (\pm 6.06)	5.51 (\pm 7.56)
South America	1.77 (\pm 0.41)	2.55 (\pm 0.42)	3.58 (\pm 0.55)	4.27 (\pm 9.70)	6.08 (\pm 16.20)	1.19 (\pm 20.19)

Present day (1980-1999) climatology

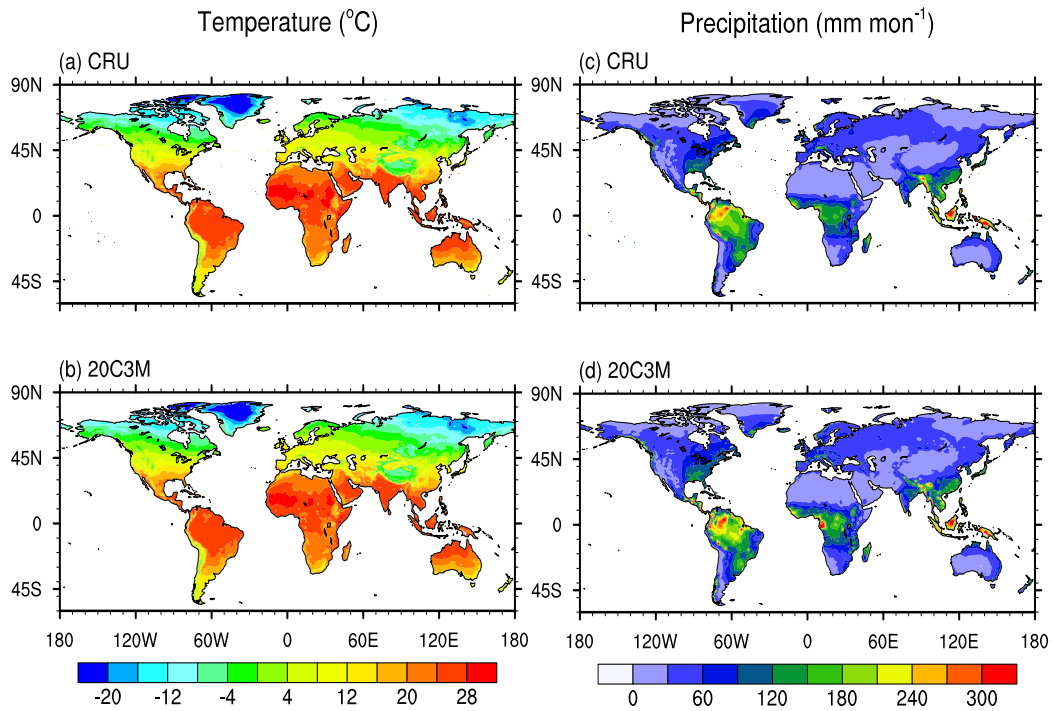


Figure 4.1. Spatial distributions of averaged temperature of (a) CRU and (b) ensemble of 20C3M simulations, and precipitation of (c) CRU and (d) ensemble of 203CM simulations for present-day (1980-2009).

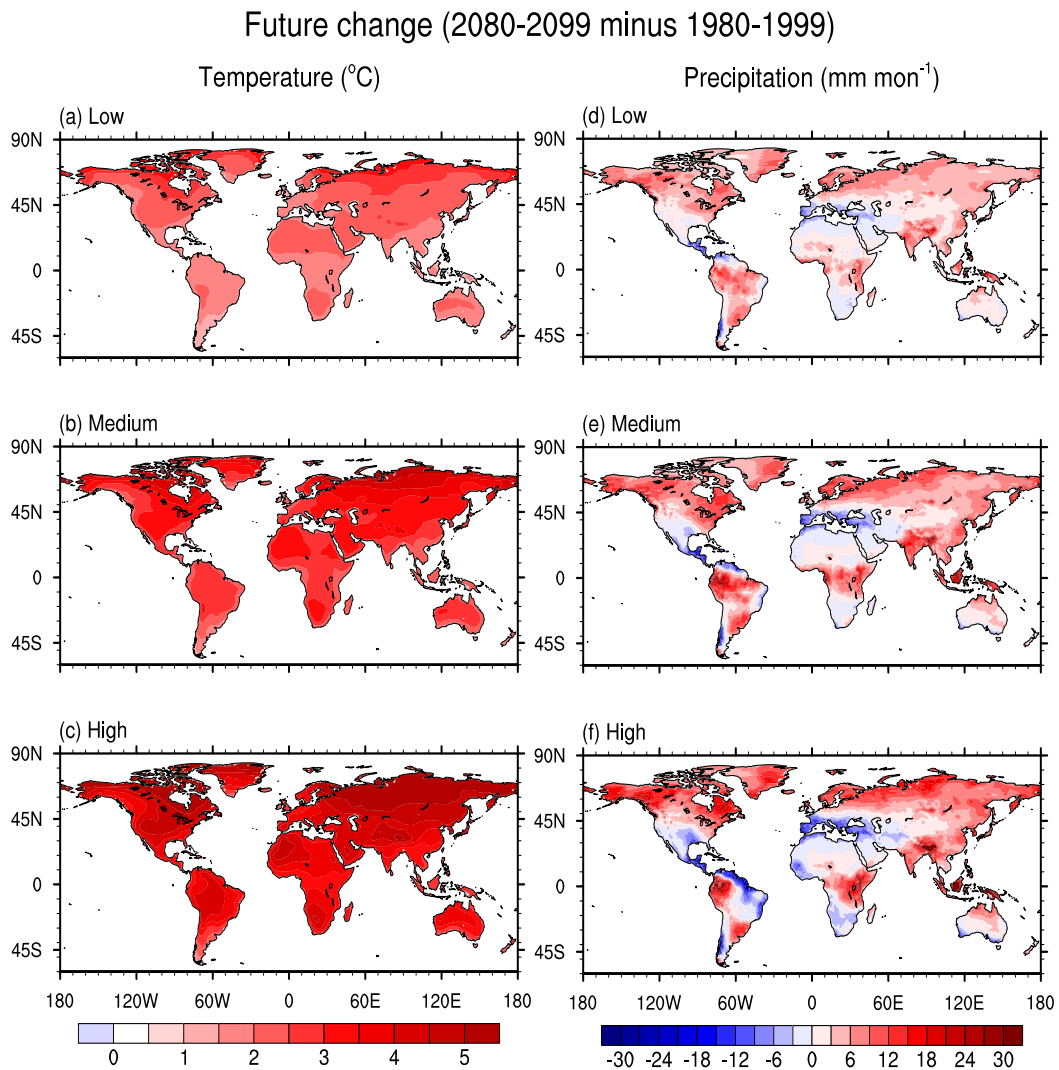


Figure 4.2. Spatial distribution of changes in averaged temperature (2080-2099 minus 1980-1999) for (a) 12 models in low, (b) 18 models in medium, and (c) 18 models in high warming threshold. (d), (e), and (f) show changes in averaged precipitation for low, medium, and high warming threshold.

4.2 Projected changes in spatial distribution of potential plant habitat

Figure 4.3 presents the spatial distributions of the eight plant habitats and desert areas in the present-day climate based on the CRU data and 20C3M GCM simulations. The habitat distributions in the late 21st century calculated for the low, medium, and high warming cases are also shown. For the present-day, the global distribution of plant habitats from the SRES 20C3M simulation is similar to the CRU-based plant habitats (Figs. 4.3a vs. 4.3b). Plant habitats calculated using the CRU and GCM temperatures vary with latitudes in general. The temperate habitats are bounded by the boreal habitats around 55°N, and most of the tropical habitats are located between 20°S and 20°N. In the eastern regions of northern Eurasia and North America, plant habitat boundaries appear at lower latitudes than in the western part of these continents. This spatial pattern of plant habitat in the present-day resembles the biome distributions from satellite retrievals (Friedl et al. 2002; Friedl et al. 2010; Sulla-Menashe et al. 2011).

The projected plant habitats in the late 21st century show clear differences of habitats from the present-day distribution, even for the lowest warming case ($\Delta T < 2.5^\circ\text{K}$) (Fig. 4.3c). In the low warming case ($\Delta T < 2.5^\circ\text{K}$), two prominent

features characterize plant habitat changes. First, tropical habitats expand substantially into adjacent temperate habitats, mainly central South America, southern Africa, northern Australia, and India. The area of tropical habitats is projected to increase by 15.4% from the present-day. This is explained by the increase in the Tr1-type habitat (tropical broadleaf green and tropical herbaceous) by up to $5.39 \times 10^6 \text{ km}^2$, about 22% of the present-day area (Table 4.3). Expansion of the tropical habitats is accompanied by contraction of two habitat types such as Te1 (tropical broadleaf green, temperate needleleaf evergreen, temperate broadleaf evergreen, and tropical herbaceous) and Te2 (temperate needleleaf evergreen, temperate broadleaf evergreen, temperate broadleaf summergreen, and temperate herbaceous), suggesting decreases in temperate woody species in temperate regions. Second, the boreal habitats decrease in the northern regions of Eurasia and North America by $3.6 \times 10^6 \text{ km}^2$, 15.1% of the present-day value (Table 4.3). The decrease in the boreal habitat is accompanied by northward propagation of the Te3- (temperate needleleaf evergreen, temperate broadleaf summergreen, and temperate herbaceous) and Te4-type (Temperate broadleaf summergreen, boreal summergreen, boreal needleleaf evergreen, and temperate herbaceous) habitats by $0.87 \times 10^6 \text{ km}^2$ and $2.33 \times 10^6 \text{ km}^2$, 13.7% and 11.7% of the present-day values, respectively (Table 4.3).

These habitat changes are further enhanced in higher warming conditions ($2.5^{\circ}\text{K} < \Delta T < 3.5^{\circ}\text{K}$ and $3.5^{\circ}\text{K} < \Delta T$) (Figs. 4.3d and 4.3e). The warming magnitude is monotonically related to the increase in the tropical habitats and the decrease in the boreal habitats. Compared to the low warming case, the tropical habitats increase further by $1.95 \times 10^6 \text{ km}^2$ and $3.80 \times 10^6 \text{ km}^2$ in the medium and high warming cases, respectively (Table 4.3). Similarly, the boreal habitats are decreased further by $1.80 \times 10^6 \text{ km}^2$ and $4.12 \times 10^6 \text{ km}^2$ in the medium and high warming cases, respectively (Table 4.3). These changes indicate that the tropical habitats will increase as much as the decrease in the boreal habitats for higher warming situations. However, the proportions of the area changes to the present-day area are up to 5.8% and 11.3% for the tropical habitats, and 7.6% and 17.3% for the boreal habitats in the medium and high warming cases, respectively. These changes suggest that the risk of changes to boreal habitats will be larger than that of tropical habitats for higher warming.

The projected spatial patterns of plant habitats in the late 21st century show that most habitat changes are observed in the boundary regions between the tropical (temperate) and temperate (boreal) plant habitats. This is evident in the zonal-mean patterns of the fractional change in plant habitat. Figure 4.4 shows the zonal-mean of the fraction of change of the tropical, temperate, and boreal habitats for the low, medium, and high warming cases in the late 21th century.

Generally, the fractional changes are most noticeable in three latitudinal belts: 10°S–25°S, 15°N–30°N, and 50°N–65°N (see the regions between dotted lines in Fig. 4.4). The amount of fractional changes also increases with the warming strength. The variation in the fractional change according to the magnitude of warming is largest in the latitudinal band 10°S–25°S where the projected maximum increase in the tropical habitats is as large as 20% (Fig. 4.4a). Around 20°S, the increase in the tropical habitats is as large as 60% for high warming, while the low warming case shows just 10% of change in the tropical habitats at the same latitude. In the regions 15°N–30°N and 50°N–65°N, the fractional changes of temperate and boreal habitats also increase with warming amplitudes (Figs. 4.4b and 4.4c). The largest difference in the fractional change between the high and low warming cases is 25% at 25°N and 20% at 55°N. Consequently, overall patterns show decreasing (or increasing) boreal (or tropical) plant habitat fractions are accompanied by increasing (or decreasing) temperate plant habitat changes.

Table 4.3. Area of observed and projected plant habitat (10^6 km^2). The numbers are the total area (in 10^6 km^2) covered by each climate type. The numbers of in parentheses are one standard deviation of total area (in 10^6 km^2) projected by 12, 18, and 18 projections in low, medium, and high warming groups.

Years	Data	Tr1	Tr2	Te1	Te2	Te3	Te4	Bo1	Bo2
1980–1999	Obs (CRU)	25.27	8.55	8.05	19.94	6.60	19.81	21.48	3.65
	All	24.66 (0.26)	9.07 (0.15)	8.36 (0.09)	20.17 (0.38)	6.62 (0.18)	19.30 (0.40)	18.84 (0.39)	4.95 (0.26)
	Low	24.72 (0.17)	9.02 (0.09)	8.32 (0.05)	20.15 (0.27)	6.66 (0.14)	19.22 (0.23)	18.85 (0.29)	4.99 (0.22)
	Medium	24.68 (0.19)	9.06 (0.11)	8.35 (0.05)	20.14 (0.23)	6.61 (0.09)	19.29 (0.25)	18.89 (0.23)	4.95 (0.18)
	High	24.62 (0.19)	9.10 (0.11)	8.38 (0.04)	20.16 (0.24)	6.61 (0.10)	19.34 (0.26)	18.84 (0.17)	4.91 (0.15)
	2080–2099	Low	30.66 (1.03)	8.28 (0.29)	6.95 (0.67)	18.73 (0.78)	7.53 (0.41)	21.55 (1.12)	17.20 (0.72)
	Medium	32.57 (0.96)	8.32 (0.30)	6.16 (0.55)	18.33 (0.79)	7.81 (0.58)	22.24 (1.32)	16.05 (0.97)	2.34 (0.50)

High	34.76	7.98	5.27	17.80	7.95	23.18	14.39	1.68
	(0.97)	(0.35)	(0.75)	(0.97)	(0.63)	(0.99)	(0.82)	(0.37)

Distribution of plant habitat

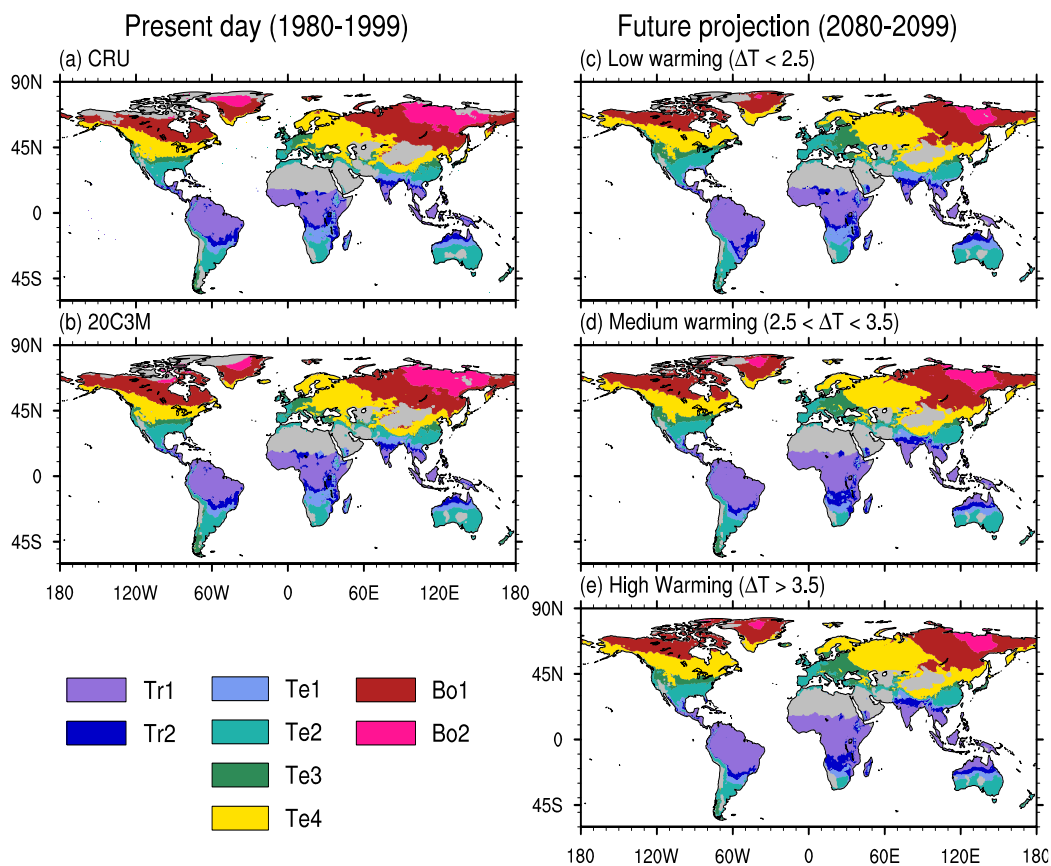


Figure 4.3. Spatial distribution of averaged plant habitat of present day (1980-1999) for (a) CRU and (b) ensemble of 20C3M simulations. Spatial distribution of averaged plant habitat of future projection (2080-2099) for (c) 12 models in low, (d) 18 models in medium, and (e) 18 models in high warming threshold. Regions with grey shading represent the desert areas.

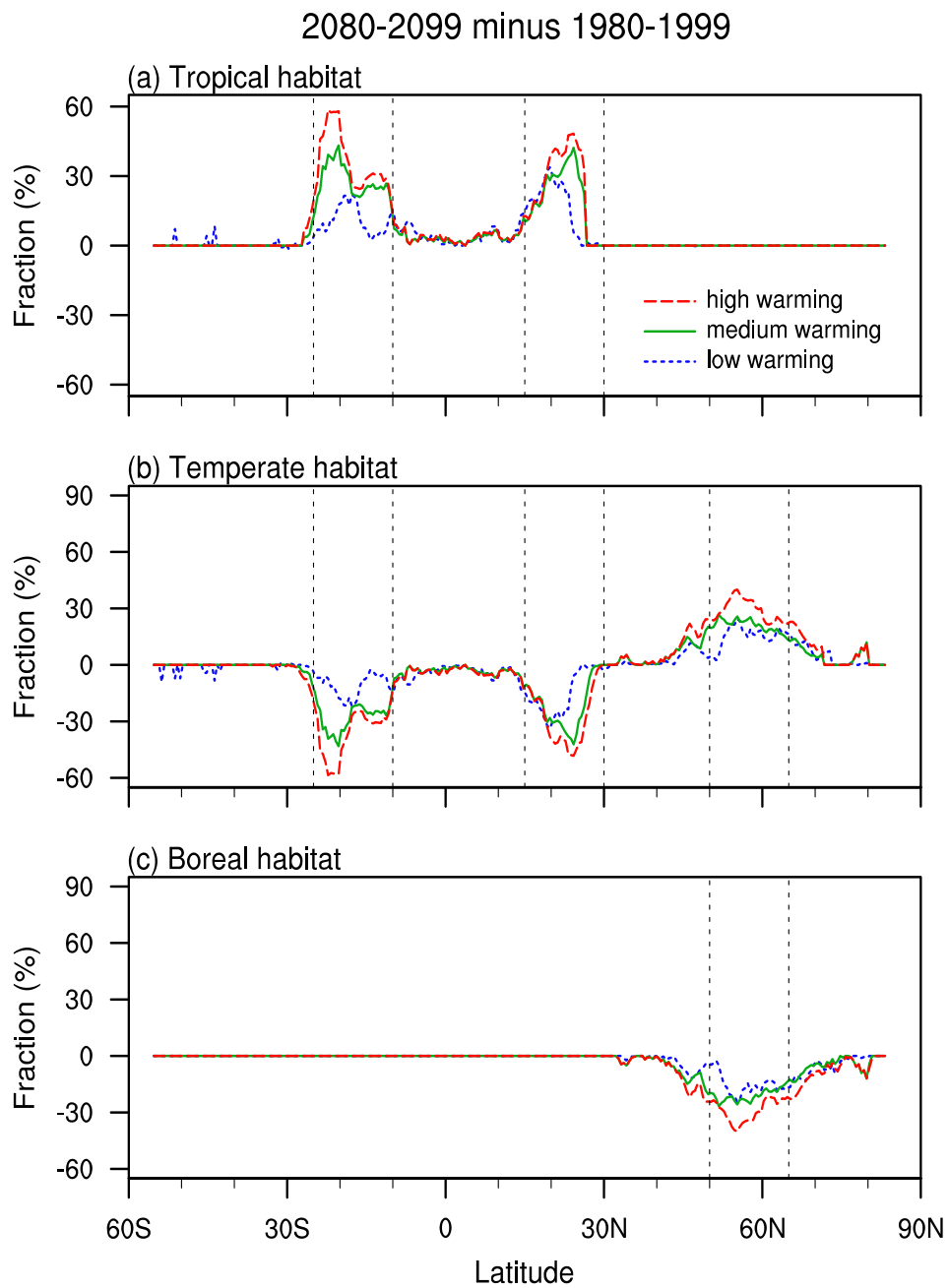


Figure 4.4. Difference of zonal-mean fractional change in plant habitat between the period of 2080–2099 and 1980–1999 for (a) tropical habitat, (b) temperate habitat, and (c) boreal habitat. Red dashed, green solid, and blue dotted line indicates high, medium, and low warming threshold.

4.3 Projected changes in the timing of plant habitat changes

4.3.1 Regional characteristics of timing of plant habitat change

Based on the changes in plant habitat for the three latitude bands, we further estimate the timing of the plant habitat change related to the three warming cases. Figure 4.5 plots the percentage of plant habitat change from the present-day (abscissa) against time (ordinate) for the three latitude bands. Due to the wide spread of the projected plant habitat changes induced by various climate model forcings, we focus on the ensemble mean of the plant habitat change between the projections (solid lines). In the regions 10°S–25°S, the ensemble mean exceeds 10% in 2032 for the high warming case (Fig. 4.5a and Table 4.4). This timing of the amount of habitat change precedes that of the low and medium warming cases by 11 and 5 years, respectively (Fig. 4.5a and Table 4.4). Increasing the threshold of fractional change to 20% and 30% also increases the difference in the timing between the high and other warming cases. The timing gap is 34 years between the low and high warming cases at 20% threshold, and 10 and 12 years between the medium and high warming cases at 20% and 30% threshold, respectively. In the regions 15°N–30°N, the mean habitat changes reach 10%, 20%, and 30% in the years 2046, 2070, and 2093, respectively in the high warming case (Fig. 4.5b and Table 4.4), earlier than those in the low warming

case by 12 years at the 10% threshold, and those of the medium warming case by 4 and 23 years at the 10% and 20% thresholds, respectively. In the latitudes 50°N–65°N, the plant habitat change also occurs earlier as the warming magnitude increases at the 20% and 30% thresholds (Fig. 4.5c and Table 4.4). For the 10% threshold, however, the timing of the low warming case precedes that of the medium warming case by 5 years (Table 4.4). This reversed relationship between the habitat-change timing and the warming magnitude is because of increase in averaged T_c of the latitudes 50°N–65°N is larger in the low warming case in the early 21st century (not shown). Despite this exception, overall patterns of projected plant habitat changes suggest that increased warming leads to faster habitat changes.

Due to the spatial heterogeneity of plant habitat changes, regional discrepancies in the timing of mean plant habitat changes are analyzed for the three latitudinal belts in each continent (Table 4.4). The most dominant features are found between southern Africa (0°–60°E) and central South America (30°W–90°W) in the latitudes 10°S–25°S. In the medium warming case, for example, the 20% habitat change occurs in 2052 for the southern Africa region, but in 2099 for the central South America region. This time gap in achieving the same amount of habitat change between these two regions indicates that southern Africa will experience larger and faster habitat change under the same global

warming. This regional variation is intensified as the warming increases. In southern Africa, the difference in the timing is 40 years for the 30% threshold between the low and high warming cases. However, central South America shows no change in the timing to achieve the 30% change for all three warming cases. Similar regional variations in the timing occur in the regions 15°N–30°N between East Asia (60°E–150°E) and northern North America (60°W–120°W) (Table 4.4); the same amount of plant habitat change occurs earlier in East Asia than in northern North America. The regional variation is amplified with increasing warming magnitudes.

For the region between 50°N–65°N, the difference between northern Eurasia (30°E–180°) and northern North America (50°W–170°W) is relatively small compared to other latitude bands (Table 4.4). The warming magnitude has only a small impact on the regional discrepancy in the timing of plant habitat change. Instead, the threshold value for the fractional habitat change is more important in examining the regional variations in the temporal changes in plant habitat. For the 10% threshold, the timing in northern Eurasia is earlier than that in northern North America, whereas this change is reversed at the 30% threshold (Table 4.4). In the high warming case, the timing is faster in northern Eurasia than in northern North America by 22 years for the 10% threshold; whereas, the timing only appears in northern North America for the 30% threshold (Table 4.4).

The ensemble mean of the timing of the plant habitat changes is analyzed by considering large variations of climate projections among model simulations. Nevertheless, the uncertainty in climate projections still exists. In figure 4.5, colored bars show the range of projected timings of plant habitat change. Upper and lower limit of the spread of timings provided as exact year for each colored bars. If upper limit is larger than 2099, the upper limit is presented upper arrow. Larger range with wider spread of projections represents larger uncertainty of projected timing. The ranges of projected timings in low warming case are generally larger than those in medium and high warming case for the 10% and 20% thresholds (Fig. 4.5). In regions of 10°N–25°N, for example, the range of projected timing is 48, 36, and 29 years for low, medium, and high warming cases at 10% thresholds. The ranges of projected timing also vary in difference latitudinal zones. The latitudes of 50°N–65°N shows broader range of projected timing than other latitudinal belts, especially at 10% thresholds of fractional change. These wide ranges of projected timings of the regions of 50°N–65°N are closely related to high uncertainty in temperature projection in high-latitudes (Meehl et al. 2007b).

Due to the ranges of projected timings, the relationship between the warming magnitude and the timing of plant habitat change is revised by changing the standard from the ensemble mean to the 90% proportion among all

models (Table 4.5). Analysis based on the timing of the 90% proportion can increase confidence level because of the 90% proportion indicates that particular habitat changes are almost certain to occur at a certain time. The timing of the 90% proportion is later than that of the ensemble mean by several decades (Table 4.5). In the case of the 90% proportion, the timing of habitat change is reduced with increased warming for all cases. Also, the 90% proportion is notable in the high warming case rather than in the low- and medium warming cases. This implies that the timing in the higher warming case makes the habitat change sure to be earlier, regardless of the uncertainty of future projections.

Table 4.4. Estimated year that ensemble mean of projected habitat changes firstly exceed 10%, 20%, and 30% threshold for all warming groups in the three latitudes belts. En-dash means that the ensemble means does not reach the three thresholds until 2099.

	Low warming ($\Delta T < 2.5^\circ\text{K}$)			Medium warming ($2.5^\circ\text{K} < \Delta T < 3.5^\circ\text{K}$)			High warming ($\Delta T > 3.5^\circ\text{K}$)		
	10%	20%	30%	10%	20%	30%	10%	20%	30%
10°S–25°S	2047	2094	-	2040	2068	2096	2034	2057	2076
southern Africa	2028	2063	2094	2026	2053	2067	2020	2044	2057
entral South America	-	-	-	2070	-	-	2059	-	-
15°N–30°N	2056	-	-	2050	2095	-	2045	2075	-
East Asia	2056	-	-	2052	2089	-	2046	2071	-
southern North America	-	-	-	2077	-	-	2065	-	-
50°N–65°N	2056	-	-	2049	2085	-	2045	2069	2097

northern Eurasia	2047	-	-	2041	2086	-	2040	2070	-
northern North America	2050	2084	-	2047	2073	2093	2039	2060	2073

Table 4.5. Estimated year that 10% and 90% of model simulations of projected habitat changes firstly exceed 10%, 20%, and 30% threshold for all warming groups in the three latitudes belts. En-dash means that the ensemble means does not reach the three thresholds until 2099.

		Low warming ($\Delta T < 2.5^\circ\text{K}$)			Medium warming ($2.5^\circ\text{K} < \Delta T < 3.5^\circ\text{K}$)			High warming ($\Delta T > 3.5^\circ\text{K}$)		
		10%	20%	30%	10%	20%	30%	10%	20%	30%
10°S–25°S	10%	2035	2066	-	2028	2057	2079	2023	2049	2067
	90%	2066	-	-	2051	2088	-	2043	2068	2087
southern Africa	10%	2019	2054	2066	2016	2039	2058	2012	2035	2046
	90%	2045	2087	-	2045	2074	2093	2040	2064	2072
central South America	10%	2065	-	-	2050	-	-	2042	-	-
	90%	-	-	-	2079	-	-	2074	-	-
15°N–30°N	10%	2044	-	-	2036	2078	-	2038	2067	2097
	90%	2073	-	-	2066	-	-	2057	2083	-
East Asia	10%	2045	2078	-	2037	2062	-	2036	2058	2087
	90%	2085	-	-	2068	-	-	2063	2087	-

southern	10%	-	-	-	2065	-	-	2052	2087	-
North America	90%	-	-	-	-	-	-	2086	-	-
<hr/>										
	10%	2035	2070	-	2030	2059	2099	2031	2058	2084
50°N–65°N	90%	2092	-	-	2068	-	-	2055	2086	-
northern Eurasia	10%	2021	2076		2013	2055	-	2009	2050	2083
	90%	-	-		2062	-	-	2059	2082	-
northern North America	10%	2013	2054	2069	2029	2048	2061	2016	2041	2059
	90%	2099	-	-	2086	-	-	2061	2076	2091
<hr/>										

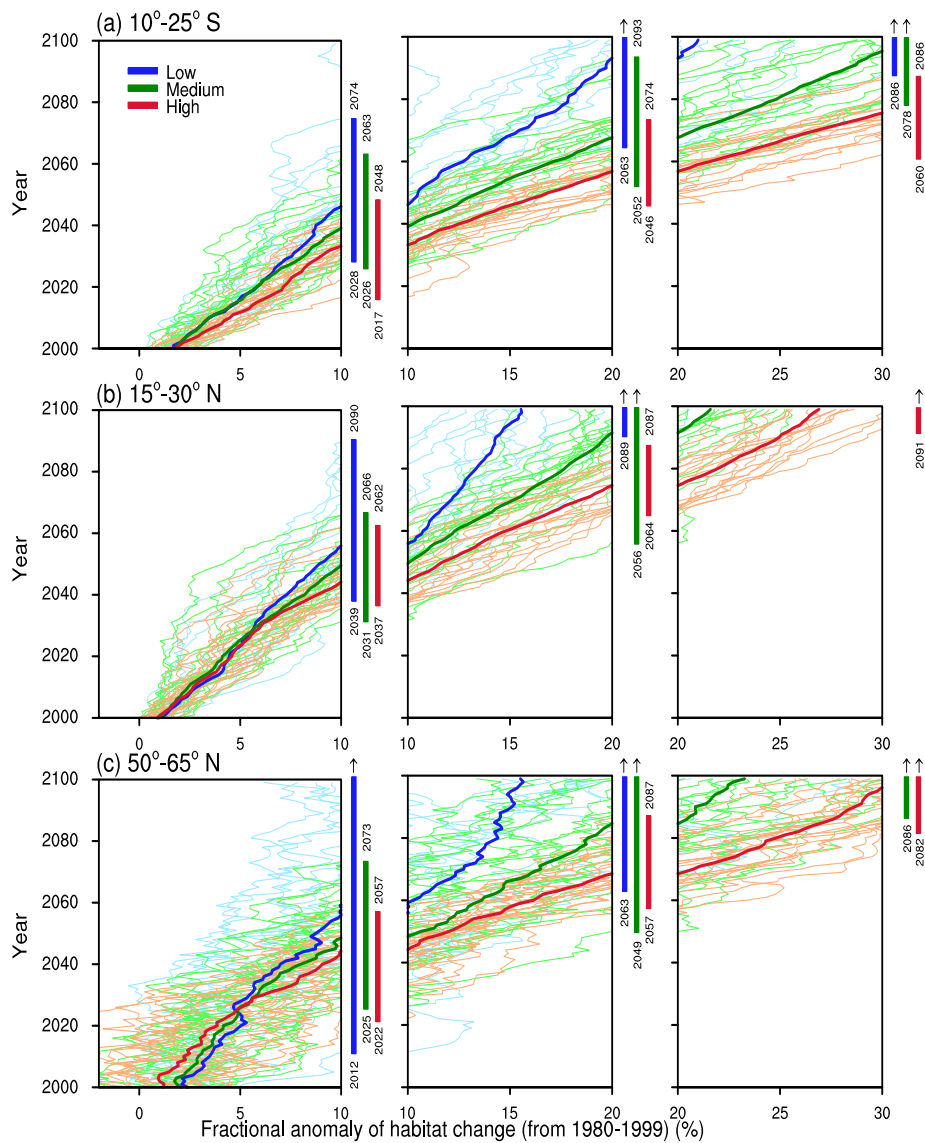


Figure 4.5. Regional mean fractional changes in plant habitats for (a) 10° – 25° S, (b) 15° – 30° N, and (c) 50° – 65° N. Each projection from the CMIP3 model simulation included in low-, medium-, and high- warming groups are shown in light blue, light green, and light orange. Blue, green, and red bars represent the range of timing when projected habitat changes might cross the 10%, 20%, and 30% thresholds of low-, medium-, and high- warming groups.

4.3.2 Relationship between national wealth and the timing of plant habitat change

Figure 4.6 shows the projected time (year) of the plant habitat change, along with the GDP values of the six nations for the three warming cases at three thresholds, respectively. For all thresholds and all warming cases, the timings of plant habitat change in Angola are overwhelmingly faster than the other countries by several decades (Figs. 4.6a and 4.6b). In particular, only Angola shows the timings of plant habitat change for the low and medium warming cases at the 30% threshold (Fig. 4.6c). The GDP of Angola is much lower than that of the other nations (Table 2.1). Thus, the vulnerability of plant habitat in Angola is amplified considering both the timing of plant habitat change and regional economic power.

The timing of the plant habitat change at all thresholds of fractional change is noticeably fast in Canada, Russia, and China (Fig. 4.6). However, these three nations have sufficiently large GDP: 1736.1, 1857.8, and 7318.5 billion US dollars for Canada, Russia, and China, respectively (Table 2.1). Thus, economic capability may allow these countries to alleviate the risk of plant habitat change. For Mexico and Brazil, the timings of plant habitat change are later than other regions by several decades in all warming cases at 10% and 20% threshold (Figs.

4.6a and 4.6b), indicating relatively low risk of plant habitat change (Figs. 4.6a and 4.6b). In addition, the large GDP values of the two nations (> 1000 billion US dollars) also decrease the adverse effects of plant habitat changes.

Timing of habitat change with GDP per Capita

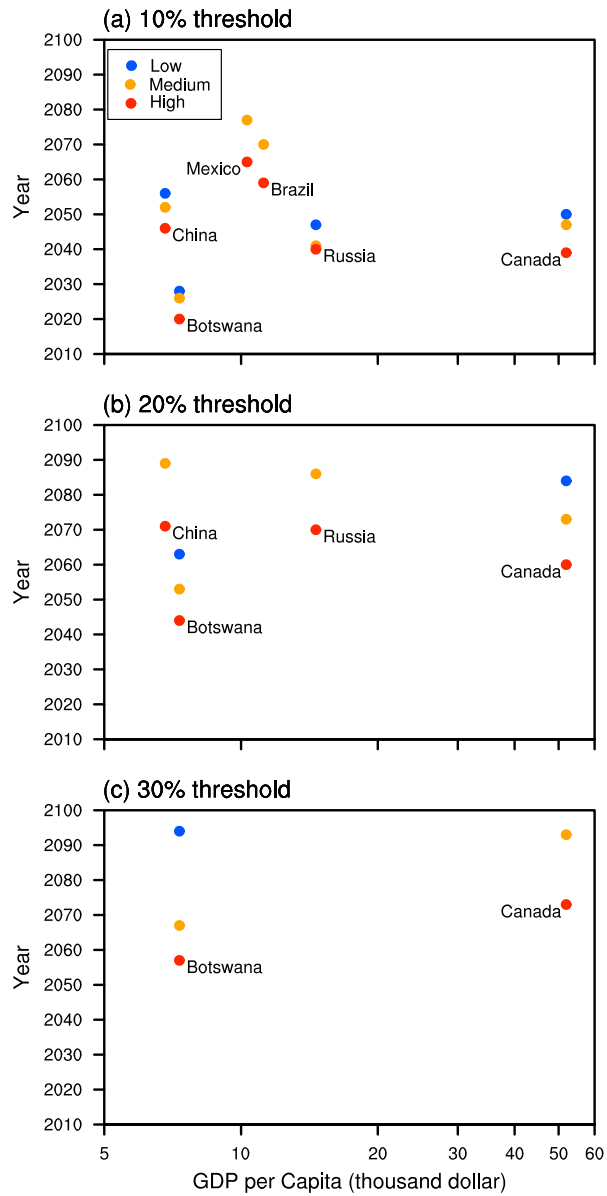


Figure 4.6. Timing of averaged plant habitat change reaches (a) 10%, (b) 20%, and (c) 30% threshold for GDP per Capita 2012 of Botswana, China, Mexico, Russia, and Canada. Blue, yellow, and red dots represent low, medium, and high warming threshold, respectively.

4.4 Summary and Discussion

Before evaluating the timing for specified plant habitat changes, the spatial patterns of plant habitat changes are analyzed in terms of global warming magnitudes. For the low warming case ($\Delta T < 2.5^\circ\text{K}$), the largest spatial changes in plant habitat are observed in the boundary regions between the tropical (10°S – 25°S), temperate (15°N – 30°N), and boreal (50°N – 65°N) habitats. With increasing magnitudes of global warming (medium case: $2.5^\circ\text{K} < \Delta T < 3.5^\circ\text{K}$ and high case: $\Delta T > 3.5^\circ\text{K}$), the fractional changes in plant habitat are increased in all three latitude zones. For example, in the regions 50°N – 65°N , boreal habitats are projected to decrease by 15.3%, 22.9%, and 32.3% in the low, medium, and high warming cases, respectively. These results are consistent with the spatial patterns of the simulated plant habitat changes in previous studies (Cramer et al. 2001; Lucht et al. 2006; Sitch et al. 2008; Gonzales et al. 2010; Jiang et al. 2012).

Estimating the timing of plant habitat changes due to global warming is one of the most important concerns that need to be improved upon from previous studies. Here the timing of plant habitat changes is firstly estimated using dominant spatial patterns of plant habitat changes over the globe. The timing of plant habitat changes is suggested for the three warming cases by specific years

when specified amounts of changes (10%, 20%, and 30%, respectively) will occur in the three latitudinal belts. Regardless of the warming magnitude, the fastest plant habitat changes appear in the regions 10°S–25°S. For the medium warming case, the plant habitat change in the latitude band 10°S–25°S exceeds 20% in 2066, faster than for the latitude bands 15°N–30°N and 50°N–65°N by 27 and 18 years, respectively (Table 4.4). In addition, the latitude band 10°S–25°S shows significant regional variations in the timing of plant habitat change. In the southern Africa region, the plant habitat change is projected to reach 30% in 2092 in the low warming case; in central South America, the projected plant habitat changes remain < 20% within the 21st century, even for the high warming case (Table 4.4). Furthermore, for all warming cases and thresholds of fractional habitat change, southern Africa shows the fastest plant habitat changes (Table 4.4). Thus, the estimated habitat-change timing indicates that the plant habitat in southern Africa is the most vulnerable to climate change.

Although the ensemble mean is used, the timing of plant habitat change still has uncertainties originated from various climate model simulations. The uncertainties in the projected timing of plant habitat change are represented by colored bars in Fig. 4.5. Due to the uncertainties the timing of plant habitat is re-estimated using both tolerant and strict standards: the 10% and 90% proportion of model projections. Comparing to the timing based on the ensemble means, the

timing of plant habitat change is advanced and delayed by several decades for the 10% and 90% proportion, respectively. This implies that the projected timing of the ensemble mean cannot guarantee that a specific amount of plant habitat change will happen at that timing. Nevertheless, there is consistency in the projected timing of plant habitat change regardless of the standards. Increasing the warming magnitude advances the timing. A specific amount of plant habitat change is appeared early in southern Africa and East Asia. Thus, the timing of plant habitat change can be a good indicator that representing regional vulnerability of ecosystem in response to climate change regardless of the uncertainty of future projections.

The estimated timing of plant habitat change presented in this study can help in planning mitigation policies, as many mitigation policies are developed for specific levels of climate change (UNFCCC 2009; Joshi et al. 2011). Nevertheless, implementation of these mitigation policies requires economic considerations (Naidoo and Ricketts 2006; IPCC 2007). Countries with weaker economic power are more vulnerable to plant habitat changes. We note that southern Africa has a low GDP and very fast timing of plant habitat change. In southern Africa, Angola shows the highest GDP of 104.3 billion dollars, which is only sixtieth in position among all nations in the world (World Bank 2012). Worse yet, the GDP of the other six nations in southern Africa is lower than 20

billion US dollars, less than one-fifth of Angola's (Table 2.1). Thus, nations in southern Africa are likely to experience greater economic hardships in coping with fast habitat changes and subsequent ecological problems, unless they achieve great economic development in a very short time. Support from the international community will be needed to mitigate the vulnerability of habitat change in southern Africa.

Information on the timing of plant habitat changes presented in this study will help to decide the optimum timing for implementing future ecosystem management policies. If plant habitat changes are reduced by timely management practice, many ecological advantages can be expected. For example, well-preserved plant habitats can protect terrestrial biodiversity from climate change due to the direct relationship between plant habitats and biodiversity (Fischlin and Midgley 2007; Giam et al. 2010; Bellard et al. 2012). Conservation of biodiversity can greatly benefit human society, as biodiversity is closely related to the ability of an ecosystem to supply goods and services (Cardinale et al. 2012), and is known to protect human society from the impact of climate change (Das and Vincent 2008; Turner et al. 2009; Nilsson and Persson 2012). In addition, regional impacts of global warming may be reduced through vegetation-climate feedback (Bonan 2008; Jackson et al. 2008). For instance, abrupt climate change and frequency of extreme weather may be prevented in

future climates by conserving plant habitat (Bounoua et al. 2010; Jeong et al. 2010).

The estimated timing of plant habitat change is limited in some aspects. Since the bio-climate rule is based only on surface temperature, the uncertainties of projected temperature are directly reflected on the projected plant habitat change, especially in high-latitudes. In addition, other important factors such as inter-species competition, physiological flexibility, and the effects of other climate variables are not included in the plant habitat changes projected in this study. Furthermore, eight types of plant habitats based on the bio-climate rule may be too simplistic for representing numerous types of plants in comparison to ecological niche models (Pearson and Dawson 2004; Morin and Thuiller 2009). Human-induced land-cover changes (or land use) can also play an important role in future changes in plant habitats (Foley et al. 2011; Lambin and Meyfroidt, 2011). Despite these limitations, which will be improved in future studies, the habitat changes projected in this study based on the bio-climate rule is generally consistent with previous studies (Cramer et al. 2001; Scholze et al. 2006; Sitch et al. 2008; Jiang et al. 2012), especially the latitudinal patterns in the plant habitats changes in previous studies on ecological responses to climate changes (Rosenzweig et al. 2008; Dillon et al. 2010). The three latitudinal zones, which are the main analysis domains in this study, also generally agree with regions

with high vulnerability to warming (Scholze et al. 2006; Williams et al. 2007; Gonzalez et al. 2010). From a global perspective, the projected timing of habitats changes is thus acceptable as one reference for designing policies for future forest management.

5. Significant drying trend over the humid area in continental East Asia by local warming

5.1 Trend in land surface dryness over continental East Asia

Figure 5.1 shows temporal variations in overall mean of annual PET/P, P, and PET over continental East Asia. For the whole period, PET/P is decreased by -2.30% decade⁻¹ due to both increase in P (2.44% decade⁻¹) and decrease in PET (-0.52% decade⁻¹). However, changes of the three variables are not monotonic. Changing point of long-term trends in PET/P is occurred in early 1980s (Methods). The trend of PET/P is negative (-1.81% decade⁻¹) and positive (1.66% decade⁻¹) for two periods of 1961-1983 and 1984-2010, respectively (Fig. 5.1a). Changes in both P and PET are consistent with the PET/P trend: increasing P and decreasing PET in former period, decreasing P and increasing PET in latter period (Figs. 5.1b, c). The decrease in PET/P before early 1980s is mainly caused by relatively large increase in P (4.56% decade⁻¹) rather than decrease in PET (-0.95% decade⁻¹). However, the increase in PET (1.22% decade⁻¹) contributes to the increase in PET/P largely in latter period.

The spatial distributions of PET/P, P, and PET trends are consistent with overall mean changes for both periods of 1961-1983 and 1984-2010 (Fig. 5.2). In

early period, about 60% of total stations shows decreasing trends of PET/P, particularly in arid (northwestern and northern China) and humid regions (southeastern China) (Fig. 5.2a). Increasing trends of PET/P are mainly shown over semi-arid region (northeastern and southwestern China), but the magnitudes are relatively small. The spatial pattern of P trends is very similar to that of P/PET trends with opposite sign, suggesting that changes in P are directly linked to those in PET/P regardless of the regional classification (Figs. 5.2a, b). PET is decreased over more than three quarters of the analysis domain with relatively small values (Fig. 5.2c). Changes in PET are meaningful on PET/P trends over the humid area only (Figs. 5.2a, c).

Spatial patterns of PET/P, P, and PET trends are drastically varied in latter period (Figs. 5.2d-f). PET/P is increased over most of analysis domain except for western part of the arid region ($< 100^{\circ}\text{E}$; northwestern China) (Fig. 5.2d). Notable shifts in PET/P trends from negative to positive values are observed in humid (southeastern China) and eastern part of arid regions (northern China) (Figs. 5.2a, d). The reversal of PET/P trends over those regions causes the increasing trend in overall mean PET/P from early 1980s considering relatively small changes in PET/P trends over other regions (Figs 5.1a, 5.2d). Spatial distribution of P trends also shows notable changes over arid and humid regions (Figs. 5.2b, e). Positive trends are reversed over eastern part of arid regions and

magnitude of increasing trends becomes smaller in humid regions. These regional patterns of P trends are consistent with PET/P trends over arid and semi-arid regions, but not in the humid area (Figs 5.2d, e). Significant increase in PET explains the inconsistency between changes in PET/P and P over the humid area (Figs. 5.2d, f). In other regions, positive trends of PET also contribute to increase PET/P.

Changes in both P and PET trends are consistent with regional pattern of climate changes appeared in continental East Asia. Trends in P over eastern part of analysis domain ($> 100^{\circ}\text{E}$) are closely related to variability of East Asian monsoon circulation. The weakening of monsoon circulation from late 1970s leads to both decreasing and increasing trends in P over arid and humid regions. However, increases in P over the humid area are much smaller than decreases over the arid regions (Fig. 5.2e). The asymmetry is come from decrease in monsoon rainfall over the humid region from early 1990s following the recovering of monsoon circulation. Notable shifts in other climate variables are connected to increasing trend in PET in latter period. For example, anthropogenic warming becomes severe in whole analysis domain after 1980s. The trend in absorbed solar radiation is changed from dimming to brightening, particularly in the humid area. Consequently, combined impacts of climate changes increase PET/P over both arid and humid regions since early 1980s.

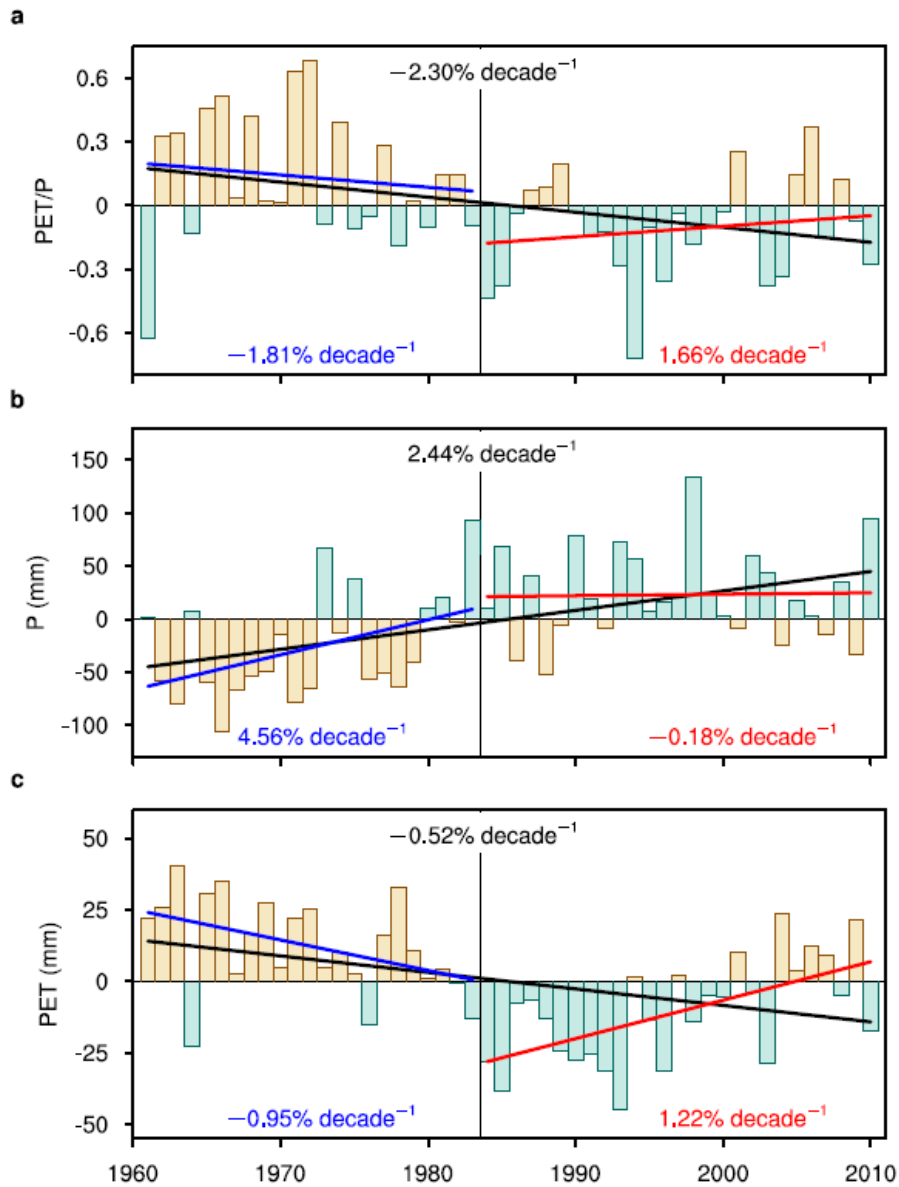


Figure 5.1. Temporal variations of annual mean PET/P, P, and PET in East Asia. a-c, PET/P (a), P (b), and PET (c). Yellow and blue bars indicate that positive and negative anomalies for PET/P and PET, but negative and positive anomalies for P. Black, blue, and red lines are linear regression lines (% decade⁻¹) for the period of 1961-2010, 1961-1983, 1984-2010, respectively.

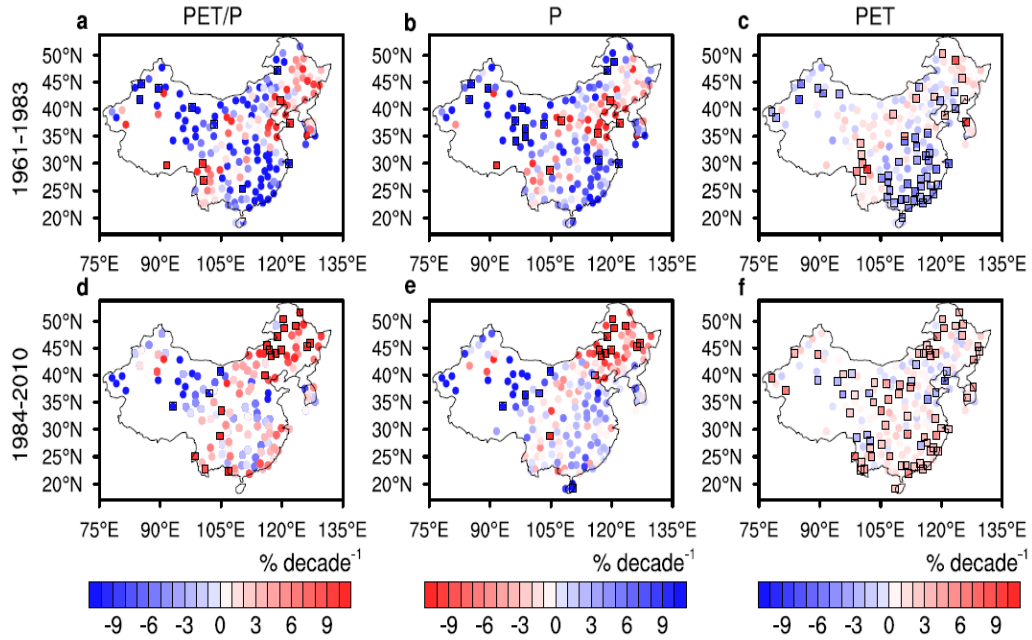


Figure 5.2. Spatial distributions of trends of PET/P, P, and PET in East Asia. a-c, The spatial distribution of trends in annual mean PET/P (a), P (b), and PET (c) for the period of 1961-1983. d-f, as a-c, but for the period of 1984-2010. The empty square indicates that the trend is significant at 95% level.

5.2 Causes of changes in land surface dryness

To determine exact causes of PET/P changes, we compute relative influences of changes in P, Rn, WS, Ta, and RH on trends in PET/P for two analysis periods (section 2.2.5). Figure 5.4 shows averaged influences of five climate parameters and their confidence intervals over three regimes for each period. Here, positive values of a particular variable indicate increasing rates of PET/P considering changes in that variable only and vice versa. Note that stations located on west of 100°E are excluded in averages. The mean climate of those regions is definitely different to other parts of continental East Asia, classified into monsoon climate region. Further, changes in land surface dryness mostly rely on variation of P rather than that of other climate variables for both analysis periods (Fig. 5.3).

Relative influences of each climate parameter are significantly different in according to both analysis periods and hydro-climate regimes, indicating that mechanisms of PET/P changes operate differently (Fig. 5.4). Over the arid region, negative impact of Rn (-1.47% decade⁻¹) looks to be offset by positive influences of P and Ta (0.83% and 0.75% decade⁻¹) before early 1980s (Fig. 5.4a). However, large confidence range of P indicates that substantial impact of P on PET/P changes locally (Fig. 5.3a). In latter period, changes in P shows the

largest influence ($3.17\% \text{ decade}^{-1}$), larger than that of other climate parameters by at least two times. These results mean that variation of P causes the significant increasing trend of PET/P over the arid region. Relative influences of climate variables over the semi-arid region are similar to those of the arid region in former period (Figs .5.4a, b). In 1984-2010, PET/P is increased by positive influences of P, Ta, and RH (1.81% , 0.90% , and $1.45\% \text{ decade}^{-1}$) despite of negative influence of WS ($-1.09\% \text{ decade}^{-1}$). Increasing trend of PET/P is contributed by both warming and decrease in P over the semi-arid area. Over the humid region, P and Rn are the primary and secondary important parameters for the PET/P decrease (-4.76% and $-2.11\% \text{ decade}^{-1}$) in early period (Fig. 5.4c). The contribution of other three variables is much smaller. In contrast, positive influences of Ta and RH (1.24% and $1.87\% \text{ decade}^{-1}$) are larger than negative influences of P and Rn (-0.95% and $-0.83\% \text{ decade}^{-1}$) in latter period. Thus, main reason for the increase in PET/P trends is warming and subsequent increase in atmospheric evaporative potential over the humid region.

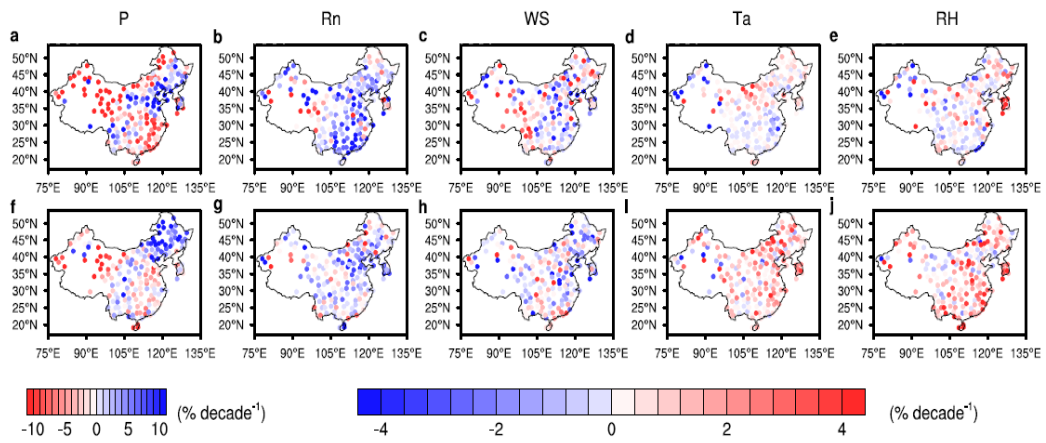


Figure 5.3. Spatial distributions of contributions of the five climate parameters on the PET/P trends in East Asia. a-e, The spatial distribution of the contribution of changes in P (a), Rn (b), WS (c), Ta (d), and RH (e) for the period of 1961-1983. f-j, as a-e, but for the period of 1984-2010.

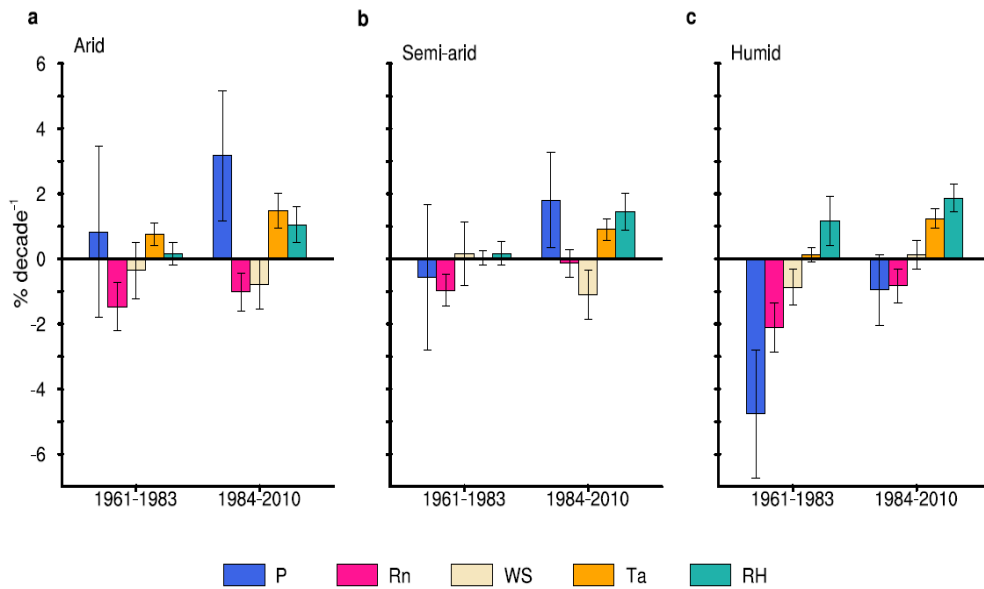


Figure 5.4. Averaged relative influences of five climate parameters on the PET/P changes. a-c, Relative influences (% decade⁻¹) of five climate parameters is averaged for the three hydro-climate regimes: arid (a), semi-arid (b), and humid (c). The averaged influences are computed for the two periods of 1961-1983 and 1984-2010. Blue, pink, beige, orange, and cyan bars represent averaged influence of P, Rn, WS, Ta, and RH, respectively. Error bars represent confidence intervals at 95% significance level.

5.3 Summary and Discussion

The above analysis clearly shows that P, Ta and RH are important three variables for increases in land surface dryness from early 1980s. Dominant influence of P on increases in PET/P in the arid region is contrast to causes of dryness increase over other water-limited regions. This contradictory comes from strong interdecadal variability of P, well known feature of East Asian monsoon region. In consistent with regional warming magnitude, the arid region shows the largest influence of Ta. However, the humid area shows the highest increasing rate of PET/P due to decrease in RH, related with increasing saturation vapor pressure (e_s) following the warming. Relationship between Ta and e_s according to Clausius-Clapeyron equation explains relatively small and large influence of RH in arid and humid regions, respectively (Fig. 5.5). Annual mean temperature is larger in the humid region than in the arid region by about 10°C (map in Fig. 5.5). Due to the difference in background air temperature, the humid region experiences steep increase in e_s and decrease in RH than the arid region despite small warming magnitude (graph in Fig. 5.5). Thus, influence of decrease in RH is relatively large in the humid region, but smaller in the arid region (bars in Fig. 5.5).

Influences of Ta and RH, always act to dry land surface, are significantly

increases in recent decades regardless of hydro-climate regions. These results could be observational evidences of the projected drying trend over the land surface during 21st century according to increase in greenhouse gas concentration. Also our results indicate that drying land surface due to warming is already in progress, not a risk of aftertime. Water management plans should consider the increased water demands due to warming to mitigate water scarcity particularly in humid areas.

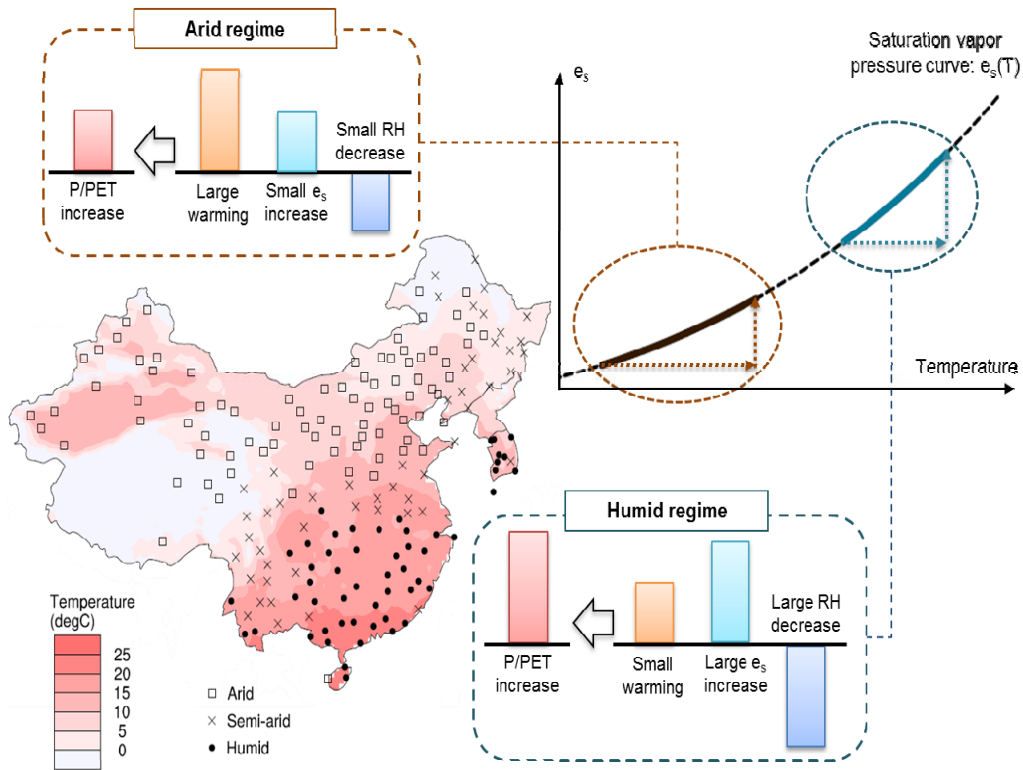


Figure 5.5. Schematic diagram explaining the small and large influence of RH on the PET/P trends in the arid and humid regions. The map shows the spatial distributions of annual mean temperature for the period of 1961-2010 (degree C). Empty squares, cross marks, and filled circles are stations that classified by arid, semi-arid, and humid regions, respectively. The map clearly shows that the arid and humid region of continental East Asia has the cold and warm climate, respectively. In the arid region, warming magnitude is large, but decrease in RH is small following the Clousius-Clapeyron relationship between the saturation vapor pressure (e_s) and T_a (brown line in the graph). In contrast, the increase in the e_s is relatively large in the humid region despite the small warming magnitude (blue line in the graph). The difference in the increment of e_s between two regions causes much larger decrease in RH, further large influence of RH on PET/P trends in the humid region.

6. Conclusions

The present thesis includes three studies about the change in vegetation and its feedback influence, and causes of changes in land surface dryness as followings:

- 1) Examination of potential impact of vegetation feedback on climate aridity over the United States in a condition of doubling CO₂ concentration
- 2) Investigation of regional plant habitat changes in according to three different warming scenarios using various future projections of fully-coupled GCMs
- 3) Emphasizing the impact of local warming on changes in land surface dryness over continental East Asia in recent decades

In chapter 3, first, increased climate aridity in according to doubled atmospheric CO₂ concentration is significantly decreased by vegetation feedback over the contiguous United States, particularly in hydrological transitional region

such as semi-arid and subhumid regions. Thornthwaite moisture index I_m is used as a represent of degree of climate aridity as well as standard of classification of hydrological climate regimes. The CAM3-DGVM model simulates the response of vegetation to climate changes due to doubled CO₂ concentration. For fixed vegetation cover and growth, warm and dry atmospheric conditions resulting from doubling CO₂ increase climate aridity over most of the US. When the vegetation actively responses to the increased CO₂ concentration and climate change, strong increases in I_m (reduced aridity) and subsequent alterations in climate types in the northwestern, midwestern, and southern contiguous US. In addition, strong impact of vegetation feedback appears in regions of subhumid climate types where large increases in aridity may occur due to CO₂-induced warming. Analysis shows that the density of vegetation is notably increased over the northwestern, midwestern, and southern contiguous US in response to doubled CO₂ centration. most part of the US. Increased evapotranspiration of dense vegetation is the key change of the decrease in climate aridity. Rich moisture amount of atmosphere according to the increase in ET is favorable condition for precipitation, indicating the increase in water supply. In addition, enhanced latent heat release due to the enhanced ET reduces water demands of atmosphere through decreasing air temperature. These results indicate that the impact of vegetation feedback on temperature and precipitation, further affects

climate aridity and climate types in future climate, particularly in intermediate climate zones.

Considering remarkable influence of vegetation feedback on future climate, accurate understanding of vegetation changes in response to climate change is important for national agencies to make various mitigation plans about agriculture, energy and water management. In chapter 4, future changes in vegetation are examined deeply using the definition of 8 plant habitat changes based on surface temperature and 64 sets of present and future projections based on 16 different fully-coupled GCMs. Spatial distributions of plant habitats in present climate are highly consistent with satellite-observed vegetation cover. In 21st century, GCMs simulate increase in global mean temperature and precipitation as rising GHGs. Changes in plant habitat changes are significant in three latitudinal zones, 10°-25°S, 15°-30°N, and 50°-65°N which are transitional regions of ecotone. In both 10°-25°S and 15°-30°N, tropical habitats are expanded accompanying poleward shift in temperature habitats. Fraction of boreal habitats is significantly decreased in latitudes 50°-65°N due to northward propagation of temperate habitats. Projected plant habitat changes are amplified with the magnitude of increase in global mean temperature.

In addition to spatial changes, the temporal side of plant habitat changes is clarified the timing of particular amounts of plant habitat change. The timing of plant habitat change is estimated on 6 continents located in latitudes 10°-25°S, 15°-30°N, and 50°-65°N to evaluate regional variability. In mid-latitude, plant habitat changes are relatively fast in Asia and Africa than America, but regional difference is small in high latitudes. Among 6 regions, the southern Africa shows the fastest changes in plant habitat. In worse, nations of weak economic power are concentrated in the southern Africa, thus the vulnerability of plant habitats in southern Africa will increase with continued warming, with potentially terrible economic and ecological consequences. The southern Africa will need the combined efforts of other nations to help mitigate the sudden plant habitat change and its impact on ecosystem and climate.

In chapter 5, lastly, concern of this thesis is returned on changes in land surface dryness. Contrasting to projected increase in land surface dryness in future due to increasing atmospheric water demands, various observations and model results show complex spatial variability of changes in land surface dryness during 20th century, but mechanisms of dryness changes are poorly understood. Thus, investigation of mechanisms of changes in land surface dryness is decided as next target. Land surface dryness is measured by the value of the ratio of PET, computed by Penman-Monteith method to P (PET/P). Over

continental East Asia, trend in overall mean PET/P shows significant changes from decrease to increase around early 1980s with consistent shift in P and PET at that timing. The shift in PET/P is noticeable in the northern and southeastern China, but mechanisms of dryness changes differ over those two regions. In arid northern China, decrease in monsoon rainfall after early 1980s mainly drives the shift in land surface dryness trend, whereas, exponentially increasing saturation vapor pressure due to atmospheric warming shows the largest impact on changes in PET/P over humid southeastern China. Results indicate that the humid area will experiences higher water need in warmer climate, may induce water scarcity.

In this thesis, both variation of precipitation and warming trend are main reason for changes in land surface dryness. Also influence of vegetation feedback could modulate the surface temperature and precipitation, further land surface dryness through changes in evapotranspiration.

Continental East Asia, target region of last study in the present thesis, experiences notable changes in composition of land surface due to urbanization and agricultural needs. The impact of land use/land cover changes (LULCC) on climate is already proved in both observations and model experiments. For example, contribution of urbanization on surface temperature increase is estimated by up to $0.2^{\circ}\text{C decade}^{-1}$ in China. Influences of LULCC may be also considered for examining historical changes in land surface dryness. Actually,

trends in atmospheric water demand show significant difference between urban and rural regions over China during 20th century. The observational evidence indicates that LULCC could be another reason for complexity of spatial changes in land surface dryness in many regions. Thus, quantification of the impact of LULCC on trend in land surface dryness can be a good topic of next study. Also this kind of study will be very helpful to establish a policy for problems associated with water availability in future.

The present thesis used CAM3-DGVM to simulate the response of vegetation in a CO₂ doubled condition and feedback influences of the changes in vegetation. Recently, next version of CAM3-DGVM, Community Earth System Model version 1, is released with new dynamic core and improved physical and chemical parameterizations. The most notable improvement in land surface model is prognostic biogeochemical cycle. Both carbon and nitrogen (CN) cycle is calculated in same time step with other physical processes in Community Land Model version 4 (CLM4). The prognostic CN cycle allows model to simulate vegetation growth adapt to immediately changed conditions of atmosphere and soil. In previous model, the speed of vegetation growth is fixed for each plant habitat changes using satellite-based phenology. Simultaneous vegetation growth shows possibility of new study to examine the impact of each climate variable on vegetation phenology. Lengthening of vegetation phenology due to climate

changes is reported by numerous assessments in globally and locally. Thus, it is valuable work to quantify the impact of various climate parameters on vegetation phenology.

References

- ACIA, 2005: *Arctic Climate Impact Assessment*. Cambridge University Press, 1042 pp.
- Adam, J. C., and D. P. Lettenmaier, 2003: Adjustment of global gridded precipitation for systematic bias. *J. Geophys. Res.*, **108**, 1–14.
- Adger, W. N., and Coauthors, 2007: Assessment of adaptation practices, options, constraints and capacity. *Climate Change 2007: Impacts, adaptation and vulnerability*, M. L. Parry et al., Eds., Cambridge University Press, 717-743.
- Allen, R.G., L.S. Pereira, D. Raes, and M. Smith, 1998: *Crop evapotranspiration – guidelines for computing crop water requirements – FAO Irrigation and drainage Paper 56*.
- Alo, C. A., and G. L. Wang, 2008: Potential future changes of the terrestrial ecosystem based on climate projections by eight general circulation models. *J. Geophys. Res-Biogeoe.*, **113**, G01004, doi:10.1029/2007JG000528.
- Barber, V.A., G.P. Juday, B.P. Finney, 2000: Reduced growth of Alaska white spruce in the twentieth century from temperature-induced drought stress, *Nature*, **405**, 668-672
- Bellard, C., C. Bertelsmeier, P. Leadley, W. Thuiller, and F. Courchamp, 2012: Impacts of climate change on the future of biodiversity. *Ecol. Lett.*, **15**, 365–377.

- Bonan, G. B., Coauthors, 2002: The land surface climatology of the Community Land Model coupled to the NCAR Community Climate Model, *J. Clim.*, **15**, 3123-3149.
- Bonan, G.B., S. Levis, S. Sitch, M. Vertenstein, K.W. Oleson, 2003: A dynamic global vegetation model for use with climate models: Concepts and description of simulated vegetation dynamics. *Glob. Change. Biol.*, **9(11)**, 1543–1566.
- Bonan, G.B., S. Levis, 2006: Evaluating aspects of the Community Land and Atmosphere Models (CLM3 and CAM3) using a dynamic global vegetation model. *J. Clim.*, **19**, 2290-2301.
- Bonan, G. B., 2008: Forests and climate change: Forcings, feedbacks, and the climate benefits of forests. *Science*, **320**, 1444–1449.
- Bounoua, L., and Coauthors, 2010: Quantifying the negative feedback of vegetation to greenhouse warming: A modeling approach. *Geophys. Res. Lett.*, **37**, L23701 doi:10.1029/2010gl045338.
- Burke, E.J., S.J. Brown, 2008: Evaluating uncertainties in the projection of future drought. *J. Hydrometeorol.*, **9**, 292–299.
- Cardinale, B. J., and Coauthors, 2012: Biodiversity loss and its impact on humanity. *Nature*, **486**, 59–67, doi:10.1038/Nature11148.
- Chan, M. A. K., L. Hoshizaki, and B. Klinkenberg, 2011: Ecosystem services in

- conservation planning: Targeted benefits vs. co-benefits or costs? *PLoS One*, **6**, doi:10.1371/journal.pone.0024378.
- Chapin, F. S., and Coauthors, 2005: Role of land-surface changes in Arctic summer warming. *Science*, **310**, 657–660.
- Chen, M., P. Xie, J. Janowiak, P.A. Arkin, 2002: Global land precipitation: A50-yr monthly analysis based on gauge observation. *J. Hydrometeorol.*, **3**, 249–266.
- Chou, C., and Coauthors, 2013: Increase in the range between wet and dry season precipitation. *Nature Geosci.* **6**, 263-267.
- Christensen, J.H., B. Hewitson, A. Busuioc, A. Chen, X. Gao, I. Held, R. Jones, R.K. Killi, W.-T. Kwon, R. Laprise, V.M. Rueda, L. Mearns, C.G. Menendez, J. Raisanen, A. Rinke, A. Sarr, P. Whetton, 2007: Regional climate projections. In: Solomon S., D. Qin, M. Manning, Z. Chen, M. Marquis, K.B. Averyt, M. Tignor, H.L. Miller (eds) *Climate change 2007: The physical science basis. Contribution of Working Group I to the fourth assessment report of the intergovernmental panel on climate change.* Cambridge University Press, Cambridge.
- Collins, W.D., coauthors, 2004: Description of the NCAR Community Atmosphere Model (CAM 3.0). Technical Note NCAR/TN-464+STR, National Center for Atmospheric Research, Boulder, CO, 214pp.

- Collins, W.D., coauthors, 2006: The Community Climate System Model Version 3 (CCSM3). *J. Clim.*, **19**, 2122-2243
- Cowling, S.A., C.D. Jones, P.M. Cox, 2009: Greening the terrestrial biosphere: simulated feedbacks on atmospheric heat and energy circulation, *Clim. Dyn.*, **32**, 287-299.
- Cramer, W., and Coauthors, 2001: Global responses of terrestrial ecosystem structure and function to CO₂ and climate change: Results from six dynamic global vegetation models. *Global Change Biol.*, **7**, 357–374. doi:10.1046/j.1365-2486.2001.00383.x.
- Dai, A., 2012: Increasing drought under global warming in observations and models. *Nature Clim. Change*. **3**, 52-28.
- Das, S., and J. R. Vincent, 2009: Mangroves protected villages and reduced death toll during Indian super cyclone. *P. Natl. Acad. Sci. USA*, **106**, 7357–7360, 0027-8424, doi:10.1073/pnas.0810440106.
- Denman, K.L., G. Brasseur, A. Chidthaisong, P. Ciais, P.M. Cox, R.E. Dickinson, D. Hauglustaine, C. Heinze, E. Holland, D. Jacob, U. Lohmann, S. Ramachandran, P.L. da Silva Dias, S.C. Wofsy and X. Zhang (2007) Couplings Between Changes in the Climate System and Biogeochemistry. In Solomon, S., D. Qin, M. Manning, Z. Chen, M. Marquis, K.B. Averyt, M.Tignor and H.L. Miller (eds) *Climate change 2007: The Physical Science*

- Basis. Contribution of Working Group I to the Fourth Assessment Report of the Intergovernmental Panel on Climate Change. Cambridge University Press, Cambridge.
- Diffenbaugh, N.S., 2009: Influence of modern land cover on the climate of the United States. *Clim. Dyn.*, **33**, 945–958.
- Dillon, M. E., G. Wang, and R. B. Huey, 2010: Global metabolic impacts of recent climate warming. *Nature*, **467**, 704–707.
- Ding, Y., Z. Wang, and Y. Sun, 2008: Inter-decadal variation of the summer precipitation in East China and its association with decreasing Asian summer monsoon. Part I: Observed evidences. *Int. J. Climatol.* **28**, 1139-1161.
- Edmonds J.A., N.J. Rosenberg, 2005: Climate change impacts for the conterminous USA: An integrated assessment summary. *Clim. Change*, **69**, 151–162.
- Fan, Y., H. van den Dool (2008) A global monthly land surface air temperature analysis for 1948-present. *J. Geophys. Res.*, 113:D01103 doi:10.1029/2007JD008470.
- Feddema, J.J. (2005a) A revised Thornthwaite-type global climate classification. *Physical Geography* 26: 442–466.
- Feng, S., R.J. Oglesby, C.M. Rowe, D.B. Loope, Q. Hu (2008) Atlantic and

- Pacific SST influences on Medieval drought in North America simulated by the Community Atmospheric Model. *J. Geophys. Res.*, 113, D11101,doi:10.1029/2007JD009347.
- Feng, S., Q. Fu, 2013: Expansion of global drylands under a warming climate. *Atmos. Chem. Phys.* **13**, 10081-10094.
- Field, C.B., L.D. Mortsch, M. Brklacich, D.L. Forbes, P. Kovacs, J.A. Patz, S.W. Running, M.J. Scott (2007) North America. In Parry, M., O. Canziani, J. Palutikof, P. Linden, C. Hansen (eds) *Climate change 2007: Impacts, adaptation and vulnerability. Contribution of Working Group II to the fourth assessment report of the Intergovernmental Panel on Climate Change.* Cambridge University Press, Cambridge.
- Fischlin, A., and Coauthors, 2007: Ecosystems, their properties, goods and services. *Climate Change 2007: Impacts, adaptation and vulnerability*, M. L. Parry et al., Eds., Cambridge University Press, 211-272.
- Foley. J. A., and Coauthors, 2011: Solutions for a cultivated planet. *Nature*, **478**, 337–342.
- Forbes, B. C., M. M. Fauria, and P. Zetterberg, P., 2010: Russian Arctic warming and ‘greening’ are closely tracked by tundra shrub willows. *Global Change Biol.*, **16**, 1542–1554.
- Friedl, M. A., and Coauthors, 2002: Global land cover mapping from MODIS:

- Algorithms and early results. *Remote Sens. Environ.*, **83**, 287–302.
- Friedl, M. A., and Coauthors, 2010: MODIS collection 5 global land cover: Algorithm refinements and characterization of new datasets. *Remote Sens. Environ.*, **114**, 168-182.
- Ge, Q., F. Wang, F., and J. Luterbacher, 2013: Improved estimation of average warming trend of China from 1951-2010 based on satellite observed land-use data. *Clim. Change* **121**, 365-379.
- Geng, Q.L., and Coauthors, 2014: Dry/wet climate zoning and delimitation of arid areas of Northwest China based on a data-driven fashion. *J. Arid. Land.* **6**, 287-299.
- Gong, D.-Y., and C.-H. Ho, 2004: Detection of large-scale climate signals in spring vegetation index (normalized difference vegetation index) over the Northern Hemisphere, *J. Geophys. Res.*, **108**, 4498, doi:10.1029/2002JG002300
- Giam, X., C. J. A. Bradshaw, H. T. W. Tan, and N. S. Sodhi, 2010: Future habitat loss and the conservation of plant biodiversity. *Biol. Conserv.*, **143**, 1594–1602.
- Gonzalez, P., R. P. Neilson, J. M. Lenihan, and R. J. Drapek, 2010: Global patterns in the vulnerability of ecosystems to vegetation shifts due to climate change. *Global Ecol. Biogeogr.*, **19**, 755–768.

- Greve, P., and Coauthors, 2014: Global assessment of trends in wetting and drying over land. *Nature Geosci.* **7**, 716-721.
- Han, S., D. Xu, and S. Wang, 2012: Decreasing potential evaporation trends in China from 1956 to 2005: Accelerated in regions with significant agricultural influence? *Agric. Forest Meteorol.* **154-155**, 44-56.
- Harris, I., P. D. Jones, T. J. Osborn, and D. H. Lister, 2012: Updated high-resolution grids of monthly climatic observations—the CRU TS3.10 dataset. *Int. J. Climatol.* (submitted).
- Hartley, I. P., and Coauthors, 2012: A potential loss of carbon associated with greater plant growth in the European Arctic. *Nature Climate Change*, **2**, 875–879.
- Hegerl, G.C., F.W. Zwiers, N.P. Braconnot, N.P. Gillett, Luo Y, J.A. Marengo Orsini, N. Nicholls, J.E. Penner, P.A. Stott, 2007: Understanding and attributing climate change. In: Solomon S., D. Qin, M. Manning, Z. Chen, M. Marquis, K.B. Averyt, M. Tignor, H.L. Miller (eds) *Climate change 2007: the physical science basis. Contribution of Working Group I to the fourth assessment report of the Intergovernmental Panel on Climate Change.* Cambridge University Press, Cambridge.
- Hegerl, G.C., and Coauthors, 2015: Challenges in quantifying changes in the global water cycle. *Bull. Amer. Meteor. Soc.* **96**, 1097-1115.

- Held, I.M., and B.J. Soden, 2006: Robust responses of the hydrological cycle to global warming. *J. Clim.* **19**, 5686-5699.
- Hightower, M., S.A. Pierce, 2008: The energy challenge. *Nature*, **452**, 285–286.
- Hoekstra, A.Y., and M.M. Mekonnen, 2012: The water footprint of humanity. *Proc. Natl Acad. Sci.* **109**, 3232-3237.
- Huo, Z., and Coauthors, 2013: Effect of climate change on reference evapotranspiration and aridity index in arid region of China. *J. Hydrol.* **492**, 24-34.
- IPCC, 2007: Summary for policymakers. *Climate Change 2007: Impacts, adaptation and vulnerability*, M. L. Parry et al., Eds., Cambridge University Press, 7-22.
- Jackson, R.B., Coauthors, 2008: Protecting climate with forests. *Environ. Res. Lett.*, doi:10.1088/1748-9326/3/4/044006.
- Jeong, S.-J., C.-H. Ho, K.-Y. Kim, J.-H. Jeong, 2009: Reduction of spring warming over East Asia associated with vegetation feedback. *Geophys. Res. Lett.*, **36**, L18705, doi: 10.1029/2009GL039114.
- Jeong, S.-J., C.-H. Ho, T.-W. Park, J. Kim, and S. Levis, 2011a: Impact of vegetation feedback on the temperature and its diurnal range over the Northern Hemisphere during summer in a $2 \times \text{CO}_2$ climate. *Clim. Dynam.*, **37**, 821–833.

- Jeong, S.-J., C.-H. Ho, M. E. Brown, J.-S. Kug, S. Piao, 2011b, Browning in desert boundaries in Asia in recent decades. *J. Geophys. Res.*, **116**, doi:10.1029/2010JD014633.
- Jia, G. J., H. E. Epstein, and D. A. Walker, 2009: Vegetation greening in the Canadian arctic related to decadal warming. *J. Environ. Monitor.*, **11**, 2231–2238.
- Jiang, Y., and Coauthors, 2012: Uncertainty analysis of vegetation distribution in the northern high latitudes during the 21st century with a dynamic vegetation model. *Ecol. Evol.*, **2**, 593–614.
- Joshi, M., E. Hawkins, R. Sutton, J. Lowe, and D. Frame, 2011: Projections of when temperature change will exceed 2°C above pre-industrial levels. *Nature Climate Change*, **1**, 407–412.
- Kundzewicz, Z.W., L.J. Mata, N.W. Arnell, P. Doll, P. Kabat, B. Jimenez, K.A. Miller, T. Oki, Z. Sen, I.A. Shiklomanov, 2007: Freshwater resources and their management. In Parry, M., O. Canziani, J. Palutikof, P. Linden, C. Hansen (eds) *Climate change 2007: Impacts, adaptation and vulnerability. Contribution of Working Group II to the fourth assessment report of the Intergovernmental Panel on Climate Change*. Cambridge University Press, Cambridge.
- Lambin, E. F., and P. Meyfroidt, 2011: Global land use change, economic

- globalization, and the looming land scarcity. *P. Natl. Acad. Sci. USA*, **108**, 3465–3472.
- Le Houerou, H.N., 1996: Climate change, drought and desertification. *J. Arid. Env.*, **34(2)**, 133–185.
- Levis, S., J.A. Foley, D. Pollard, 2000: Large-scale vegetation feedbacks on doubled CO₂ climate. *J. Clim.*, **13**, 1313–1325.
- Levis, S., G.B. Bonan, M. Vertenstein, K.W. Oleson, 2004: The Community Land Model's Dynamic Global Vegetation Model (CLM-DGVM): Technical description and user's guide. Technical Note NCAR/TN-459+IA, National Center for Atmospheric Research, Boulder, Colorado, 50 pp.
- Liu, Z., M. Notaro, J. Kutzbach, N. Liu, 2006: Assessing global vegetation-climate feedbacks from observations. *J. Clim.*, **19**, 787–814.
- Liu, M., Y. Shen, Y. Zeng, and C. Liu, 2010: Trends of pan evaporation in China in recent 50 years in China. *J. Geogr. Sci.* **20**, 557-568.
- Liu, H.W., T.J. Zhou, Y.X. Zhu, and Y.H. Lin, 2012: The strengthening East Asia summer monsoon since the early 1990s. *Chinese Sci. Bull.* **57**, 1553-1558.
- Liu, X., D. Zhang, Y. Luo, and C. Liu, 2013: Spatial and temporal changes in aridity index in northwest China: 1960 to 2010. *Theor. Appl. Climatol.* **112**, 307-316.
- Lucht, W., S. Schaphoff, T. Erbrecht, U. Heyder, and W. Cramer, 2006:

- Terrestrial vegetation redistribution and carbon balance under climate change. *Carbon Balance and Management*, **1**, doi:10.1186/1750-0680-1-6.
- Mather, J.R., J.J. Feddema, 1986: Hydrologic consequences of increases in trace gases and CO₂ in the atmosphere. In: James GT Effects of changes in stratospheric ozone and global climate volume 3: climate change, U.S. Environmental Protection Agency, Washington D.C.
- Maurer, E. P., J. C. Adam, and A. W. Wood, 2009: Climate model based consensus on the hydrologic impacts of climate change to the Rio Lempa basin of Central America. *Hydrology and Earth System Sciences*, **13**, 183–194.
- McCabe, G.J., D.M. Wolock, L.E. Hay, M.A. Ayers, 1990: Effects of climate change on the Thornthwaite moisture index. *Journal of the American Water Resources Association*, **26**, 633–643.
- McCabe, G.J., D.M. Wolock, 1992: Effects of climatic change and climatic variability on the Thornthwaite moisture index in the Delaware River basin. *Clim. Change*, **20**, 143–153.
- McKee, T.B., N. J. Doesken, J. Kleist, 1993: The relationship of drought frequency and duration to time scales. In Proceedings of the 8th Conference of Applied Climatology, 17-22 January 1993, Anaheim, CA. American Meteorological Society. pp.179-184.

- Meehl, G. A., and Coauthors, 2007a: The WCRP CMIP3 multi-model dataset: A new era in climate change research. *Bull. Amer. Meteor. Soc.*, **88**, 1383–1394.
- Meehl, G.A., and Coauthors, 200b: Global climate projection. *Climate Change 2007: The Physical Science Basis*, S. Solomon et al., Eds., Cambridge University Press, 747-846.
- Menzel, A., P. Fabian, 2000: Growing season extended in Europe. *Nature*. **397**, 659.
- Morin, X., and W. Thuiller, 2009: Comparing niche- and process-based models to reduce prediction uncertainty in species range shifts under climate change. *Ecology*, **90**, 1301–1313.
- Myneni, R.B., C.D. Keeling, C.J. Tucker, G. Asrar, R.R. Nemani, 1997: Increased plant growth in the northern high latitudes from 1981 to 1991, *Nature*, **386**, 698-702.
- Naidoo, R., and Coauthors, 2006: Integrating economic costs into conservation planning. *Trend in Ecology and Evolution*, **21**, 681–687.
- Naidoo, R., and T. H. Ricketts, 2006: Mapping the economic costs and benefits of conservation. *PLoS Biology*, **4**, e360, doi:10.1371/journal.pbio.0040360.
- Neale, R.B., Coauthors, 2010: Description of the NCAR Community Atmosphere Model (CAM 4.0). Technical Note NCAR/TN-???+STR,

- National Center for Atmospheric Research, Boulder, CO, 206pp.
- Nilsson, M., and A. Persson 2012: Reprint of “Can Earth system interactions be governed? Governance functions for linking climate change mitigation with land use, freshwater and biodiversity protection”. *Ecological Economics*, **75**, 61–71.
- Notaro, M., Z. Liu, J.W. Williams, 2006: Observed vegetation-climate feedbacks in the United States. *J. Clim.*, **19**, 763–785.
- Oleson, K.W., Coauthors, 2010: Technical Description of version 4.0 of the Community Land Model (CLM). Technical Note NCAR/TN-478+STR, National Center for Atmospheric Research, Boulder, CO, 257pp.
- Park, C.-E., C.-H. Ho, S.-J. Jeong, J. Kim, and S. Feng, 2012: Impact of vegetation on feedback to alleviate climate aridity over the United States associated with a $2 \times \text{CO}_2$ climate condition, *Clim. Dynam.*, **38**, 1489-1500, doi:10.1008/s00382-011-1150-x.
- Parmesan, C., and G. Yohe, 2003: A globally coherent fingerprint of climate change impacts across natural systems. *Nature*, **421**, 37–42.
- Pearson, R. G., and T. P. Dawson, 2003: Predicting the impacts of climate change on the distribution of species: are bioclimate envelope models useful? *Global Ecol. Biogeogr.*, **12**, 361–374.
- Penman, H.L., 1948: Natural evaporation from open water, bare soil and grass.

- Proc. Roy. Soc. Lond.* **193**, 120-145.
- Piao, S., A. Mohammat, J. Fang, Q. Cai, J. Feng, 2005: NDVI-based increase in growth of temperate grasslands and its responses to climate changes in China. *Glob. Env. Change*, **16**, 340-348.
- Piao, S., and Coauthors, 2010: The impacts of climate change on water resources and agriculture in China. *Nature* **467**, 43-51.
- Rosenzweig, C., and Coauthors, 2007: Assessment of observed changes and responses in natural and managed systems. *Climate Change 2007: Impacts, adaptation and vulnerability*, M. L. Parry et al., Eds., Cambridge University Press, 79-131.
- Rosenzweig, C., and Coauthors, 2008: Attributing physical and biological impacts to anthropogenic climate change. *Nature*, **453**, 353–358.
- Sala, O., 2005: Biodiversity across scenarios. *Millenium Ecosystem Assessment, volume 2: Scenarios*. Island Press, 375-408.
- Scholze, M., W. Knorr, N. W. Arnell, and I. C. Prentice, 2006: A climate-change risk analysis for world ecosystems. *P. Natl. Acad. Sci. USA*, **103**, 13116–13120.
- Seager, R., A. Tzanova, J. Nakamura, 2009: Drought in the southeastern United States: Causes, variability over the last millennium, and the potential for future hydroclimate change. *J. Clim.*, **22(19)**, 5021–5045.

- Sheffield, J., G. Goteti, E.F. Wood, 2006: Development of a 50-Year High-Resolution Global Dataset of Meteorological Forcings for Land Surface Modeling. *J. Clim.*, **19**, 3088-3111
- Sheffield, J., E.F. Wood, 2008: Projected changes in drought occurrence under future global warming from multi-model, multi-scenario, IPCC AR4 simulations. *Clim. Dyn.*, **31**, 79–105.
- Sherwood, S., and Q. Fu, 2014: A Drier Future? *Science* **343**, 737-739.
- Shi, Y., and Coauthors, 2007: Recent and future climate change in northwestern China. *Clim. Change* **80**, 379-393.
- Sitch, S., and Coauthors, 2003: Evaluation of ecosystem dynamics, plant geography and terrestrial carbon cycling in the LPJ dynamic global vegetation model. *Global Change Biol.*, **9**, 161–185.
- Sitch, S., and Coauthors, 2008: Evaluation of the terrestrial carbon cycle, future plant geography and climate-carbon cycle feedbacks using five dynamic global vegetation models (DGVMs). *Global Change Biol.*, **14**, 2015–2039.
- Song, S., L. Li, X. Chen, and J. Bai, 2015: The dominant role of heavy precipitation in precipitation change despite opposite trends in west and east of northern China. *Int. J. Climatol.* doi:10.1002/joc.4290.
- Sturm, M., C. Racine, and K. Tape, 2001: Climate change–increasing shrub abundance in the Arctic. *Nature*, **411**, 546–547.

- Sulla-Menashe, D., and Coauthors, 2011: Hierarchical mapping of Northern Eurasian land cover using MODIS data. *Remote Sens. Environ.*, **115**, 392-403
- Tang, W.-J., and Coauthors, 2011: Solar radiation trend across China in recent decades: a revisit with quality-controlled data. *Atmos. Chem. Phys.* **11**, 393-406.
- Thomas, J. A., and R. T. Clarke, 2004: Extinction risk from climate change. *Nature*, **427**, 145–148.
- Thornthwaite, C.W., 1948: An approach toward a rational classification of climate. *Geogr. Rev.*, **38**, 55–94.
- Trenberth, K.E., P.D. Jones, P. Ambenje, R. Bojariu, D. Easterling, A.K. Tank, D. Parker, F.Rahimzadeh, J.A. Renwich, M. Rusticucci, B. Soden, P. Zhai, 2007: Observations: Surface and atmospheric climate change. In: Solomon S., D. Qin, M. Manning, Z. Chen, M. Marquis, K.B. Averyt, M. Tignor, H.L. Miller (eds) *Climate change 2007: the physical science basis. Contribution of Working Group I to the fourth assessment report of the Intergovernmental Panel on Climate Change*. Cambridge University Press, Cambridge.
- Turner, W. R., M. Oppenheimer, D. S., Wilcove, 2009: A force to fight global warming. *Nature*, **462**, 278–279.

- van Mantgem, P.J., Coauthors, 2009: Widespread increase of tree mortality rates in the western United States. *Science*, **323(5913)**, 521–524.
- United Nations Environment Programme (UNEP), 2009: *Global Deserts Outlooks*. Eds. Ezcurra, Nairobi, 164pp.
- United Nations Framework Convention on Climate Change (UNFCCC), 2007: Investment and financial flows to address climate change. UNFCCC, 273pp.
- Wang, G., 2005: Agricultural drought in a future climate: results from 15 global climate models participating in the IPCC 4th assessment. *Clim. Dyn.*, **25**, 739–753.
- Wang, B., and Q. Ding, 2006: Changes in global monsoon precipitation over the past 56 years. *Geophys. Res. Lett.* **33**, L06711.
- Wang, L., and W. Chen, 2014: A CMIP5 multimodel projection of future temperature, precipitation, and climatological drought in China. *Int. J. Climatol.* **34**, 2059-2078.
- Williams, J. W., S. T. Jackson, and J. E. Kutzbach, 2007: Projected distributions of novel and disappearing climates by 2100 AD. *P. Natl. Acad. Sci. USA*, **104**, 5738–5742.
- Williamson, D.L., 2002: Time-split versus process-split coupling of parameterizations and dynamical core. *Mon. Wea. Rev.*, **130**, 2024-2041
- Wilmking, M., Juday, G.P., Barber, V.A., Zald, H.S., 2004: Recent climate

- warming forces contrasting growth responses of white spruce at treeline in Alaska through temperature thresholds, *Glob. Change Biol.*, **10**, 1724–1736, 2004.
- Wood, A. W., L. R. Leung, V. Sridhar, and D. P. Lettenmaier, 2004: Hydrologic implications of dynamical and statistical approaches to downscaling climate model outputs. *Climatic Change*, **62**, 189–216.
- Wu, S., Y. Yin, D. Zheng, and Q. Yang, 2006: Moisture conditions and climate trends in China during the period 1971-2000. *Int. J. Climatol.* **26**, 193-206.
- The World Bank, 2012: *Gross domestic production 2011 included in World development indicators*.
<http://databank.worldbank.org/databank/download/GDP.pdf>.
- Xu, L., and Coauthors, 2013: Temperature and vegetation seasonality diminishment over northern lands. *Nature Climate Change*, **3**, 581–586, doi::10.1038/nclimate1836.
- Yin, Y., D. Ma, S. Wu, and T. Pan, 2015: Projections of aridity and its regional variability over China in the mid-21st century. *Int. J. Climatol.* doi:10.1002/joc.4295.
- Yohe, G.W., R.D. Lasco, Q.K. Ahmad, N.W. Arnell, S.J. Cohen, C. Hope, A.C. Janetos, R.T. Perez, 2007: Perspectives on climate changes and sustainability. In Parry, M., O. Canziani, J. Palutikof, P. Linden, C. Hansen

- (eds) Climate change 2007: Impacts, adaptation and vulnerability. Contribution of Working Group II to the fourth assessment report of the Intergovernmental Panel on Climate Change. Cambridge University Press, Cambridge.
- Yue, T.-X., and Coauthors, 2013: Climate change trend in China, with improved accuracy. *Clim. Change* **120**, 137-151.
- Zhang, J., J.E. Walsh, 2006: Thermodynamic and hydrological impacts of increasing greenness in northern high latitudes. *J. Hydrometeorol.*, **7**, 1147–1163.
- Zhang, L.X., and T.J. Zhou, 2011: An assessment of monsoon precipitation changes during 1901-2001. *Clim. Dyn.* **37**, 279-296.
- Zhou, L.M., C.J. Tucker, R.K. Kaufmann, D. Slayback, N.V. Shabanov, and R.B. Myneni, 2001: Variations in northern vegetation activity inferred from satellite data of vegetation index during 1981-1999, *J. Geophys. Res.*, **106**, 20,069-20,083.
- Zhu, C., B. Wang, W. Qian, and B. Zhang, 2012: Recent weakening of northern East Asian summer monsoon: A possible response to global warming. *Geophys. Res. Lett.* **39**, doi:10.1029/2012GL051155.

국문 초록

기후 변화에 따라 지속적으로 변화하는 지면의 특성 중, 식생과 지표 건조도의 변화는 지면의 반응들 중에서도 가장 중요한 두 가지라 할 수 있다. 식생은 지면의 70%를 차지할 뿐 아니라 지면의 물리, 화학 과정에 지대한 영향을 끼치는 요소로서 식생 변화 및 그에 따른 되먹임 효과에 대한 연구는 현재 기후 변화에 대한 이해 및 미래 기후 예측에 있어 매우 중요한 요소이다. 또한 지표 건조도 변화는 지면 물 순환 변화와 밀접하게 관련되어 있으며 농업과 물 관리의 측면에서 매우 중요하게 다루어지고 있다. 식생 및 지표 건조도 변화는 기후뿐 아니라 사회, 경제적으로도 큰 영향을 끼치며 이에 따라 관련 연구들은 기후 변화 적응 및 완화에 있어 매우 중요하다. 본 학위 논문은 식생 및 지표 건조도에 대한 세 가지 연구 내용으로 이루어져 있다.

첫 번째로 미국 지역에서 이산화탄소 배증에 의한 식생 증가의 효과가 여름철 지표 건조도를 감소시키는 것을 식생 역학 모델이 접합된 전구기후모델 실험을 통해 밝혀내었다. 지표 건조도는 Thornthwaite의 습윤 지수(Thornthwaite's moisture index)를 이용하여 측정하였으며 습윤 지수의 변화를 통해 미국 지역의 건조도가 증가 혹은 감소하는 것을 보였다. 이산화탄소 배증 시 미국 지역의 지표 건조도가 증가하며 이는 늘어난 강수량보다 온도 증가에 따른 잠재증발량(potential evapotranspiration)의 증가량이 더 크기 때문이다. 이 때, 식생 변화가 고려될 경우, 이산화탄소 및 온도 증가에 따른 식생 밀도의 증가는 지표면에서의 증발량 및 이에 따른 잠열 방출을 활발하게 하여 기온 증가를 완화하는 효과가 있고, 이는 결국 지표 건조도를 낮추는 것으로 나타난다. 이와 같은 효과는 특히 식생 밀도 증가가 뚜렷한 미국 동부 및 동남부, 북서부에서 뚜렷하게 나타나고 있다.

두 번째 연구는 온난화에 따른 21세기의 식생 서식지 변화 시기를 세 개의 온난화 강도에 따라 측정하였다. 식생 서식지의 정의는 현재 식생 역학

모델에서 식생 구분을 위해 쓰는 생물기후학적 규칙 (bio-climate rule)을 이용하였으며 실제 식생 구분 및 식생 변화 시기 예측을 위한 현재 및 미래 기후 자료는 IPCC 4차 보고서에 쓰인 16개의 전구 기후 모형을 이용하여 생산되었다. 식생 변화 시기는 각 식생 서식지의 변화 비율이 처음으로 10%, 20%, 30%가 되는 시기로 정의하였다. 또한 식생 변화 시기와 온난화 강도와와의 관계를 알기 위하여 전구 평균 지면 온도 변화 (ΔT)를 이용, 미래 예측 자료를 약한 온난화 ($\Delta T < 2.5K$), 중간 온난화 ($2.5K < \Delta T < 3.5K$), 강한 온난화 ($\Delta T > 3.5K$)의 세 가지로 나누어 식생 변화 시기를 추정하였다. 분석 결과, 21세기 식생 변화는 온난화 강도와 관계 없이 다른 종의 식생이 같이 분포하는 지역에서 뚜렷하게 나타나는 것을 확인하였다. 식생 변화 시기는 온난화가 심할수록 빨라졌으며 남부 아프리카 및 아시아 지역에서의 식생 변화 시기가 같은 위도의 다른 지역에 비해 매우 빠른 것으로 나타났다. 특히 남부 아프리카 지역에서의 식생 변화가 가장 빠르게 나타났는데, 온난화가 약한 경우에도 식생이 10%만큼 변화하는 시기가 아메리카 대륙에 비해 약 70년이나 빠른 것을 확인하였다. 이에 더해 식생 변화가 빠르게 나타나는 아프리카 및 아시아 지역은 경제력이 낮은 국가가 밀집되어 있어 식생 변화에 의한 피해가 더욱 크게 나타날 가능성이 있는 것으로 분석되었다.

마지막으로 최근 동아시아 지역에서 나타나는 지표 건조도 변화에 대한 5가지 주요 기후 요소들의 영향을 정량적으로 측정하여 지표 건조도 변화의 원인을 제시하였다. 위의 분석을 위해 동아시아의 189개 기상 관측 지점에서 제공하는 1961년부터 2010년까지 50년 동안의 일별 기후 자료를 이용하였으며 해당 지역을 수문학적으로 습윤, 반건조, 건조의 세 가지 지역으로 나누어 분석하였다. 동아시아는 전체 기간에 대해서는 습윤해지는 것처럼 보이나 실제로는 1980년대 초반부터 건조해지는 것을 알 수 있다. 이는 몬순의 영향을 받는 동경 100° 동쪽 지역에서 나타나며 건조 지역과 습윤 지역에서 뚜렷하게 나타나고 있다. 건조 지역의 건조화 경향은 강수량 감소가 주요 원

인이나 습윤 지역의 경우, 온도 증가에 따른 상대 습도 감소가 가장 중요한 원인인 것으로 나타났다.

본 학위 논문의 연구 결과들이 시사하는 점은 다음과 같이 세 가지가 있다. 첫 번째로 증가한 식생의 되먹임 효과에 따른 지표 건조도 감소 결과는 기후 변화에 취약한 지역에서 뚜렷하기 때문에 건조화에 대한 완화 대책에 중요할 것이다. 두 번째로 경제력이 약한 아시아 및 아프리카 지역의 빠른 식생 변화 및 이에 따른 피해를 줄이기 위한 국제적인 공조가 필요하다는 것을 알려준다. 마지막으로 온난화에 의한 지표 건조도 상승은 매우 급격하게 나타나고 있으므로 미래의 물 부족을 피하기 위해서는 이를 고려한 물 관리 정책이 필요하다는 것이다.

주요어: 기후 변화, 식생 변화, 지표 건조도, 식생 되먹임, 건조 지수,
대기의 물 요구량

학 번: 2010-30105



저작자표시-비영리-변경금지 2.0 대한민국

이용자는 아래의 조건을 따르는 경우에 한하여 자유롭게

- 이 저작물을 복제, 배포, 전송, 전시, 공연 및 방송할 수 있습니다.

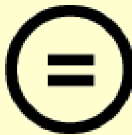
다음과 같은 조건을 따라야 합니다:



저작자표시. 귀하는 원저작자를 표시하여야 합니다.



비영리. 귀하는 이 저작물을 영리 목적으로 이용할 수 없습니다.



변경금지. 귀하는 이 저작물을 개작, 변형 또는 가공할 수 없습니다.

- 귀하는, 이 저작물의 재이용이나 배포의 경우, 이 저작물에 적용된 이용허락조건을 명확하게 나타내어야 합니다.
- 저작권자로부터 별도의 허가를 받으면 이러한 조건들은 적용되지 않습니다.

저작권법에 따른 이용자의 권리는 위의 내용에 의하여 영향을 받지 않습니다.

이것은 [이용허락규약\(Legal Code\)](#)을 이해하기 쉽게 요약한 것입니다.

[Disclaimer](#)

Thesis for a Ph. D. Degree

A study on changes in the vegetation
and land surface dryness
in present and future climate

현재 및 미래기후에서의 식생 및
지면 건조도 변화에 대한 연구

Chang-Eui Park

February 2016

School of Earth and Environmental Sciences

Graduate School

Seoul National University

A study on changes in the vegetation
and land surface dryness
in present and future climate

By
Chang-Eui Park

Dissertation Submitted to the Faculty of the Graduate School of the
Seoul National University in Partial Fulfillment of the Requirement
for the Degree of Doctor of Philosophy

Degree Awarded:
February 2016

Advisory committee:

Professor	Wookap Choi, Chair
Professor	Chang-Hoi Ho,
Professor	Song-You Hong
Professor	Eun-Ju Lee
Professor	Yong-Sang Choi
Doctor	Kwang-Ya Lee

이학박사학위논문

현재 및 미래기후에서의 식생 및
지면 건조도 변화에 대한 연구

A study on changes in the vegetation and land surface
dryness in present and future climate

2016년 2월

서울대학교 대학원

지구환경과학부

박 창 의

Abstract

Historical observations show various responses to global warming over the land surface, one of important elements of Earth's climate system as well as living place of humanity. Among those responses over the land, both changes in vegetation and land surface dryness are regarded as two major phenomena. Vegetation, occupies about 70% of whole land surface, is a key element of both physical and chemical processes over the land surface. Exact understanding of the vegetation change and its feedback influences on climate is essential for both investigating observed climate change and projection of future climate. Changes in land surface dryness are invisible, but important for the hydrological condition over the land, largely influences on agriculture and water management. Thus, researches on changes in both vegetation and land surface dryness contribute to mitigate risks of climate change because of both vegetation and land surface dryness has numerous socio-economic impacts on society. The present dissertation provides remarkable results of three studies about changes in vegetation and land surface dryness.

First, the potential impact of vegetation feedback on land surface dryness in summer season is examined in a condition of doubling of atmospheric CO₂ concentration over the contiguous United States (US) using a set of 100-year-

long climate simulations integrated by global climate model (GCM) interactively coupled with a dynamic vegetation model. The Thornthwaite moisture index (I_m), which quantifies land surface dryness on the basis of atmospheric water supply (i.e. precipitation, P) and atmospheric water demand (i.e., potential evapotranspiration, PET), is used to measure changes in the surface dryness. Warmer atmosphere and drier surface resulting from increased CO₂ concentration increase land surface dryness over most of the contiguous US. This phenomenon is due to larger increments in PET than in P, regardless of the presence or absence of vegetation feedback. Compared to simulation without active dynamic vegetation feedback, the presence of vegetation feedback significantly alleviates the increase in land surface dryness. This vegetation-feedback effects is most notable in the subhumid regions such as southern, Midwestern and northwestern US, primarily by the increasing vegetation greenness. In these regions, the greening in response to warmer temperatures enhances moisture transfer from soil to atmosphere by evapotranspiration (ET). The increased et and subsequent moistening over land areas result in weaker surface warming (1–2 K) and PET (3–10 mm month⁻¹), and greater P (4–10 mm month⁻¹). Collectively, changes in temperature, PET, and P due to vegetation feedback result in moderate increases in I_m , indicating decrease in land surface dryness.

Next, the change in vegetation due to global warming is examined in detail focusing on its speed during twenty-first century using both a definition of plant habitat based on surface temperature and climate scenarios from multiple GCMs. The plant habitat changes are predicted by driving the bioclimate rule in a dynamic global vegetation model using the climate projections from 16 coupled GCMs. The timing of plant habitat change is estimated by the first occurrence of specified fractional changes (10%, 20%, and 30%). All future projections are categorized into three groups by the magnitude of the projected global-mean land surface temperature changes: low (<2.5K), medium (2.5-3.5K), and high (>3.5K) warming. During the course of the twenty-first century, dominant plant habitat changes are projected in ecologically transitional (i.e., from tropical to temperate and temperate to boreal) regions. The timing of plant habitat changes varies substantially according to regions. In the low-warming group, habitat changes of 10% in southern Africa occur in 2028, earlier than in the Americas by more than 70 yrs. Differences in the timing between regions increase with the increase in warming and fractional threshold. In the sub-tropics, fast plant habitat changes are projected for the Asia and Africa regions, where countries of relatively small gross domestic product (GDP) per capita are concentrated. Ecosystems in these regions will be more vulnerable to global warming, because countries of low economic power lack the capability to deal with the warming-induced habitat

changes.

Causes of changes in land surface dryness are not clear due to various attributions of climate variables on dryness changes. For exact understanding on complex spatial variability of land surface dryness changes, relative influences of five climate variables on dryness changes are quantified over continental East Asia, covering diverse hydro-climate regimes from humid to arid regions, by using observations from 189 stations for the period of 1961-2010. For the whole analysis period, the land surface dryness is decreased by both increasing P and decreasing PET, but the increasing trend is not monotonic. Since early 1980s, increasing trend of the land surface dryness is shown over monsoon climate area ($> 100^{\circ}\text{E}$), but different climate variables drive the drying trend in each hydro-climate regimes. Dryness increases over the arid region are mostly explained by decrease in precipitation. In the humid area, increasing saturation vapor pressure following warming primarily contributes to dry surface despite continuous increase in precipitation. These results suggest increased evaporative potential, the secondary impact of atmospheric warming, plays a considerable role in changes in land surface dryness over the humid area even though sufficient atmospheric moisture exists at there.

Conclusions of the present thesis suggest three meaningful implications. 1)

Moistening by enhanced vegetation feedback may prevent aridification under climatic warming especially in areas vulnerable to climate change, with consequent implication for mitigation strategies. 2) The spatial distribution of plant habitat is projected to change quickly over countries of low economic power located on Asia and Africa. It is important to establish international collaboration via which developed countries provide assistance to mitigate the impacts of global warming. 3) The global warming sharply increases atmospheric water demands, inducing the risk of drying out over the land surface. Water management plans should consider the ongoing trend of drying accompanied by warming to mitigate the water scarcity in future.

Keywords: Vegetation Change, Land Surface Dryness, Climate Change, Vegetation Feedback, Aridity Index, Atmospheric Water Demand

Student Number: 2010-30105

Table of Contents

Abstract	i
Table of Contents.....	vii
List of Tables.....	x
List of Figures	xii
1. Introduction	1
1.1 Backgrounds	1
1.2 Motivation and objectives.....	5
1.3 Thesis organization	12
2. Data and Method	13
2.1 Data.....	14
2.2 Method.....	20

3. Vegetation feedback impact on climate aridity.....	33
3.1 Models	33
3.2 Experimental design.....	37
3.3 Changes in climate types	41
3.4 Changes in LAI and surface evapotranspiration.....	46
3.5 Changes in water supply and water demand	51
3.6 Summary and Discussion	58
3.6.1 Comparison of impact of change in ET with change in vegetation physiology and soil moisture.....	58
3.6.2 Importance of vegetation feedback and limitation of potential vegetation and I_m.....	62
4. Understanding of present and future changes in vegetation.....	65
4.1 Temperature and precipitation in present and future climate.....	65
4.2 Projected changes in spatial distribution of potential plant habitat.....	71
4.3 Projected changes in the timing of plant habitat changes..	79
4.3.1 Regional characteristics of timing of plant habitat change	79
4.3.2 Relationship between national wealth and the timing of plant habitat change	89
4.4 Summary and Discussion	92

5. Significant drying trend over the humid area in continental East Asia by local warming.....	99
5.1 Trend in land surface dryness over continental East Asia.	99
5.2 Causes of changes in land surface dryness	104
5.3 Summary and Discussion	108
6. Conclusions.....	111
References.....	118

국문 초록

감사의 글

List of Tables

Table 2.1. The gross domestic product (GDP) of nations which total or some part of territory is included in each region (The World Bank, 2012).....	19
Table 2.2. Bio-climate limits for plant habitats: $T_{c,min}$ is the minimum coldest-month temperature for survival; $T_{c,max}$ is the maximum coldest-month temperature for survival.....	23
Table 2.3. Future projection of 16 climate models included in three warming thresholds.....	24
Table 2.4. Climate types defined in terms of the original Thornthwaite moisture index.....	27
Table 3.1. Equilibrium experiments using CAM3-DGVM. Identifiers for each simulation, sea surface temperature (SST), atmospheric CO ₂ concentrations (CO ₂), integration time (Years), number of ensemble (Ensembles), and model horizontal resolution (Resolution).	40
Table 4.1. Annual mean temperature and precipitation (\pm standard deviation) of CRU and 20C3M simulations for present-day.....	67
Table 4.2. Projected changes in annual mean temperature and precipitation (\pm standard deviation) for low, medium, and high warming groups in future (2080-2099).	68
Table 4.3. Area of observed and projected plant habitat (10^6 km ²). The numbers	

are the total area (in 10^6 km^2) covered by each climate type. The numbers of in parentheses are one standard deviation of total area (in 10^6 km^2) projected by 12, 18, and 18 projections in low, medium, and high warming groups. 75

Table 4.4. Estimated year that ensemble mean of projected habitat changes firstly exceed 10%, 20%, and 30% threshold for all warming groups in the three latitudes belts. En-dash means that the ensemble means does not reach the three thresholds until 2099. 84

Table 4.5. Estimated year that 10% and 90% of model simulations of projected habitat changes firstly exceed 10%, 20%, and 30% threshold for all warming groups in the three latitudes belts. En-dash means that the ensemble means does not reach the three thresholds until 2099. 86

List of Figures

Figure 3.1. Spatial distribution of Thornthwaite moisture index over the US in boreal summer for VegOff_1× (a), and 30-year climatology of CPC monthly analysis of global surface air temperature and land precipitation for the period 1980–2009 (b).....	44
Figure 3.2. Spatial distribution of changes in Thornthwaite moisture index by radiative effect (a), radiative and vegetation feedback effect (b), and vegetation feedback only (c). Blue dots and red dots represent regions that the climate type change more humid and arid, respectively.....	45
Figure 3.3. Spatial distribution of leaf area index over the US in boreal summer for VegOff_1× (left) and changes in leaf area index between VegOn_2× and VegOff_1× (right). Black dots represent the regions that changes in leaf area are statistically significant at the 95% confidence level.....	49
Figure 3.4. Spatial distribution of changes in total evaporation, canopy evaporation, canopy transpiration, and soil evaporation due to radiative effect (a–d), radiative and vegetation feedback effect (e–h), and vegetation feedback only (i–l). Black dots represent the regions that changes are statistically significant at the 95% confidence level.....	50
Figure 3.5. Spatial distribution of changes in precipitation, temperature, and PET	

over the US due to radiative effect (a-c), radiative and vegetation feedback effect (d-f), and vegetation feedback only (g-i). Black dots represent the regions that changes are statistically significant at the 95% confidence level. 56

Figure 3.6. Scatter plot of the values of I_m in present climate run (VegOff_1x) with respect to ratio of precipitation to PET. Black, blue, and red dots represent the ratio of VegOff_1x, VegOff_2x, and VegOn_2x, respectively. 57

Figure 3.7. Spatial distribution of changes in vertically integrated volumetric soil water due to radiative effect (a), radiative and vegetation feedback effect (b), and vegetation feedback only (c). 61

Figure 4.1. Spatial distributions of averaged temperature of (a) CRU and (b) ensemble of 20C3M simulations, and precipitation of (c) CRU and (d) ensemble of 203CM simulations for present-day (1980-2009). 69

Figure 4.2. Spatial distribution of changes in averaged temperature (2080-2099 minus 1980-1999) for (a) 12 models in low, (b) 18 models in medium, and (c) 18 models in high warming threshold. (d), (e), and (f) show changes in averaged precipitation for low, medium, and high warming threshold. 70

Figure 4.3. Spatial distribution of averaged plant habitat of present day (1980-1999) for (a) CRU and (b) ensemble of 20C3M simulations. Spatial distribution of averaged plant habitat of future projection (2080-2099) for (c) 12 models in low, (d) 18 models in medium, and (e) 18 models in high warming threshold.

Regions with grey shading represent the desert areas. 77

Figure 4.4. Difference of zonal-mean fractional change in plant habitat between the period of 2080–2099 and 1980–1999 for (a) tropical habitat, (b) temperate habitat, and (c) boreal habitat. Red dashed, green solid, and blue dotted line indicates high, medium, and low warming threshold. 78

Figure 4.5. Regional mean fractional changes in plant habitats for (a) 10°–25°S, (b) 15°–30°N, and (c) 50°–65°N. Each projection from the CMIP3 model simulation included in low-, medium-, and high- warming groups are shown in light blue, light green, and light orange. Blue, green, and red bars represent the range of timing when projected habitat changes might cross the 10%, 20%, and 30% thresholds of low-, medium-, and high- warming groups. 88

Figure 4.6. Timing of averaged plant habitat change reaches (a) 10%, (b) 20%, and (c) 30% threshold for GDP per Capita 2012 of Botswana, China, Mexico, Russia, and Canada. Blue, yellow, and red dots represent low, medium, and high warming threshold, respectively. 91

Figure 5.1. Temporal variations of annual mean PET/P, P, and PET in East Asia. a-c, PET/P (a), P (b), and PET (c). Yellow and blue bars indicate that positive and negative anomalies for PET/P and PET, but negative and positive anomalies for P. Black, blue, and red lines are linear regression lines (% decade⁻¹) for the period of 1961-2010, 1961-1983, 1984-2010, respectively. 102

Figure 5.2. Spatial distributions of trends of PET/P, P, and PET in East Asia. a-c, The spatial distribution of trends in annual mean PET/P (a), P (b), and PET (c) for the period of 1961-1983. d-f, as a-c, but for the period of 1984-2010. The empty square indicates that the trend is significant at 95% level. 103

Figure 5.3. Spatial distributions of contributions of the five climate parameters on the PET/P trends in East Asia. a-e, The spatial distribution of the contribution of changes in P (a), Rn (b), WS (c), Ta (d), and RH (e) for the period of 1961-1983. f-j, as a-e, but for the period of 1984-2010. 106

Figure 5.4. Averaged relative influences of five climate parameters on the PET/P changes. a-c, Relative influences ($\% \text{ decade}^{-1}$) of five climate parameters is averaged for the three hydro-climate regimes: arid (a), semi-arid (b), and humid (c). The averaged influences are computed for the two periods of 1961-1983 and 1984-2010. Blue, pink, beige, orange, and cyan bars represent averaged influence of P, Rn, WS, Ta, and RH, respectively. Error bars represent confidence intervals at 95% significance level. 107

Figure 5.5. Schematic diagram explaining the small and large influence of RH on the PET/P trends in the arid and humid regions. The map shows the spatial distributions of annual mean temperature for the period of 1961-2010 (degree C). Empty squares, cross marks, and filled circles are stations that classified by arid, semi-arid, and humid regions, respectively. The map clearly shows that the arid

and humid region of continental East Asia has the cold and warm climate, respectively. In the arid region, warming magnitude is large, but decrease in RH is small following the Clousius-Clapeyron relationship between the saturation vapor pressure (e_s) and T_a (brown line in the graph). In contrast, the increase in the e_s is relatively large in the humid region despite the small warming magnitude (blue line in the graph). The difference in the increment of e_s between two regions causes much larger decrease in RH, further large influence of RH on PET/P trends in the humid region. 110

1. Introduction

1.1 Backgrounds

As climate changes according to rising concentration of greenhouse gases (GHGs), the land surface experiences enormous changes, bring significant impacts on regional climate through variations of surface temperature, radiation, and cloudiness (Denman et al. 2007). Changes in plant habitats are among the key responses of terrestrial ecosystems to climate change (Sturm et al. 2001; Rosenzweig et al. 2007; Xu et al. 2013). Recent observational studies show that the global warming induced by the emissions of anthropogenic greenhouse gases may have caused notable habitat changes, particularly for shrub- and grasslands in the high latitudes (Parmesan and Yohe 2003; ACIA 2005; Jia et al. 2009; Forbes et al. 2010). Future climate projection studies also suggest that global warming may accelerate the current global habitat changes (Sala et al. 2005; Sitch et al. 2008; Gonzalez et al. 2010). The plant habitat changes can cause various ecological effects such as decline in biodiversity, increased extinction risks, and alterations in biogeochemical cycles (Thomas et al. 2004; Bellard et al. 2012; Hartley et al. 2012), which can further alter local/regional climate through vegetation-climate feedback (Chapin et al. 2005; Bonan 2008; Jeong et al. 2011a; Park et al. 2012). Thus, understanding plant habitat changes due to global

warming is crucial for mitigating and adapting to future climate and ecological changes.

The vegetation change in response to climate change have been projected using dynamic global vegetation models (DGVMs) and bioclimate envelope models either driven by climate model forcing (Cramer et al. 2001; Sitch et al. 2008; Bellard et al. 2012) or equipped with global climate model (Boudena et al. 2010; Jeong et al. 2011a). Previous studies show that future vegetation change is drastic in the northern high-latitudes (Sitch et al. 2003; Scholze et al. 2006; Jia et al. 2012). It is because of the large temperature increase induces profound penetration of the grasses and shrubs into non-vegetation regions in the high-latitudes (Wang et al. 2008; Jeong et al. 2011a). In mid-latitude and tropics, changes in the vegetation are mainly represented by changes in density of forests. With increasing the warming magnitude, more severe vegetation changes are appeared surely.

Altered vegetation influences regional climate through vegetation feedback by changing land-atmosphere interaction (Bonan et al. 2003; Jackson et al. 2008; Jeong et al. 2011a). Changes in the surface albedo and ET are the two main mechanisms involved in vegetation feedback with the surface climate. For example, an increase in vegetation greenness reduces surface albedo to favor

surface warming. This warming effect is countered by the cooling due to enhanced evapotranspiration (ET). The net impact of the two opposite effects determines the surface air temperature changes. Further, changes in vegetation may alter regional precipitation and water cycle. Through diverse regional features of the net effects (i.e., both temperature and moisture effects), vegetation feedback determines the magnitude of the changes in regional temperatures and water cycle (Notaro et al. 2007; Liu et al. 2006; Diffenbaugh 2009).

In warmer climate, water holding capacity of atmosphere is exponentially increased based on the relationship between saturation vapor pressure (e_s) and air temperature following Clausius-Clapeyron equation (Tsonis 2002; Hegerl et al. 2007). The increased capability of water vapor of the atmosphere induces two contrasting impact on land surface dryness. Large amount of water vapor is regarded as a favor condition of cloud formation (Held and Soden 2006; Meehl et al. 2007b). The amount of P is surely increased over the land surface, indicating moistening of the land. However, increased water demand of the atmosphere could dry out the land surface through increasing surface evaporation (Denman et al. 2007; Hegerl et al. 2015). Relative importance of two contrasting impacts is regionally different due to spatial heterogeneity of both characteristics of the land surface and mean climate condition (Greve et al. 2014).

Changes in land surface dryness have substantial socio-economic influences on human society. Projected increase in surface dryness with increasing GHGs may increase in natural disaster and social problems related to water availability such as drought (Meehl et al. 2007b; Sheffield and Wood 2008), desertification (Le Houerou 1996), vegetation die-out (van Mantgem et al. 2009), famine (Wang 2005; Edmonds and Rosenberg 2005), water management (Kundzewicz et al. 2007; Yohe et al. 2007), and energy production (Filed et al. 2007; Hightower and Pierce 2008). Among those problems, drought is one of significant extreme event because of it can induce a severe socio-economic impact by extremely large water stress (Bruke and Brown 2008; Seager et al. 2009). Over the 20th century, risk of drought occurrence is increased over Sahel, Mediterranean, and Asia where decreasing trend of Palmer Drought Severity Index (PDSI) is shown (Trenberth et al. 2007). In addition, analysis of GCM projections in IPCC AR4 consistently shows that occurrence and duration of drought will be increased with GHGs induced warming (Wang 2005; Meehl et al. 2007; Bruke and Brown 2008).

1.2 Motivation and objectives

Projected changes in land surface dryness shows large uncertainties related to land surface conditions and its feedback (Notaro et al. 2007; Meehl et al. 2007a; Christensen et al. 2007). Surely, the land surface dryness is influenced by vegetation feedback, playing considerable roles on surface hydrology (Bonan 2008; Jeong et al. 2011a). The first objective of present thesis is to examine the feedback impact of vegetation change on climate aridity, representing the degree of land surface dryness. Projections of several global climate models (GCM) in IPCC Fourth Assessment Report (IPCC AR4) show increasing trend of surface air temperature during 2000-2099, particularly over continental mid- and high-latitude in northern hemisphere (Meehl et al. 2007b). This warming lead to increase in moisture transport from surface to atmosphere due to increased atmospheric water-holding capacity (Hegerl et al. 2007). Hence, water stress will increase due to larger water demand associated with warmer temperature. Precipitation regarded as a water supply, however, is generally decreased over the subtropics in the future warmer climate (Meehl et al. 2007b). Thus, climate of continental subtropics is getting more arid due to increasing atmospheric water demand and decrease in water supply.

The potential impact of vegetation feedback on the climate aridity in warmer climate condition is examined using the results of atmosphere-land-vegetation coupled model. As mentioned above, the vegetation feedback is considered as one of important modulator of regional climate in future climate projection by changing surface energy budget and hydrological cycle (Bonan et al. 2003; Diffenbaugh 2009; Jeong et al. 2009; Jeong et al. 2011a). However, previous studies are not sufficient to explain the impact of vegetation change on climate aridity. Hence, it is valuable work that evaluating the impact of vegetation feedback on drought potential and projecting potential impact of vegetation change on climate aridity.

Next target of present thesis is changes in vegetation in future focusing on changing speed. Projections of ecosystem-level plant habitat changes in response to climate change have been made using dynamic global vegetation models (DGVMs) and bio-climate envelope models either driven by climate model forcing (Cramer et al. 2001; Sitch et al. 2008; Bellard et al. 2012) or coupled with global climate models (GCMs) (Bounoua et al. 2010; Jeong et al. 2011a). Plant habitat changes are investigated by contrasting the time-mean geographical distributions of plant habitats in a future period against that in a present-day period, in general (e.g., 2071–2100 minus 1961–1990 in Scholze et al. (2006)). This method is useful for measuring the amount of habitat change in targeted

regions and periods (Lucht et al. 2006; Alo and Wang 2008), but is not suitable for obtaining the point of time (i.e., timing) at which a specified amount of habitat change will occur. The timing of plant habitat change can tell us which parts of the world will experience faster changes, indicating higher risks from habitat change. This also allows us to estimate the amount of time required for the occurrence of a specific amount of habitat change for a specific level of climate change. Information on the timing to exceed a particular threshold value is useful for the development and timely implementation of management plans to adapt to and mitigate the impact of plant habitat changes (IPCC 2007; Joshi et al. 2011).

The second objective of this study is to evaluate the regional variations in the timing of plant habitat changes corresponding to a specified level of global warming in terms of the surface air temperature. Forest management plans have been generally developed at regional or national levels (Adger et al. 2007). Thus regional variations in the timing of plant habitat changes are directly useful in forest management practices. We also examine the relationship between the gross domestic product (GDP) per capita and the projected timing of plant habitat changes to help individual nations in developing ecosystem management plans. Ecosystem management policy needs sufficient economic capability. Adaptation policies and actions cannot be implemented if the associated cost is

too large for a nation to afford (Naidoo et al. 2006; IPCC 2007; Chan et al. 2011). Nations with weaker economic capability will experience difficulties in implementing mitigation plans, thus are more vulnerable to the same amount of habitat changes than wealthier nations.

To obtain future global plant habitat changes, this study projects the spatial and temporal variations in the changes of woody plant habitats in the 21st century using the bio-climate rule and multiple global warming scenarios from multiple atmosphere-ocean coupled GCMs. Because the bio-climate rule describes the plant habitat changes only in terms of the surface air temperature, the biotic factors such as the physiological impacts of CO₂ fertilization on plant habitat and competition among plant species under given climate change are not included in the projections. This may be an over-simplification in projecting plant habitat changes, however, a hierarchical framework in Turner et al. (2001) showed that climate is the highest environmental constrain for distribution of plant habitat in the global scale. This hierarchy of environmental variables is supported by limited impacts of the biotic factors when the climate change is less severe (Brown and Lomolino 1998; Pearson and Dawson 2003). Thus, global plant habitat changes in response to climate change obtained using the bio-climate rule is reliable although it does not include the effects of other factors such as CO₂ fertilization. This study have utilized all available climate model

outputs from the Intergovernmental Panel on Climate Change (IPCC) Fourth Assessment Report (AR4) archives to calculate the response of plant habitats to climate change (Meehl et al. 2007a). Ensemble of various projected habitat changes could cope with a wide range of inter-GCM variations in climate sensitivity (Meehl et al. 2007b).

The third topic is about examining exact mechanisms of changes in land surface dryness induced by present climate changes. Recent studies reveal that complex spatial variability of dryness changes over the land that contrasts to the “dry gets drier, wet gets wetter” paradigm (Greve et al. 2014; Hegerl et al. 2015). However, causes of changes in land surface dryness are not clear due to various attributions of climate variables on dryness changes (Estes et al. 2014; Christensen et al. 2007; Greve et al. 2014). The mechanism of changes in surface dryness over the land fundamentally differs from that over the ocean due to limited surface moisture availability (Feng and Fu 2013; Sherwood and Fu 2014). In many assessments, variation of precipitation (P), representing the amount of moisture supply, is regarded as a key variable for historical changes in land surface dryness, particularly over monsoon climate zones (Piao et al. 2010; Estes et al. 2014). For example, land surface dryness changes over East Asia are generally summarized by “Dry western region ($< 100^{\circ}\text{E}$) is getting wetter, dry northern region ($> 100^{\circ}\text{E}$, $35^{\circ}\text{-}45^{\circ}\text{N}$) drier, and wet southern region ($> 100^{\circ}\text{E}$,

25°-35°N) wetter” based on changes in annual mean P (Wang and Ding 2006; Piao et al. 2010). However, climate changes lead to significant changes in pan evaporation and potential evapotranspiration (PET), measurement of the amount of atmospheric moisture demand (Liu et al. 2010; Han et al. 2012). PET changes show large influence on the dryness trend over many regions according to changes in absorbed radiation, surface wind, and air temperature (Westerling et al. 2006; Estes et al. 2014). Thus, it is necessary to quantify impacts of each climate parameters on land surface dryness over various hydro-climate regimes for comprehensive understanding of complicated dryness changes over the land.

To investigate exact causes of changes in land surface dryness over continental East Asia, relative influences of five climate parameters on dryness changes are compared. Relative influences are computed using climate records at 179 and 10 meteorological stations of China and South Korea during the period of 1961-2010. Continental East Asia may be appropriate target region for examining the impact of climate variables on changes in land surface dryness due to both observed abrupt climate change and widespread of various hydro-climate regimes. An aridity index, defined as PET based on Penman-Monteith equation divided by P (PET/P), is used to determine changes in land surface dryness (Penmen 1948; Allen et al. 1998). If PET/P is decreased, it means that the land surface gets wetter; if it rises, the land surface is getting drier. In addition, the

analysis domain is divided into three hydro-climate regimes using 50-year climatology of PET/P: arid ($PET/P > 2$), semi-arid ($1 < PET/P < 2$), and humid ($PET/P < 1$). This classification is essential considering the spatial variability of changes in land surface dryness. Through using this method, we estimate influence of changes in P, net radiation (R_n), wind speed (WS), surface air temperature (T_a), and relative humidity (RH) on the changes in PET/P over three hydro-climate regimes of continental East Asia to present exact causes of changes in land surface dryness.

1.3 Thesis organization

The present thesis is organized as the following.

The data and analysis methods are mentioned in chapter 2. The data section includes descriptions of station based climate record, reanalysis field, model outputs from CMIP3, and satellite-observed vegetation. The method section explains the calculation of PET based on both Thornthwaite's equation and Penman-Monteith equation, and the land surface dryness (Thornthwaite aridity index and aridity index). Also the definition of plant habitats based on surface temperature is described in the method section. In chapter 3, influences of vegetation feedback on the climate aridity are investigated using several set of coupled GCM outputs in a condition of doubled CO₂ concentration. Chapter 4 deals with when the timing of plant habitat changes is occurred for multiple warming scenarios and regions. Chapter 5 reveals the exact causes of changes in land surface dryness over continental East Asia by comparing relative influences of five climate parameters using observational record of 1961-2010. Overall conclusions of the present thesis and possible future works are proposed in chapter 6.

2. Data and Method

The employed data sets are consists of the observed climate records from ground stations, satellite-retrieved observations, reanalysis data, and future projections of fully coupled GCM. The ground observation consists of 179 and 10 stations of China and South Korea for the period of 1961-2010. The satellite observations of NDVI are regarded as vegetation greenness and used as observation. Land surface temperature and precipitation of Climate Research Unit Time Series v3.0 (CRU TS3.0) is used as environmental climate of present-day. In addition, long-term integrations of 16 fully coupled GCMs in the third phase of the Coupled Model Intercomparison Project (CMIP3: Meehl et al. 2007a) are used as hindcast and future projections of climate.

Present-day and future plant habitat of woody plant species are examined using the bio-climate rule of plant functional types (PFTs) in the Lund-Potsdam-Jena dynamic global vegetation model (LPJ-DGVM) (Sitch et al. 2003). The timing of plant habitat change is estimated based on the computed plant habitat. In addition, Thornthwaite moisture index is used as a quantifier of climate aridity on the basis of atmospheric water supply (i.e., precipitation) and atmospheric water demand (i.e., potential evapotranspiration: PET). Climate observations of

ground stations are used to compute PET following FAO Penman-Monteith method.

2.1 Data

2.1.1 Station based climate records

The climate data for the period of 1961-2010 are come from selected 179 and 10 meteorological sites of China and South Korea, respectively. Data includes daily mean air temperature, precipitation, wind speed, relative humidity, sunshine duration, and several other variables. The quality of this data is controlled by National Meteorological Center of China Meteorological Administration and Korea Meteorological Administration. Selection of meteorological sites is carried out by two two conditions: 1) existence of all climate parameters of the year 2010, 2) continuous records of at least 10-year for both analysis periods.

2.1.2 Normalized Difference Vegetation Index (NDVI)

To determine the area of vegetation and soil, satellite-derived NDVI data is used in this study. The NDVI is the contrast between red and near-infrared reflectance of vegetation. This contrast is indicative of the abundance of pigments such as chlorophyll, or simply, leaf area. It is calculated from reflectances in channel 1 (0.58-0.68 μm) and channel 2 (0.73-1.1 μm) and is defined as

$$\text{NDVI} = (\text{Channel 2} - \text{Channel 1}) / (\text{Channel 2} + \text{Channel 1}).$$

The NDVI is expressed on a scale between -1 to +1, and ranges between -2 and 0.1 for snow, inland water bodies, deserts, and 85 exposed soils, and increases from about 0.1 to 0.7 for increasing amounts of vegetation, but saturates in the case of dense leaf canopies, e.g., the humid tropical forests. The primary data source are measurements from the Advanced Very High Resolution Radiometers (AVHRR) on board the afternoon-viewing NOAA series satellites (NOAA 7, 9, 11 and 14), which were processed to NDVI by the Global Inventory Monitoring and Modeling Systems (GIMMS) group. The important data processing features contained improved navigation, sensor calibration, and atmospheric correction for stratospheric aerosols. Details on development of the GIMMS NDVI data set and its quality can be found in *Zhou et al. (2001)*. Residual problems from lack of an explicit atmospheric correction for

tropospheric aerosols, water vapor absorption, surface anisotropy, etc. can be identified in this data set (Zhou et al. 2001). To minimize such effects, Los et al. (2000) developed a four-step procedure, which involved a Fourier Adjustment of outliers in the time series, Solar zenith angle correction, Interpolation for missing data, and Reconstruction of NDVI values over tropical rain forests. This data set overcomes most problems noted in previous generation of NDVI data sets. In this study, we used $0.5^\circ \times 0.5^\circ$ and monthly temporal resolution for the period 1982-2007.

2.1.3 Climate Research Unit Time Series v3 (CRU TS3.0)

CRU TS3.0 dataset is high-resolution gridded datasets presented by Climate Research Unit (Harris et al. 2013). The CRU TS3.0 is constructed by composing land surface observations of > 4000 stations. In the CRU TS3.0 datasets, 9 kinds of meteorological variables are provided for land surface: mean temperature, minimum temperature, maximum temperature, precipitation, daily temperature range, vapor pressure, cloud cover, wet day frequency, and frost day frequency. The CRU TS3.0 has $0.5^\circ \times 0.5^\circ$ horizontal resolution and monthly temporal resolution for the period from 1901 to 2005. In this thesis, land surface

temperature and precipitation data are used to determine the plant habitat for the present-day (1980-1999).

2.1.4 CMIP3 multi-model dataset

The third phase of Coupled Model Intercomparison Project (CMIP3) is huge project, which provides simulations of many atmosphere-ocean global climate models for assessment of climate variability and climate change (Meehl et al. 2007a). Long-term simulation of 16 fully coupled GCMs is obtained from CMIP3. Surface temperature and precipitation of multi-model dataset is used to identify present and future distribution of plant habitat. All GCM outputs are first statistically downscaled onto a $0.5^\circ \times 0.5^\circ$ latitude-longitude grid for the period 1950–1999 using the bias-corrected spatial downscaling (BCSD) scheme of Wood et al. (2004) in conjunction with the gridded observations of Adam and Lettenmaier (2003). We analyzed a total of 64 sets of downscaled GCM simulations: 16 present-day simulations following the Special Report on Emissions Scenarios (SRES) 20C3M for 1950–1999 and 48 (= 16×3) future projections corresponding to the SRES B1, A1b, and A2 emissions scenarios for 2000–2099.

2.1.5 Gross Domestic Product

The Gross Domestic Product (GDP) is the market value of all officially recognized final goods and services produced within a nation in a year. The GDP could represent the total economic size of each nation, thus the GDP is adopted to evaluate the relationship between the timing of plant habitat change and regional economic power. Table 2.1 shows the 2011 GDP values of all nations that have some or all of their territory located in the latitude bands 10°S – 25°S , 15°N – 30°N , and 50°N – 65°N (World Bank 2012). Notice that these three latitude bands are found to have significant plant habitat changes (see results section later). The six selected nations (Angola, Brazil, China, Mexico, Russia, and Canada) have the largest GDP values in each region, representing the upper limits of regional economic power. The United States is excluded from the representative nations because only a small part of its territory is located within the latitudes 15°N – 30°N and 50°N – 65°N .

Table 2.1. The gross domestic product (GDP) of nations which total or some part of territory is included in each region (The World Bank, 2012).

Latitudinal belt	Region	Nation	GDP (billion US dollar)
10°S–25°S	southern Africa	Angola	104.3
		Zambia	19.2
		Namibia	12.3
		Botswana	17.3
		Zimbabwe	9.7
		Mozambique	12.8
		Madagascar	9.9
	central South America	Brazil	2476.7
		Bolivia	23.9
Paraguay		23.8	
15°N–30°N	East Asia	Pakistan	210.2
		India	1848.0
		Bangladesh	111.9
		Lao PDR	8.3
		Thailand	345.7
		Vietnam	123.6
		Philippine	224.8
		Nepal	18.9
		Bhutan	1.7
		China	7318.5
		southern North America	Mexico
Cuba	-		
United States	14991.3		
50°N–65°N	northern Eurasia	Russia	1857.8
		Kazakhstan	188.1
	northern North America	Canada	1736.1
		United States	14991.3

2.2 Method

2.2.1 The bio-climate rule and plant habitats

Habitat changes of woody plant species in response to global warming are assessed using the bio-climate rule of plant functional types (PFTs) in the Lund-Potsdam-Jena dynamic global vegetation model (LPJ-DGVM) (see Table 2 in Sitch et al. 2003) where the bio-climate rule for woody PFTs is defined by temperature-based bio-climatic limitation of survival and establishment. The climatic limitation is represented by range of the coldest-month temperature in the 20-year running mean (T_c). For example, in regions where T_c ranges between 3°C and 15.5°C, temperate needleleaf evergreen, temperate broadleaf evergreen, temperate broadleaf summergreen, and temperate herbaceous plants can coexist. The bio-climate rule has been used in a number of previous studies on future vegetation changes using LPJ-DGVM based models (Lucht et al. 2006; Alo and Wang 2008; Scholze et al. 2008; Jiang et al. 2012). On the basis of the bio-climate rule, eight plant habitats are defined according to dominant PFTs (Table 2.2); tropical (Tr-type: Tr1 and Tr2), temperate (Te-type: Te1, Te2, Te3, and Te4), and boreal (Bo-type: Bo1 and Bo2). For every year in the analysis period, the spatial distribution of T_c is transformed into the spatial distribution of plant habitats following the T_c ranges in table 2.2. Thus, the distribution of plant

habitats is calculated at annual time steps with the horizontal resolution same as T_c . To remove remaining non-vegetative regions, i.e., deserts, the tropical and temperate regions with annual precipitation totals < 200 mm (UNEP 2009; Jeong et al. 2011b) are excluded. Polar deserts in the arctic region are defined as the areas of annual precipitation totals < 250 mm with the warmest-month temperatures $< 10^\circ\text{C}$ (UNEP 2009). In addition, the land cover product from MODIS retrievals is used to verify the present-day distributions of the eight plant habitats and deserts (Friedl et al. 2002).

2.2.2 Temperature-based approach for plant habitat change

Instead of the SRES emission scenarios, the global-mean warming thresholds are used to calculate habitat changes corresponding to specified amounts of increased global mean surface temperature. The global-mean surface temperature is conventionally used to represent the degree of climate change (Scholze et al. 2006; Solomon et al. 2007) because different degrees of global-mean temperatures are reflected by combined impacts of land-use and greenhouse gas changes (Joshi et al., 2011). In addition, the global-mean temperature change is relevant to planning mitigation policies about the impact of climate change (Meinshausen et al. 2009; UNFCCC 2009). Thus, assessing the climate change impact as a function of the global-mean temperature change is a rational way to

quantify the climate change impacts (Scholze et al. 2006; Joshi et al. 2011). The 48 sets of GCM projections are grouped into three categories following the projected global-mean land surface temperature differences (ΔT) between the late 21st century period (2080–2099) and the present-day period (1980–1999): $\Delta T < 2.5^\circ\text{K}$ as low warming, $2.5^\circ\text{K} < \Delta T < 3.5^\circ\text{K}$ as medium warming, and $\Delta T > 3.5^\circ\text{K}$ as high warming. These warming thresholds are larger than in Scholze et al. (2006) by 0.5°K because the warming signal is generally larger over lands than ocean surfaces (Meehl et al. 2007b). Using these threshold values, 12, 18, and 18 sets of GCM projections are categorized into the low, medium, and high warming groups, respectively. (Table 2.3). For all warming thresholds, the timing at which a plant habitat changes by 10%, 20%, and 30% is estimated. In a specific analysis domain, the fractional change is computed by a ratio of the area where plant habitat change occurs to the total area in that region. A year at which the ratio first exceeds 10%, 20%, or 30% indicate the timing of 10%, 20%, or 30% habitat change, respectively. The timing is computed based not only on the ensemble mean, but on 10% and 90% of model projections to deal with the uncertainty in model simulations. Because previous studies showed that the regional-mean fraction of wood species is likely to be $< 20\%$ over the globe, these three habitat-change thresholds must be sufficiently large to capture meaningful habitat changes (Scholze et al. 2006; Sitch et al. 2008).

Table 2.2. Bio-climate limits for plant habitats: $T_{c,min}$ is the minimum coldest-month temperature for survival; $T_{c,max}$ is the maximum coldest-month temperature for survival.

	Plant habitat	$T_{c,min}$ (°C)	$T_{c,max}$ (°C)
Tropical PFTs dominated habitat (Tr-type)	Tr1 tropical broadleaf green tropical herbaceous	22	-
	Tr2 tropical broadleaf green temperate needleleaf evergreen tropical herbaceous	18.8	22
Temperate PFTs dominated habitat (Te-type)	Te1 tropical broadleaf green temperate needleleaf evergreen temperate broadleaf evergreen tropical herbaceous	15.5	18.8
	Te2 temperate needleleaf evergreen temperate broadleaf summergreen temperate herbaceous	3	15.5
	Te3 temperate needleleaf evergreen temperate broadleaf summergreen temperate herbaceous	-2	3
	Te4 temperate broadleaf summergreen boreal summergreen boreal needleleaf evergreen temperate herbaceous	-17	-2
Boreal PFTs dominated habitat (Bo-type)	Bo1 boreal summergreen boreal needleleaf evergreen temperate herbaceous	-32.5	-17
	Bo2 temperate herbaceous	-	-32.5

Table 2.3. Future projection of 16 climate models included in three warming thresholds.

	Low warming ($\Delta T < 2.5^\circ\text{C}$)	Medium warming ($2.5^\circ\text{C} < \Delta T < 3.5^\circ\text{C}$)	High warming ($\Delta T > 3.5^\circ\text{C}$)
BCCR-BCM2.0	B1	A1b, A2	
CGCM3.1 (T63)	B1	A1b	A2
CCSM3	B1	A1b	A2
CNRM-CM3	B1	A1b	A2
CSIRO-MK3.0	B1, A1b	A2	
ECHAM5/MPI-OM		B1	A1b, A2
ECHO-G		B1	A1b, A2
GFDL-CM2.0		B1	A1b, A2
GFDL-CM2.1	B1		A1b, A2
GISS-ER	B1	A1b, A2	
INMCM3.0	B1	A1b	A2
IPSL-CM4		B1	A1b, A2
MIROC3.2(M)		B1	A1b, A2
MRI-CGCM2.3.2	B1	A1b, A2	
PCM	B1, A1b	A2	
UKMO-HadCM3		B1	A1b, A2

2.2.3 Thornthwaite moisture index

The Thornthwaite moisture index (Thornthwaite 1948; hereafter I_m) is used as a measure of climate aridity in this study as in changes in climate aridity (e.g., Mather and Feddema 1986; McCabe et al. 1990; McCabe and Wolock 1992). I_m is defined in terms of the atmospheric water supply and demand represented by precipitation (P) and potential evapotranspiration (PET), respectively. The moisture index consists of two indices: I_a that represents the potential aridity and I_h the potential humidity. These two indices are separately calculated based on moisture surplus and deficit from the water budget as

$$I_a = 100 \frac{D}{N} \quad (2.2.1)$$

$$I_h = 100 \frac{S}{N} \quad (2.2.2)$$

where D is water deficit defined as the sum of monthly PET minus P for $PET > P$, S is water surplus defined as the sum of monthly P minus PET for $P > PET$, and N is water need defined as the sum of monthly PET. The moisture index I_m is represented by combining of these two indices as

$$I_m = I_h - 0.6I_a. \quad (2.2.3)$$

Negative values of I_m imply arid climate where atmospheric water demand exceeds atmospheric water supply, and vice versa. The factor of 0.6 accounts for the assumption that water can infiltrate into soil more easily than it is extracted (Thornthwaite 1948). Monthly PET is calculated using an empirical formula as a function of mean surface air temperature (Thornthwaite 1948). In addition, I_m is used to separate climate type based on regional moisture condition. Table 2.4 provides that 9 climate types based on I_m .

Table 2.4. Climate types defined in terms of the original Thornthwaite moisture index.

Climate Type	Minimum	Maximum
A Perhumid	100	Infinite
B₄ Humid	80	100
B₃ Humid	60	80
B₂ Humid	40	60
B₁ Humid	20	40
C₂ Moist Subhumid	0	20
C₁ Dry Subhumid	-20	0
D Semiarid	-40	-20
E Arid	-60	-40

2.2.4 FAO Penman-Monteith method

In the FAO Penman-Monteith method, daily PET values are estimated for a reference crop defined as a hypothetical crop assumed by a height of 0.12 m, surface resistance of 70 s m^{-1} , and an albedo of 0.23. The computed daily PET closely resembles the evaporation of an extension surface of green grass of uniform height, actively growing and adequately watered. The formulation of daily PET following FAO Penman-Monteith method is written as:

$$\text{PET} = \frac{0.408\Delta(R_n - G) + \gamma\left(\frac{900}{T + 273}\right)U_2(e_s - e_a)}{\Delta + \gamma(1 + 0.34U_2)} \quad (2.2.4)$$

where R_n is the net radiation at the crop surface ($\text{MJ m}^{-2} \text{ day}^{-1}$), G the soil heat flux density ($\text{MJ m}^{-2} \text{ day}^{-1}$), T the air temperature at 2 m height, U_2 the wind speed at 2m height, e_s the saturation vapor pressure of the air (kPa), e_a the actual vapor pressure (kPa), Δ the slope of the vapor pressure curve ($\text{kPa } ^\circ\text{C}^{-1}$) at T , and γ the psychrometric constant ($\text{kPa } ^\circ\text{C}^{-1}$). The complete equation set for all variables is described in the FAO56 report (Allen et al. 1998).

2.2.5 Change-point method

Two methods are used to find change-point of temporal variation of PET/P.

One method defines the change-point when cumulative sum of PET/P variation for t th year (C_t) is the largest (Pettitt 1980). The cumulative sum C_t is provided as following:

$$C_0 = 0$$

$$C_t = C_{t-1} + (X_t - \bar{X}) \quad (2.2.5)$$

where X_t is PET/P in year t , and \bar{X} the averaged PET/P for whole analysis period.

In the other change-point model, X_t is same, PET/P of t th year and Y_t is defined as $\log_{10}(X_t + 1)$. The step variable S_t is defined for an integer l that changes from 2 to $m = N - 1$ as following:

$$S_t(l) = \begin{cases} 0, & t < l \\ 1, & t \geq l \end{cases} \quad (2.2.6)$$

where N is the total years of analysis period 1961-2010. Using the step variable S_t , a simple linear first-order regression model is suggested for an integer l as following:

$$Y_t = \beta_0(l) + \beta_1(l)S_t(l) + \epsilon_t(l) \quad (2.2.7)$$

where $\beta_0(l)$ is the intercept, $\beta_1(l)$ the slope and $\epsilon_t(l)$ the error of residual at Y_t for a fixed l . In addition, the value of $L(l)$ is computed by

$$L(l) = \hat{\beta}_1(l) / \text{se}[\hat{\beta}_1(l)] \quad (2.2.8)$$

where $se[\beta_1(t)]$ is the standard error of $\beta_1(t)$.

Let $L(l_1) = \max\{|L(2)|, |L(3)|, \dots, |L(m)|\}$. The l_1 can be a change-point if the $L(l_1)$ is statistically significant (Chu 2002).

2.2.6 Computing relative influences of climate parameters on PET/P trends

The relative influences of the five climate parameters on the PET/P changes are estimated by applying stepwise regression method to 189 meteorological stations¹⁹. In the regression, annual mean PET/P is derived by annual P, Rn, WS, Ta, and RH as shown in the following equation:

$$\frac{PET}{P} = a_1P + a_2R_n + a_3WS + a_4T_a + a_5RH + b \quad (2.2.9)$$

where a_1 - a_5 are the regression coefficients of the climate parameters and b is the intercept.

The product of the regression coefficient and annual trends of each climate parameters (P, Rn, WS, Ta, and RH) are regarded as the relative influence of the climate parameter on the PET/P trends as follows:

$$\Delta\left(\frac{PET}{P}\right) = a_1\Delta P + a_2\Delta R_n + a_3\Delta WS + a_4\Delta T_a + a_5\Delta RH \quad (2.2.10)$$

where ΔP , ΔR_n , ΔWS , ΔT_a , and ΔRH are the trend slope of annual P,

Rn, WS, Ta, and RH, respectively. $\Delta\left(\frac{PST}{\rho}\right)$ is the computed trend slope based on sum of influences of five climate parameters.

3. Vegetation feedback impact on climate aridity

The change in temperature and precipitation leads to the climate aridity change by modulating regional balance between water deficit or water surplus. As mentioned in section 1, change in vegetation in response to climate change has feedback impact on climate through changes in albedo and ET (Bonan et al. 2008). Future changes in vegetation and its feedback impact on climate aridity is examined in this section using CAM-DGVM simulations.

3.1 Models

The global climate model (GCM) used in this study is the National Center for Atmospheric Research (NCAR) Community Atmospheric Model version 3 (CAM3) configured with a T42 horizontal resolution and 26 hybrid-sigma vertical layers. Climate Land Model version 3 (CLM3) is used for Land Surface Model to calculate land surface processes. CLM3 contains the dynamic global vegetation model (DGVM), a modified version of the Lund-Potsdam-Jena (LPJ) DGVM (Levis et al. 2004), to compute vegetation dynamics as a function of climate variables. The CLM-DGVM and CAM3-DGVM models have been widely used in many previous climate studies (e.g., Bonan and Levis 2006).

3.1.1 CAM3

The CAM3 is the fifth version of atmospheric general circulation model (AGCM) developed by the National Center for Atmospheric Research (NCAR). The standard NCAR CAM3 is described in *Collins et al.* (2004).

The CAM3 can be run either as an independent AGCM or as a component of the Community Climate System Model version 3 (CCSM3; *Collins et al.* 2006). As a stand-alone AGCM, CAM3 is integrated together with the Community Land Model (CLM; *Bonan et al.* 2002), a thermodynamic sea ice model, and a data ocean or optional slab ocean model. CAM3 includes Eulerian spectral and semi-Lagrangian and finite volume (FV) dynamical core. This dynamical core is perfectly separated from the physical part and can be coupled to the physics in a time-split or process-split approximation (Williamson 2002). Parameters are configured for the Eulerian dynamical core at T31, T42, and T85 spectral truncation and for FV core at $2^\circ \times 2.5^\circ$ horizontal resolution. Zonal resolutions of the Eulerian truncations are from 3.87° for the T31 configuration to 1.41° for the T85 configuration.

The code, documentation, input datasets, and model simulations for CAM3 are freely available from the CAM Web site (www.cesm.ucar.edu/models/atm-cam).

3.1.2 CLM3

The CLM3 has significantly improved over its earlier versions as a result of algorithmic improvements, better input from its parent atmosphere, and use of a higher spatial resolution by its parent model. In the CLM3, land region comprises 3799 gridcells, each of which can have a difference number of landunits as subgrid representation. The landunit includes physically distinct surface types (glacier, lake, wetland, urban, vegetation areas). To capture variability in the soil and snow state variables within a single landunit, the landunit is divided into 10 soil columns and 5 snow columns. As final subgrid, the vegetated subgrid is composed of up to 4 different plant functional types (PFTs) from a total 15 types. In the CLM3, ecological and physical characteristics of vegetation is either prescribed by satellite-derived values or interactively calculated by DGVM.

3.1.3 DGVM

The DGVM were introduced as a practical and ecologically realistic means of simulation vegetation changes in global climate models (Sitch et al. 2003, Bonan et al. 2003). DGVMs coupled to climate models have been used to

simulate vegetation for past, present, and future climates to assess the interactions among climate, CO₂, and vegetation (Levis et al. 2004; Cowling et al. 2009). In this study, we used the CLM-DGVM, which is a modified version from the LPJ DGVM (Levis et al. 2004) to the CLM following the IBIS approach (Foley et al. 1996). The CLM-DGVM consists of CLM3 plus a set of routines that allow vegetation cover and structure to be simulated instead of prescribed from data. The model represents spatial heterogeneity in land cover by dividing each grid cell into four land cover types: glacier, lake, wetland, and vegetation (Bonan et al., 2002). The vegetated portion of the grid cell is further divided into several patches of plant functional types (PFTs). The PFTs consist of 10 different types depending on the climate of grid cell. Two tropical trees, three temperate trees, and two boreal trees are differentiated by bioclimatology, leaf form (broadleaf, needleleaf), phenology (evergreen, summergreen, raingreen), physiology, and response to disturbance. Three grasses are distinguished by bioclimatology and photosynthetic pathway (C3, C4). The plant functional types are similar to those used in versions of LPJ and are a subset of those used in LSM.

The vegetation dynamics of LPJ can be readily incorporated into CLM. LPJ couples fast hydrological and physiological processes with slower ecosystem processes using time-scales of daily (soil water, soil temperature, snow canopy

physiology, phenology), monthly (soil microbial processes), and yearly (vegetation dynamics). In coupling CLM and LPJ, we omitted fast LPJ processes already present in CLM, altered LPJ algorithms to meet the requirements of a climate model, and scaled LPJ's daily and monthly respiration to fit CLM's 20 min coupling with the atmosphere. We retained LPJ's daily time step for leaf phenology and LPJ's annual time step for changes in community composition and ecosystem structure.

3.2 Experimental design

Using the CAM3-DGVM model, three sets of model experiments have been performed. The first one is under the present-day CO₂ concentration ($1 \times \text{CO}_2 = 355$ ppmv, parts per million in volume) with monthly vegetation specified from the climatological mean vegetation state (CMVS) defined below for the simulation period (hereafter VegOff_1×). The other two experiments are under $2 \times \text{CO}_2 (=710$ ppmv) conditions with interactive vegetation feedback (hereafter VegOn_2×) and specified monthly vegetation from CMVS (hereafter VegOff_2×), that is active and inactive DGVM for VegOn_2× and VegOff_2×, respectively. Prior to all model integrations, the CAM3-DGVM model was spun

up for 500 years to obtain the potential vegetation under the present-day climate. Starting from the bare ground, the CAM3-DGVM vegetation achieved an equilibrium climate-vegetation state after about 400 years. CMVS that is defined as the mean state over the last 30 years of the 500-year spin up run is used as the initial or perpetual vegetation fields for all three experiments above. Table 3.1 provides that summary these three experiments.

Each experiment consists of five ensemble members with varying atmospheric initial conditions randomly selected in the last 5 years of the 500-year spin-up run. To include the impacts of the CO₂ increase on oceanic state, sea surface temperatures (SSTs) and sea ice covers (SICs) derived from the 1990 control run and the 2 × CO₂ run of Community Climate System Model version 3 (CCSM3; Collins et al. 2006) are prescribed in the present-day and 2 × CO₂ simulations. Thus the feedback between vegetation effects and oceanic circulation is not included in this experiment. From the three sets of ensemble simulations, we separate the effect of elevated CO₂ from the vegetation feedback as follows: VegOff_2× minus VegOff_1× indicates the effect of elevated CO₂ only, defined as the radiative effect; VegOn_2× minus VegOff_1× includes both the radiative and the vegetation feedback effect; VegOn_2× minus VegOff_2×

isolates the vegetation feedback only. More detailed descriptions on these experiments are documented in *Jeong et al. (2011a)*.

Table 3.1. Equilibrium experiments using CAM3-DGVM. Identifiers for each simulation, sea surface temperature (SST), atmospheric CO₂ concentrations (CO₂), integration time (Years), number of ensemble (Ensembles), and model horizontal resolution (Resolution).

	Identifier	SST	CO₂	Vegetation	Years	Ensembles	Resolution
Spin-up	Spin-up	Present climatology	Present climatology	Dynamic	500	1	T42
Equilibrium	VegOff_1×	CCSM Present	335 ppmv	Fixed	100	5	T42
	VegOff_2×	CCSM CO ₂ doubling	710 ppmv	Fixed	100	5	T42
	VegOn_2×	CCSM CO ₂ doubling	710 ppmv	Dynamic	100	5	T42

3.3 Changes in climate types

Climate types over the contiguous US region is classified in terms of I_m vary in a wide range from -60 to infinity (Table 2.4). Note that aridity increases as I_m decreases (Thornthwaite 1948). Figure 3.1 presents the climate types determined on the basis of I_m calculated using climatology for the last 30 years of present-day CO_2 concentration run (i.e., VegOff_1 \times). It also shows climatology from the 0.5° Climate Prediction Center's (CPC) monthly analysis of global surface air temperature and land precipitation for a 30-year period (1980–2009) (Chen et al. 2002; Fan and van den Dool 2008). The climate types computed with the CPC data shows that three climate types dominate most of the contiguous US region: the arid type to the west of the Rocky Mountains, the semiarid type over the western Great Plains and Rocky Mountain States, and dry subhumid type over the eastern Great Plains and East Coast (Fig. 3.1b). The VegOff_1 \times run reproduces well the arid climate found to the west of the Rocky Mountains and the dry subhumid type found over the eastern Great Plains and East Coast (Fig. 3.1a). The relatively wetter climates in the eastern half and drier climates in the western half of the contiguous US region also agree with previous observation-based studies (Thornthwaite 1948; Feddema 2005a). The most notable model errors are the wet biases over the Rocky Mountains and the western Great Plains,

especially Colorado, Nebraska, and Kansas (Fig. 3.1a). This wet bias is also evident in previous modeling studies using CAM3 (e.g., Meehl et al. 2006, Feng et al. 2008). Overall, the simulated present-day regional climate types are largely consistent with the observation-based climate type.

Figure 3.2 shows the changes in I_m and the subsequent climate types over the US by; (a) the radiative effect due to doubling of CO₂ concentration only (VegOff_2× minus VegOff_1×), (b) the combination of the radiative and vegetation-feedback effects (VegOn_2× minus VegOff_1×), and (c) vegetation-feedback effects only (VegOn_2× minus VegOff_2×). Blue (red) dots indicate that the regions shift to a more humid (arid) climate type due to the increase in CO₂ and/or vegetation feedback. In the 2 × CO₂ climate, I_m decreases by the radiative effect suggesting increases in aridity in most (> 75%) of the contiguous US region, (Fig. 3.2a). The most noticeable decrease in I_m appears in Texas, Arkansas, and Louisiana. By contrast, a notable increase in I_m appears in the northern part of the Mountainous regions, especially around Wyoming. The changes in I_m and subsequently the climate types, induced by the radiative effect are generally consistent with the previous studies of Meehl et al. (2007) and Christensen et al. (2007).

Vegetation feedback appears to strongly modify the changes in I_m calculated in the radiative effects only case (Fig. 3.2b). The most noticeable features are the increase in I_m (i.e., decreased aridity) over the Midwest, the East South Central division, and the Northwest. The impacts of vegetation feedback on I_m and subsequent climate types are clearly shown in Fig. 3.2c. Positive I_m anomalies occur in over 75% of the contiguous US region. Due to the large increase in I_m in these regions, climate types in Montana, Wyoming, South Dakota, Illinois, and northern Texas become more humid. In particular, significant drying in the northern Texas region due to the radiative effect (Fig. 3.2a) is reversed into a wetter type due to the inclusion of vegetation feedback (Fig. 3.2c). On the other hand, only small changes in I_m are found over the Northeast and Southwest. I_m even decreases due to vegetation feedback over the southeastern US. Despite those regional differences, Fig. 3.2 shows that the increase in aridity by the radiative effects is generally suppressed by vegetation feedback. The mechanisms by which vegetation feedback alleviates the increasing aridity by the radiative effects are investigated in the next two sections.

Present Climate Type

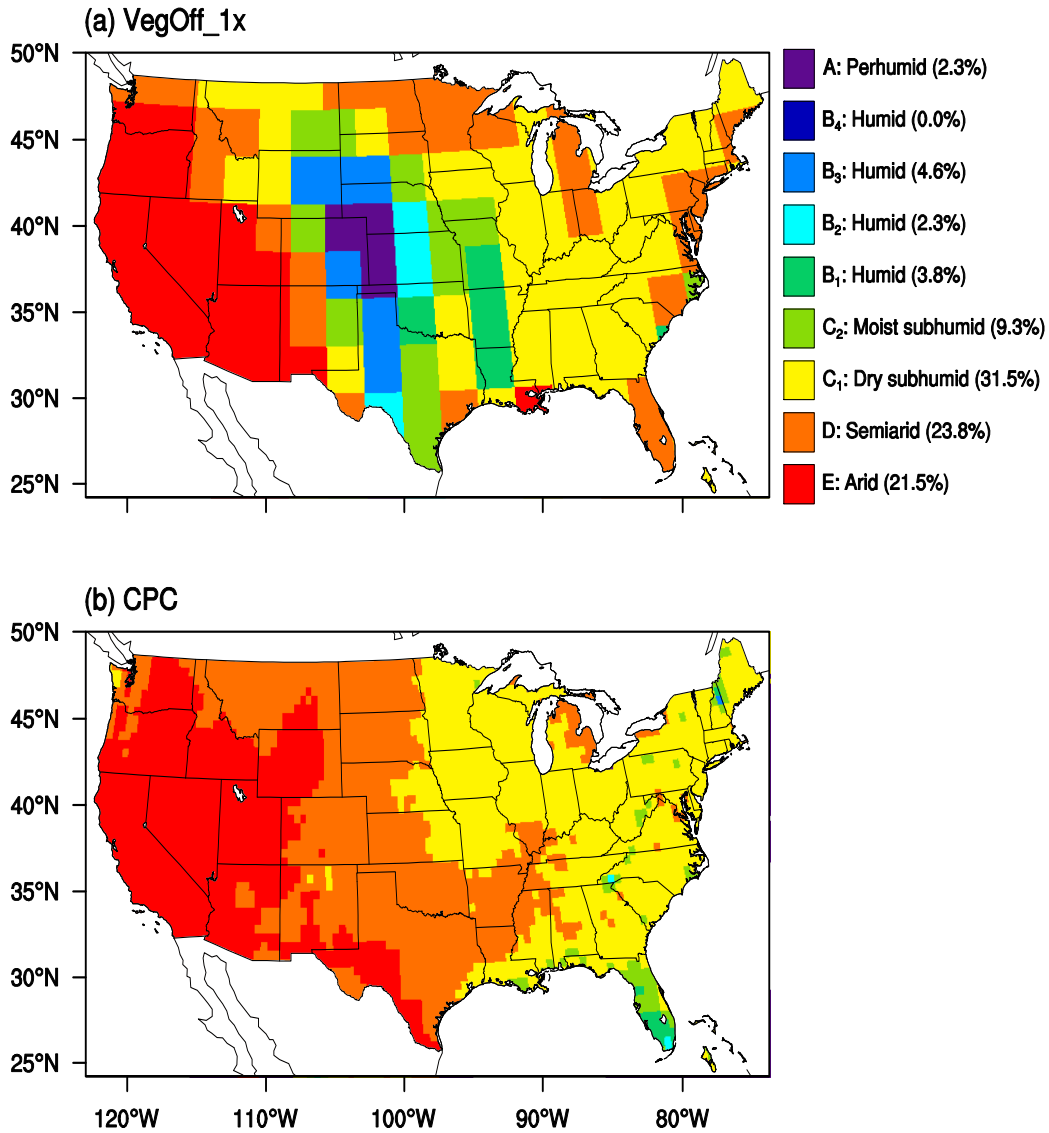


Figure 3.1. Spatial distribution of Thornthwaite moisture index over the US in boreal summer for VegOff_1x (a), and 30-year climatology of CPC monthly analysis of global surface air temperature and land precipitation for the period 1980–2009 (b).

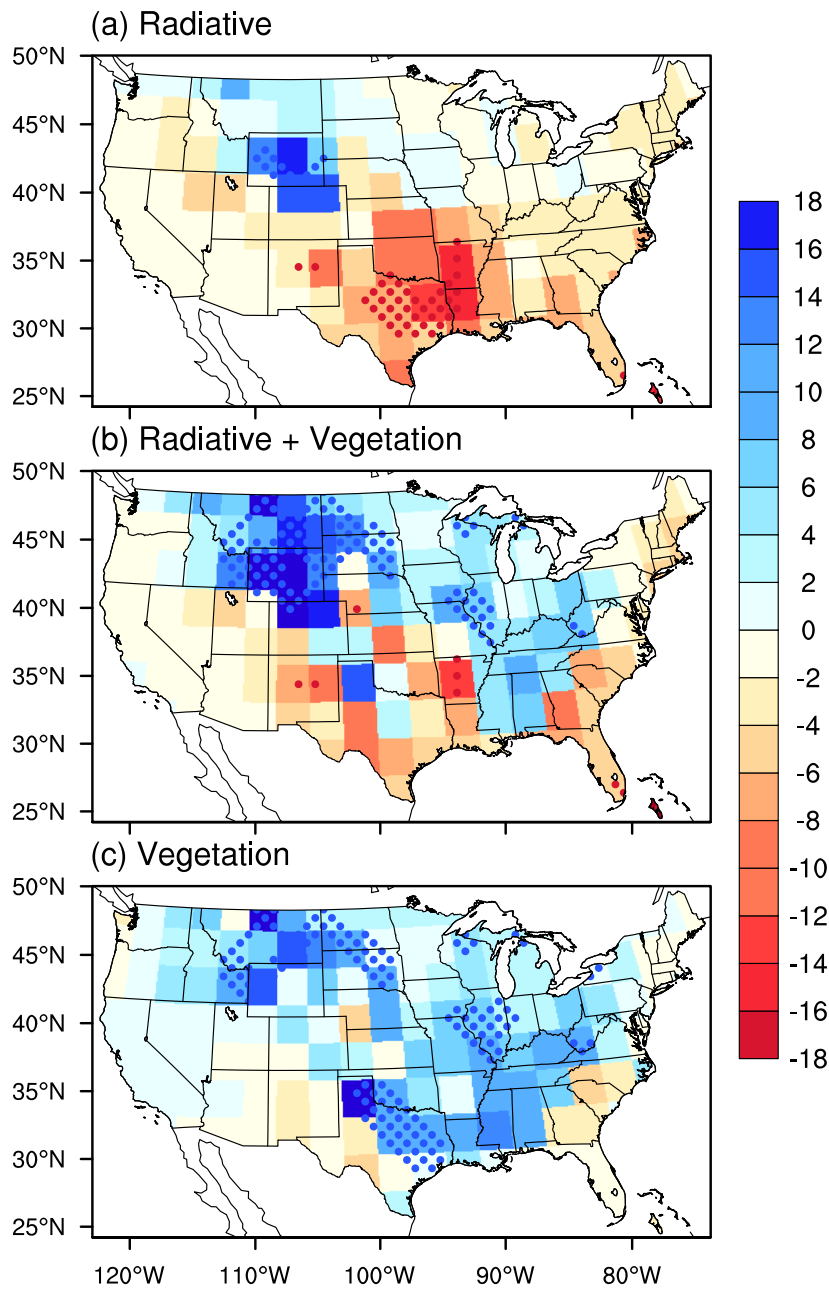


Figure 3.2. Spatial distribution of changes in Thornthwaite moisture index by radiative effect (a), radiative and vegetation feedback effect (b), and vegetation feedback only (c). Blue dots and red dots represent regions that the climate type change more humid and arid, respectively.

3.4 Changes in LAI and surface evapotranspiration

Vegetation feedback in climate model occurs mostly through the changes in PFTs or LAI or both (Bonan et al. 2003; Jeong et al. 2011a). These two variables combined represent vegetation “greenness”. There are two types of vegetation feedback through changes in vegetation greenness (combined effects of PFTs and LAI): 1) vegetation–albedo feedback acting to alter land surface albedo and hence the amount of shortwave absorption, and 2) vegetation–evaporation feedback resulted from changes in ET. Changes in PFTs are minimal in the analysis region, suggesting it plays only a minor role in affecting I_m . A previous study (Jeong et al. 2010) suggested that the impact of vegetation–evaporation feedback through the increase in LAI dominates in the mid-latitude regions, especially Europe and North America. Thus we will focus on the effects through LAI in the following.

Figure 3.3 shows the LAI simulated with the present-day CO₂ concentration and the changes in LAI due to increasing CO₂ concentration. In the present-day climate condition, large LAI values occur in the East Coast region, southern US, western Great Plains, and the Pacific Northwest coastal regions (Fig. 3.3a). Small LAI values can be found in the arid southwestern US region. These spatial distributions and magnitudes of the present-day LAI are generally consistent

with satellite observations, except the unrealistically large values over parts of the southern Great Plains region (approximately 30-40°N, 97-105°W) (Bonan et al. 2003). With $2 \times \text{CO}_2$ concentration, the simulated LAI values increase significantly in most of the contiguous US region (Fig. 3.3b). The greening may be explained by enhanced vegetation productivity and water-use efficiency in the warmer climate under the higher CO_2 concentration (Levis et al. 2000; Jeong et al. 2011a). Noticeable greening is also observed over the Midwest, East South Central division, and northern part of Mountain division. These regions are mostly classified as dry subhumid climate types in the present climate (see Fig. 3.3a). In addition, these greening regions are similar to regions where an increase in I_m is shown on Fig. 3.2c. The consistent increases in I_m and LAI indicate that the enhanced vegetation growth is a key factor in reducing aridity in the VegOn_2× simulation.

Changes in LAI can significantly modulate the magnitude and composition of surface ET, thereby alter the surface water cycle and energy budget (Jeong et al. 2011a). Figure 3.4 illustrates the spatial distribution of the projected changes in the total evaporation, canopy evaporation, canopy transpiration, and bare-soil evaporation by the radiative effect only (Figs. 3.4a–3.4d), the combined radiative and vegetation-feedback effects (Figs. 3.4e–3.4h), and the vegetation-feedback effect only (Figs. 3.4i–3.4l). The total evaporation increases over most of the

contiguous US due to the CO₂-induced radiative effect by as much as 15 mm month⁻¹. The increase in total evaporation is likely to be caused by increased atmospheric water-holding capacity due to CO₂-induced warming (Hegerl et al. 2007). Spatial distribution of the changes in canopy evaporation, canopy transpiration, and bare-soil evaporation are similar to the changes in the total evaporation (Figs. 3.4b–3.4d) indicating evaporation from soil and vegetation responds to the radiative effects in a similar way.

With the inclusion of vegetation feedback (VegOn_2× minus VegOff_1×), the total evaporation increases further (Fig. 3.4e). The increase in evapotranspiration and the decrease in bare-soil evaporation appear clearly over the Midwest, South, and Northwest (Figs. 3.4f–3.4h) where LAI increases significantly (see Fig. 3.3b), especially in western Montana where the canopy and soil evaporation changes by as much as 50 mm month⁻¹. The vegetation-feedback effect increases the total evaporation by as much as 15 mm month⁻¹ in the Midwest, Northwest, and the East South Central division (Figs. 3.4i–3.4l). In addition, significant increase in the total evaporation appears in Idaho, Montana, North Dakota, Tennessee, Mississippi, and Alabama because the sum of the increase in the canopy evaporation and canopy transpiration is larger than the decrease in the bare-soil evaporation.

JJA Leaf Area Index

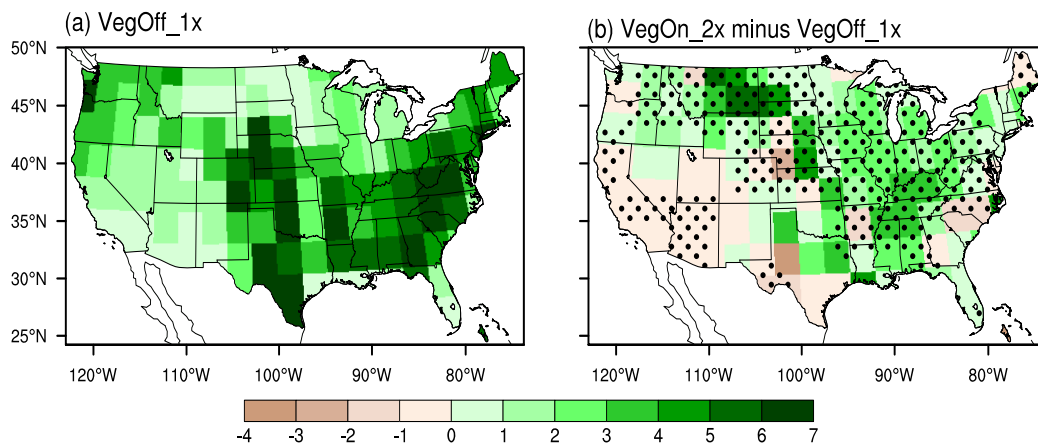


Figure 3.3. Spatial distribution of leaf area index over the US in boreal summer for VegOff_1x (left) and changes in leaf area index between VegOn_2x and VegOff_1x (right). Black dots represent the regions that changes in leaf area are statistically significant at the 95% confidence level.

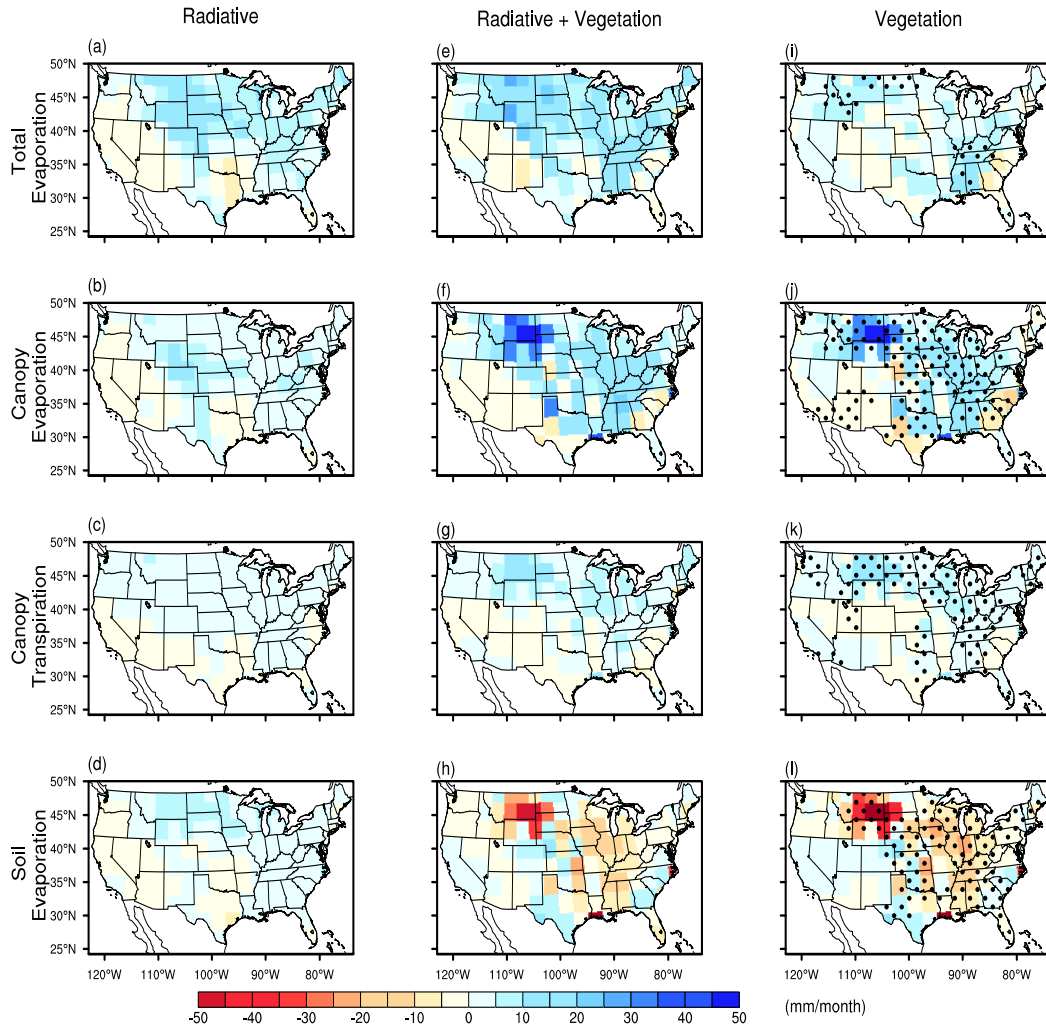


Figure 3.4. Spatial distribution of changes in total evaporation, canopy evaporation, canopy transpiration, and soil evaporation due to radiative effect (a–d), radiative and vegetation feedback effect (e–h), and vegetation feedback only (i–l). Black dots represent the regions that changes are statistically significant at the 95% confidence level.

3.5 Changes in water supply and water demand

In the simulation with active vegetation feedback, LAI is positively correlated with ET over most of the contiguous US region. The CO₂-induced changes in precipitation and surface temperatures are modified by the increase in surface evaporation and evaporative cooling, respectively, through enhanced surface latent heat flux. Those changes indicate that the water supply and demand (precipitation and PET, respectively) are influenced by the increase in evaporation combined with the presence of vegetation feedback. These changes in water supply and demand terms are directly linked with the changes in I_m and subsequent climate types. Figure 3.5 illustrates changes in precipitation, temperature, and PET caused by the radiative effects of the CO₂ increase, the combined radiative and vegetation-feedback effects, and vegetation-feedback effects alone. The radiative effects increase precipitation in the northeastern, midwestern, and some part of southern US regions, and decrease precipitation in the western states except northern Washington, Idaho, and the West South Central division (Fig. 3.5a). These changes in precipitation are consistent with projections made by the climate models included in the IPCC fourth assessment report, at least qualitatively (Karl et al., 2009). With active vegetation feedback, precipitation increases in most contiguous US regions except the southwestern inland region including the Nevada, Arizona, western New Mexico, and

southwestern Utah (Fig. 3.5d) with largest precipitation increases of up to 30 mm month⁻¹ in the Rocky Mountains region (Montana, Wyoming, and Colorado). The results from vegetation feedback only clearly show that this factor increases precipitation (Fig. 3.5g) especially in Idaho, Alabama, Georgia, Tennessee, and Kentucky. Further analysis shows that vegetation feedback increases convective precipitation but slightly reduces large-scale precipitation (not shown) suggesting that the positive feedback between the changes in local precipitation and LAI is mainly through the increase in local convection caused by enhanced ET rather than changes in the large scale circulation.

Spatial distributions of the surface temperature changes due to radiative effects are shown in Fig. 3.5b. In most of the contiguous US, the warming exceeds 2 K, except in regions along the Gulf of Mexico. The CO₂-induced warming is substantially reduced in the Midwest, East South Central division, and northern part of Mountain division when both radiative and vegetation-feedback effects are included (Fig. 3.5e). Vegetation feedback (Fig. 3.5h) alleviates surface warming caused by radiative effects by as much as 2 K over 80% of the total analysis area. Significant cooling effects were observed in wide regions over the Midwest, Northwest, and East South Central division via the enhancement of surface latent heat fluxes by the increase in ET and the decrease in solar radiation resulting from increased cloud cover (Jeong et al. 2011a).

According to the definition used in this study (Thornthwaite 1948), PET is directly influenced by the changes in surface temperatures. Figure 3.5c shows the PET changes due to CO₂-induced surface warming. In general, the increase in PET is largely shown occurring over the southern part of the US, including the South and Southwest whereas a relatively small increase occurs in the Northwest. Due to additional evaporative cooling induced by vegetation feedback, the increment in PET is largely suppressed over the analysis domain (Fig. 3.5f). In particular, strong negative anomalies of PET occur over the eastern US (Fig. 3.5i). Compared to the changes in surface temperatures, changes in PET are generally concentrated in the southern US region, probably because there are nonlinear empirical relationships between surface temperature and PET (Thornthwaite 1948).

Changes in water supply (precipitation) and demand (PET) lead to changes in I_m as inferred from Eqs. 2.2.1 and 2.2.2. The radiative effect increases aridity in most of the contiguous US through the increase in D (water deficit in Eq. 2.2.1) or the decrease in S (water surplus in Eq. 2.2.2) because PET increases are larger than precipitation increases. The increase in aridity is particularly strong in the southwestern US and the West South Central division, where PET increases and precipitation decreases. In the northern part of Mountain division, on the contrary, a large increase in precipitation leads to an increase in S , resulting in

increased I_m . When vegetation feedback is introduced, the changes in water balance induced by the radiative effect are greatly modified. Increases in precipitation and weakened PET increases lead to the decrease in aridity over the Midwest, East South Central division, and the northern part of Mountain division. When the impact of the radiative effect is removed, a decrease in aridity induced by vegetation feedback is clearly shown through enhanced precipitation and reduced PET over most of the contiguous US.

Overall, the changes in atmospheric water supply and demand are consistent with the changes in I_m and the subsequent climate type shown in Fig. 3.6. Decreases (increases) in I_m corresponding to the increase (decrease) in climate aridity occur in the regions where the increase in water demand exceeds the increase in water supply. In addition, changes in climate type appear in regions with notably large changes in both water supply and demand. These changes in water supply and demand, and I_m levels resulting from the radiative effect and vegetation feedback are summarized in Fig. 3.6. The vertical axis indicates I_m in the present-day climate run (VegOff_1×) and the horizontal axis indicates the ratio of precipitation (water supply) and PET (water demand) that is clearly proportional to I_m . The black dots depict the P/PET ratio in the present-day climate simulation. Orange cross markers and green open circles indicate the changes in the P/PET ratio when the radiative effect alone and

radiative/vegetation feedback effects are included, respectively. In general, orange cross markers appear to the left of black dots implying decreases in the P/PET ratio and a shift to a drier climate than the present-day climate. Green open circles, on the contrary, are generally located to the right of black dots implying an increase in the P/PET ratio. This clearly shows that vegetation feedback leads to a more humid climate in the CO₂ doubling condition compared to the radiation effects only case. Additionally, noticeable changes in the P/PET ratio, denoted by the orange cross markers and green open circles, are mainly observed in the subhumid climate type ($-20 < I_m < 20$) represented by the two dashed lines in Fig. 6. Because the subhumid climate type occurs in a large portion (> 40%) of the US, our results would suggest that vegetation feedback could have a considerable influence over changes in aridity induced by the increase in atmospheric CO₂ concentration.

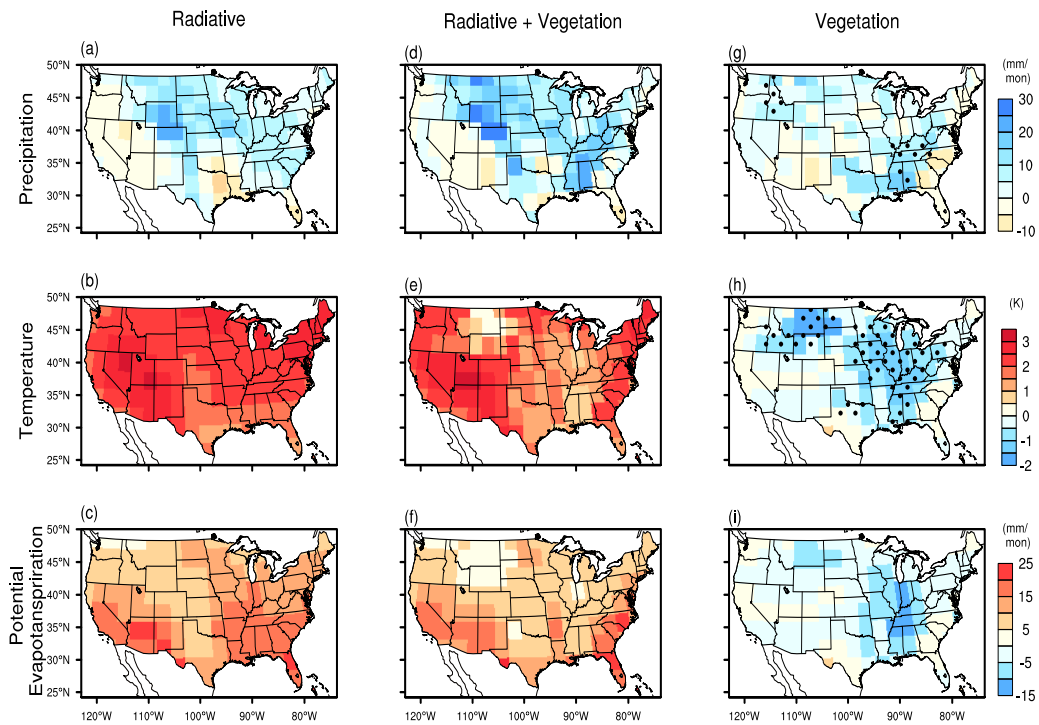


Figure 3.5. Spatial distribution of changes in precipitation, temperature, and PET over the US due to radiative effect (a–c), radiative and vegetation feedback effect (d–f), and vegetation feedback only (g–i). Black dots represent the regions that changes are statistically significant at the 95% confidence level.

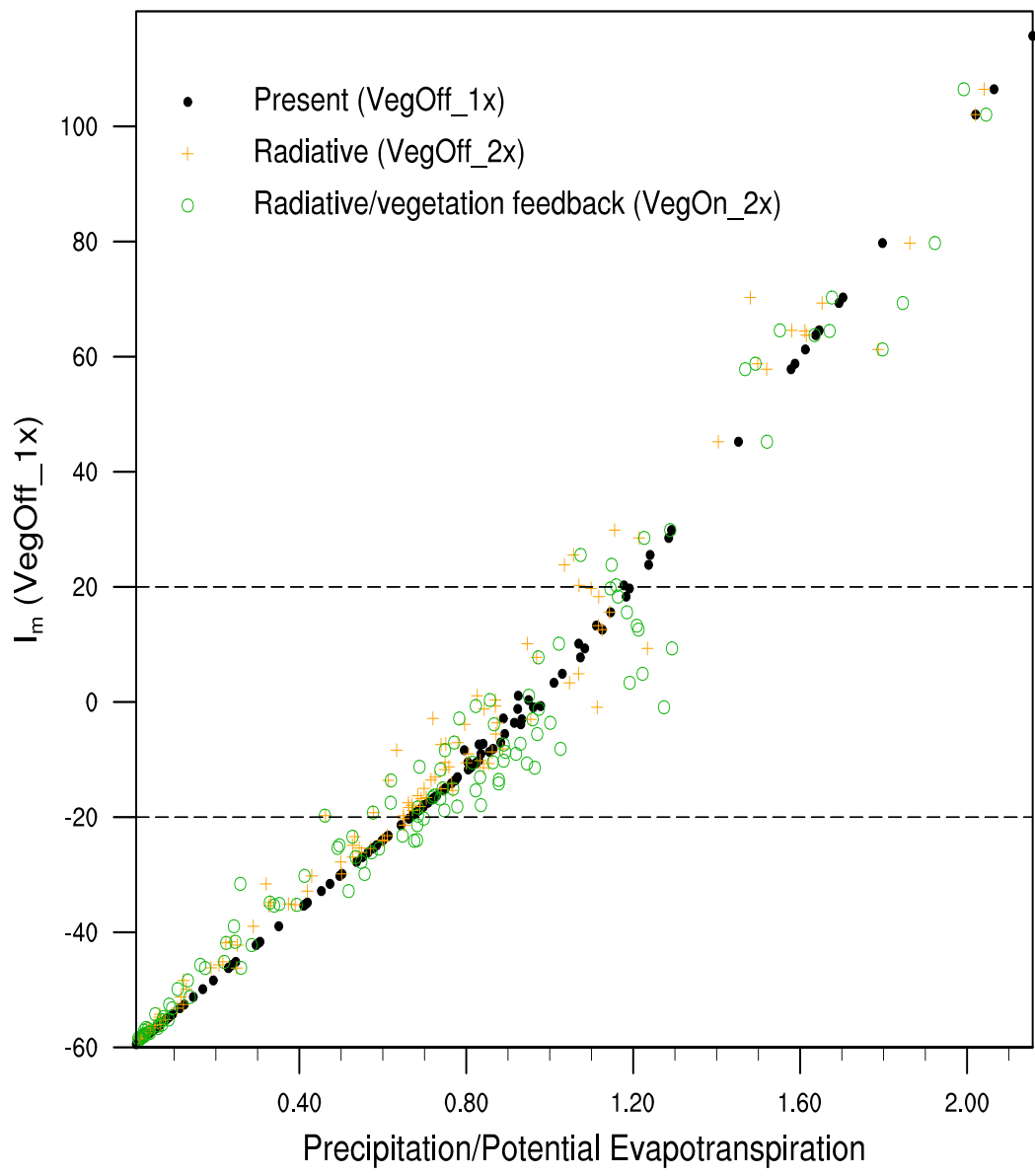


Figure 3.6. Scatter plot of the values of I_m in present climate run (VegOff_1x) with respect to ratio of precipitation to PET. Black, blue, and red dots represent the ratio of VegOff_1x, VegOff_2x, and VegOn_2x, respectively.

3.6 Summary and Discussion

3.6.1 Comparison of impact of change in ET with change in vegetation physiology and soil moisture

As examined in earlier studies (Notaro et al. 2006; Sitch et al 2008; Jeong et al. 2010), the coupled GCM experiments are focused on the combined impact of CO₂ doubling and the associated structural changes in vegetation such as PFTs and LAI. The results show that the increase in LAI, which is contributed by combined effect of direct CO₂ fertilization and indirect climatic warming, is notable structural change and main reason for vegetation feedback effect. But the impact of warming and CO₂ fertilization cannot be separately measured because of our experimental design. The relative contribution between direct CO₂ fertilization and indirect CO₂ induced climatic warming on LAI increases depends on region and climatic conditions. For instance, *Piao et al. (2006)* showed increase in LAI in moisture limited region is mostly explained by CO₂ fertilization over the regions where exhibited sufficient soil moisture. In contrast, increase in LAI in boreal region dominantly explained by temperature increases rather than CO₂ fertilization (Levis et al. 2000, Jeong et al 2011a).

The physiological responses of vegetation to carbon dioxide also cannot be isolated by the CAM3-DGVM model. Under increased CO₂ condition,

physiological effects may enhance the CO₂ induced warming and increase the surface runoff through suppression of plant stomata and transpiration (Seller et al. 1996; Betts et al. 2007; Cao et al. 2010). When structural changes in vegetation exist, however, the changes in surface albedo and ET are the two main mechanisms involved in vegetation feedback with the surface climate (Betts et al. 1997; Notaro et al 2007; Bonan 2008). For example, positive feedback between vegetation cover and surface temperature has been observed in the northern US during spring (March–May) via negative anomalies in surface albedo (Notaro et al. 2006). Potentially, replacing mixed crop land and urban built-up areas with vegetation could cause strong cooling in the Great Plains and the Midwest by increasing evaporation and surface albedo, respectively (Diffenbaugh 2009). Additionally, as a response to increasing GHGs, negative anomalies in surface albedo can induce positive anomalies in surface temperature and extreme warm events in the western US (Diffenbaugh 2005a, and b). Further, increase in vegetation greenness brings dominant vegetation–evaporative cooling over mid-latitudes and warming over high latitudes through a decrease in surface albedo (Jeong et al. 2010).

Soil moisture is another key variable in land-atmosphere interaction and climate aridity (Manabe et al. 2004; Seneviratne et al. 2010), further vegetation feedback (Hoffman and Jackson 2000; Kim and Wang 2007; Mendez-barroso et

al. 2009). Following the method used to calculate I_m , the impact of soil moisture on climate aridity may be ignored in our analysis. However, changes in I_m are connected with soil moisture through precipitation and temperature. Increase in precipitation naturally induces higher soil moisture except few cases (Seneviratne et al. 2010). Surface cooling, which leads to reduction of PET and increase in I_m , also produces higher soil moisture through negative correlation between temperature and soil moisture (Koster et al. 2006; Seneviratne et al. 2006). Additional analysis shows that changes in soil moisture due to radiative and vegetation-feedback-effects are consistent with the changes in precipitation and temperature in the eastern US, but inconsistent in western US (Fig. 3.7).

Volumetric Soil Water

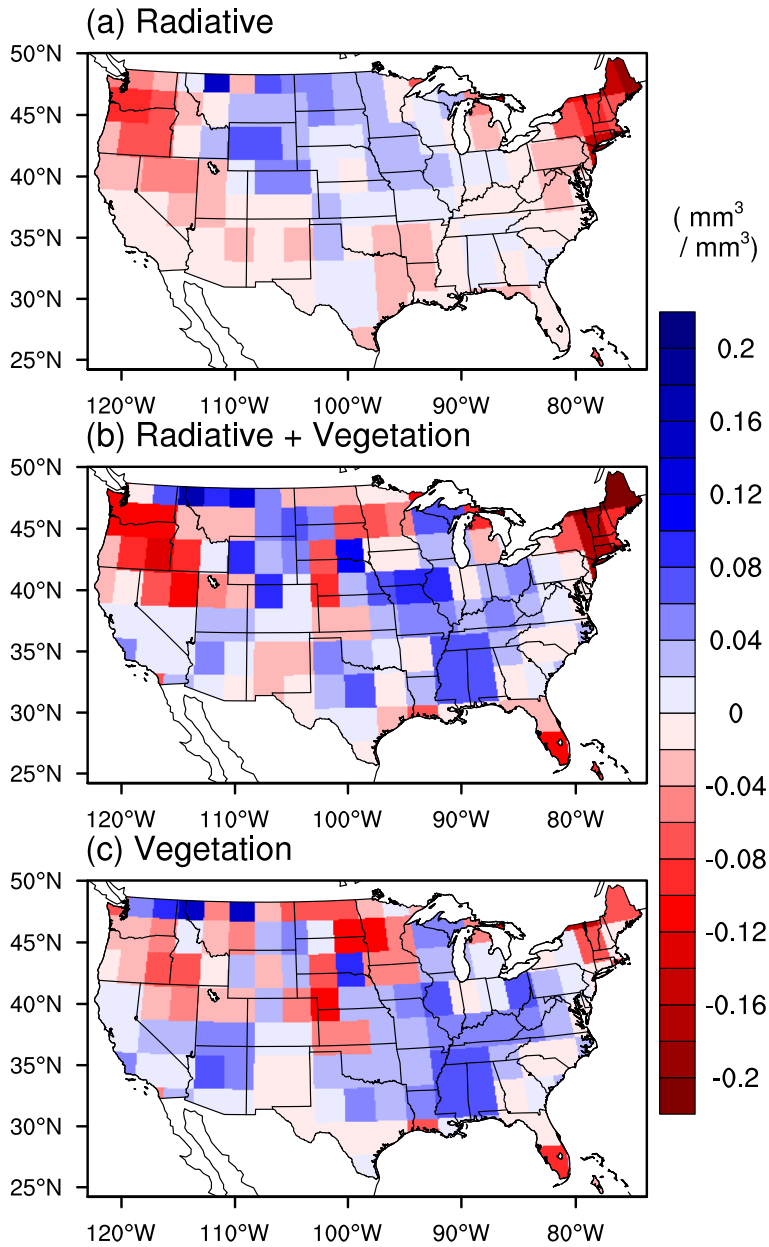


Figure 3.7. Spatial distribution of changes in vertically integrated volumetric soil water due to radiative effect (a), radiative and vegetation feedback effect (b), and vegetation feedback only (c).

3.6.2 Importance of vegetation feedback and limitation of potential vegetation and I_m

If the vegetation feedback is not considered, previous climate model projections with increasing GHGs suggested that increasing aridity may elevate natural disaster and social problems linked with water availability. For example, increasing aridity leads to longer periods of drought (Wang 2005; Sheffield and Wood 2008), greater water demands for irrigation (Edmonds and Rosenberg 2005), more difficult water management (Kundzewicz et al. 2007; Yohe et al. 2007), and difficulties in energy production resulting from limited water supplies (Filed et al. 2007; Hightower and Pierce 2008). *Bonan* (2008) and *Jackson et al.* (2008) reported that vegetation feedback is important to mitigate the impact of climate change and reduce the social and economic costs required to manage those problems. A key result of the present study points to decreases in summer dryness through vegetation feedback, providing additional evidence that vegetation can alleviate climate change. Further, vegetation feedback exerts favorable influences on subhumid climate types that are vulnerable to climate change. Thus, the impact of vegetation feedback is an important component for projection and mitigation of climate change, especially for climate hot spots.

In this thesis, the I_m and related climate types is used to visualize and interpret the impact of radiative and vegetation feedback on climate aridity

because of I_m is known for a reliable index for water balance (Feddemma 2005a). The key advantage of I_m is that it is simple, being only defined by monthly temperature and precipitation. Thus, the results are easy to interpret and understand. Though the advantage, formulation of I_m has two limitations. One is the empirical algorithm used to estimate the monthly PET (Thornthwaite 1948). The simple formula used merely monthly air temperature to estimate PET may cause some bias because the effects of wind speed, humidity, and net radiation are not included in the calculation of PET (Allen et al., 1998). This bias, however, has little impact on our result because of diverse validation tests showed that the PET estimated by Thornthwaite method is comparable to PETs calculated from various complex methods in the US (Hulme et al. (1992); Mintz and Walker (1993)).

In the present study, we only focused on potential vegetation which is only modulated by climate, but anthropogenic land cover change can also influence changes in climate regime. Previous studies reported (Zhao and Pitman 2002; Feddemma et al. 2005b) that changes in land use/cover, such as for agriculture and urbanization, can potentially influence regional climate over developed regions. Though CAM3-DGVM simulates reliable low-level circulation and spatial distribution of precipitation, in addition, the T42 horizontal resolution may be too coarse to represent complex local topography, particularly over the western

US (Diffenbaugh et al. 2005b). The impact of local topography on regional circulation cannot be well simulated by this coarse spatial resolution model, which likely explains the wet biases in Rocky Mountains and western Great Plains regions (Meehl et al. 2006). Despite these limitations, the CAM3-DGVM has been widely and successfully used to evaluate the impact of land use change and vegetation feedback on North America (Oleson et al. 2004). In addition, positive temperature anomalies in the western US obtained in our simulations are consistent with those obtained by RCM simulation with fine spatial resolution (Diffenbaugh 2005b). Therefore, the CAM3-DGVM model used in this study is sufficient, though certainly not perfect, for estimating the potential impact of vegetation feedback on broader scale summer aridity across the US.

4. Understanding of present and future changes in vegetation

4.1 Temperature and precipitation in present and future climate

Figure 4.1 shows that the 20C3M runs reasonably simulate the present-day (1980-1999) climatology of temperature and precipitation depicted by CRU with the Pearson correlation coefficients of spatial patterns of 0.99 and 0.95 for the temperature and precipitation, respectively. The differences in the global means are also small: 0.44°C for temperature and $-1.83 \text{ mm mon}^{-1}$ for precipitation, respectively (Table 4.1). Also the regional mean of the simulated temperature and precipitation is similar to CRU for each continent (Table 4.1). Figure 4.2 shows the temperature and precipitation changes for the low, medium, and high warming groups in the period 2080–2099. For all these groups, surface temperature increases for all of land surfaces (Figs. 4.2a, 4.2b, and 4.2c) with the global-mean changes of 2.10°C , 3.01°C , and 4.10°C in the low, medium, and high warming groups, respectively (Table 4.2). For each continent, the increase in surface temperatures is proportional to the amount of global warming (Table 4.2). Precipitation changes are generally positive but precipitation changes are small or negative for the central Asia, Mediterranean, southern Africa, and

central America regions (Figs. 4.2d, 4.2e, and 4.2f). The global-mean precipitation increases by 3.45, 4.76, 4.35 mm mon⁻¹ in the low, medium, and high warming groups, respectively (Table 4.2). In contrast to the temperature change, the continental change in precipitation is largest in the medium warming group except for North America and Asia (Table 4.2) due to large decrease in precipitation on South America, southern Africa, and Mediterranean in the high warming group (Fig. 4.2f).

Table 4.1. Annual mean temperature and precipitation (\pm standard deviation) of CRU and 20C3M simulations for present-day.

Continent	Temperature ($^{\circ}\text{C}$)		Precipitation (mm mon^{-1})	
	CRU	20C3M	CRU	20C3M
Globe	13.45	13.01 (± 0.09)	68.89	70.72 (± 1.26)
Africa	23.54	23.30 (± 0.06)	48.72	56.59 (± 1.05)
Asia	9.15	8.37 (± 0.11)	53.19	52.71 (± 1.05)
Australia	21.96	21.69 (± 0.07)	44.72	40.63 (± 1.25)
Europe	10.60	10.09 (± 0.10)	52.60	55.84 (± 1.01)
North America	6.01	5.23 (± 0.12)	62.76	65.30 (± 1.20)
South America	21.80	21.81 (± 0.06)	128.69	137.10 (± 2.03)

Table 4.2. Projected changes in annual mean temperature and precipitation (\pm standard deviation) for low, medium, and high warming groups in future (2080-2099).

Continent	Temperature			Precipitation		
	Low	Medium	High	Low	Medium	High
Globe	2.10 (\pm 0.48)	3.01 (\pm 0.50)	4.10 (\pm 0.57)	3.45 (\pm 5.15)	4.76 (\pm 7.17)	4.34 (\pm 8.91)
Africa	2.02 (\pm 0.43)	2.87 (\pm 0.45)	3.82 (\pm 0.45)	1.20 (\pm 4.51)	1.64 (\pm 5.91)	1.04 (\pm 7.19)
Asia	2.25 (\pm 0.52)	3.26 (\pm 0.53)	4.47 (\pm 0.59)	3.82 (\pm 3.76)	5.45 (\pm 4.97)	6.36 (\pm 6.20)
Australia	1.85 (\pm 0.31)	2.58 (\pm 0.43)	3.31 (\pm 0.45)	1.48 (\pm 4.26)	2.31 (\pm 4.74)	2.02 (\pm 7.37)
Europe	2.06 (\pm 0.44)	3.05 (\pm 0.54)	4.00 (\pm 0.60)	1.04 (\pm 3.56)	0.77 (\pm 4.58)	-0.97 (\pm .29)
North America	2.26 (\pm 0.50)	3.19 (\pm 0.55)	4.39 (\pm 0.66)	4.25 (\pm 4.77)	5.18 (\pm 6.06)	5.51 (\pm 7.56)
South America	1.77 (\pm 0.41)	2.55 (\pm 0.42)	3.58 (\pm 0.55)	4.27 (\pm 9.70)	6.08 (\pm 16.20)	1.19 (\pm 20.19)

Present day (1980-1999) climatology

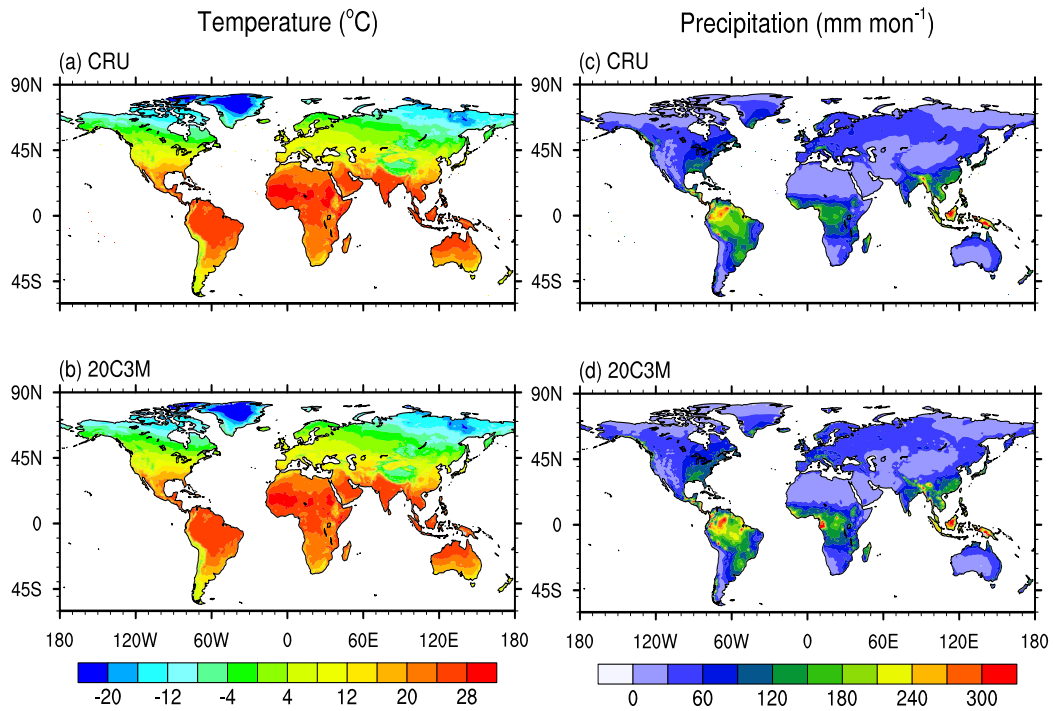


Figure 4.1. Spatial distributions of averaged temperature of (a) CRU and (b) ensemble of 20C3M simulations, and precipitation of (c) CRU and (d) ensemble of 203CM simulations for present-day (1980-2009).

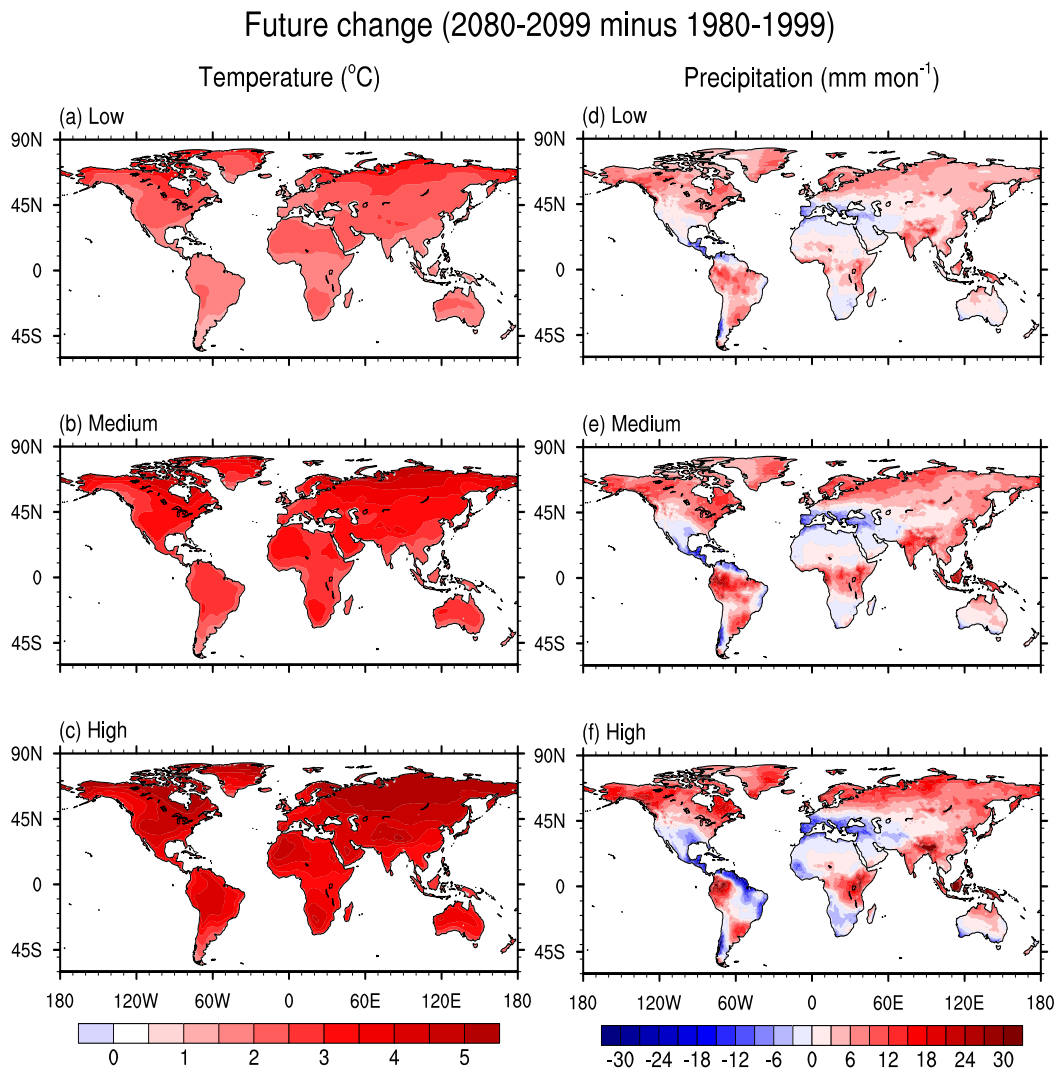


Figure 4.2. Spatial distribution of changes in averaged temperature (2080-2099 minus 1980-1999) for (a) 12 models in low, (b) 18 models in medium, and (c) 18 models in high warming threshold. (d), (e), and (f) show changes in averaged precipitation for low, medium, and high warming threshold.

4.2 Projected changes in spatial distribution of potential plant habitat

Figure 4.3 presents the spatial distributions of the eight plant habitats and desert areas in the present-day climate based on the CRU data and 20C3M GCM simulations. The habitat distributions in the late 21st century calculated for the low, medium, and high warming cases are also shown. For the present-day, the global distribution of plant habitats from the SRES 20C3M simulation is similar to the CRU-based plant habitats (Figs. 4.3a vs. 4.3b). Plant habitats calculated using the CRU and GCM temperatures vary with latitudes in general. The temperate habitats are bounded by the boreal habitats around 55°N, and most of the tropical habitats are located between 20°S and 20°N. In the eastern regions of northern Eurasia and North America, plant habitat boundaries appear at lower latitudes than in the western part of these continents. This spatial pattern of plant habitat in the present-day resembles the biome distributions from satellite retrievals (Friedl et al. 2002; Friedl et al. 2010; Sulla-Menashe et al. 2011).

The projected plant habitats in the late 21st century show clear differences of habitats from the present-day distribution, even for the lowest warming case ($\Delta T < 2.5^\circ\text{K}$) (Fig. 4.3c). In the low warming case ($\Delta T < 2.5^\circ\text{K}$), two prominent

features characterize plant habitat changes. First, tropical habitats expand substantially into adjacent temperate habitats, mainly central South America, southern Africa, northern Australia, and India. The area of tropical habitats is projected to increase by 15.4% from the present-day. This is explained by the increase in the Tr1-type habitat (tropical broadleaf green and tropical herbaceous) by up to $5.39 \times 10^6 \text{ km}^2$, about 22% of the present-day area (Table 4.3). Expansion of the tropical habitats is accompanied by contraction of two habitat types such as Te1 (tropical broadleaf green, temperate needleleaf evergreen, temperate broadleaf evergreen, and tropical herbaceous) and Te2 (temperate needleleaf evergreen, temperate broadleaf evergreen, temperate broadleaf summergreen, and temperate herbaceous), suggesting decreases in temperate woody species in temperate regions. Second, the boreal habitats decrease in the northern regions of Eurasia and North America by $3.6 \times 10^6 \text{ km}^2$, 15.1% of the present-day value (Table 4.3). The decrease in the boreal habitat is accompanied by northward propagation of the Te3- (temperate needleleaf evergreen, temperate broadleaf summergreen, and temperate herbaceous) and Te4-type (Temperate broadleaf summergreen, boreal summergreen, boreal needleleaf evergreen, and temperate herbaceous) habitats by $0.87 \times 10^6 \text{ km}^2$ and $2.33 \times 10^6 \text{ km}^2$, 13.7% and 11.7% of the present-day values, respectively (Table 4.3).

These habitat changes are further enhanced in higher warming conditions ($2.5^{\circ}\text{K} < \Delta T < 3.5^{\circ}\text{K}$ and $3.5^{\circ}\text{K} < \Delta T$) (Figs. 4.3d and 4.3e). The warming magnitude is monotonically related to the increase in the tropical habitats and the decrease in the boreal habitats. Compared to the low warming case, the tropical habitats increase further by $1.95 \times 10^6 \text{ km}^2$ and $3.80 \times 10^6 \text{ km}^2$ in the medium and high warming cases, respectively (Table 4.3). Similarly, the boreal habitats are decreased further by $1.80 \times 10^6 \text{ km}^2$ and $4.12 \times 10^6 \text{ km}^2$ in the medium and high warming cases, respectively (Table 4.3). These changes indicate that the tropical habitats will increase as much as the decrease in the boreal habitats for higher warming situations. However, the proportions of the area changes to the present-day area are up to 5.8% and 11.3% for the tropical habitats, and 7.6% and 17.3% for the boreal habitats in the medium and high warming cases, respectively. These changes suggest that the risk of changes to boreal habitats will be larger than that of tropical habitats for higher warming.

The projected spatial patterns of plant habitats in the late 21st century show that most habitat changes are observed in the boundary regions between the tropical (temperate) and temperate (boreal) plant habitats. This is evident in the zonal-mean patterns of the fractional change in plant habitat. Figure 4.4 shows the zonal-mean of the fraction of change of the tropical, temperate, and boreal habitats for the low, medium, and high warming cases in the late 21th century.

Generally, the fractional changes are most noticeable in three latitudinal belts: 10°S–25°S, 15°N–30°N, and 50°N–65°N (see the regions between dotted lines in Fig. 4.4). The amount of fractional changes also increases with the warming strength. The variation in the fractional change according to the magnitude of warming is largest in the latitudinal band 10°S–25°S where the projected maximum increase in the tropical habitats is as large as 20% (Fig. 4.4a). Around 20°S, the increase in the tropical habitats is as large as 60% for high warming, while the low warming case shows just 10% of change in the tropical habitats at the same latitude. In the regions 15°N–30°N and 50°N–65°N, the fractional changes of temperate and boreal habitats also increase with warming amplitudes (Figs. 4.4b and 4.4c). The largest difference in the fractional change between the high and low warming cases is 25% at 25°N and 20% at 55°N. Consequently, overall patterns show decreasing (or increasing) boreal (or tropical) plant habitat fractions are accompanied by increasing (or decreasing) temperate plant habitat changes.

Table 4.3. Area of observed and projected plant habitat (10^6 km^2). The numbers are the total area (in 10^6 km^2) covered by each climate type. The numbers of in parentheses are one standard deviation of total area (in 10^6 km^2) projected by 12, 18, and 18 projections in low, medium, and high warming groups.

Years	Data	Tr1	Tr2	Te1	Te2	Te3	Te4	Bo1	Bo2
1980–1999	Obs (CRU)	25.27	8.55	8.05	19.94	6.60	19.81	21.48	3.65
	All	24.66 (0.26)	9.07 (0.15)	8.36 (0.09)	20.17 (0.38)	6.62 (0.18)	19.30 (0.40)	18.84 (0.39)	4.95 (0.26)
	Low	24.72 (0.17)	9.02 (0.09)	8.32 (0.05)	20.15 (0.27)	6.66 (0.14)	19.22 (0.23)	18.85 (0.29)	4.99 (0.22)
	Medium	24.68 (0.19)	9.06 (0.11)	8.35 (0.05)	20.14 (0.23)	6.61 (0.09)	19.29 (0.25)	18.89 (0.23)	4.95 (0.18)
	High	24.62 (0.19)	9.10 (0.11)	8.38 (0.04)	20.16 (0.24)	6.61 (0.10)	19.34 (0.26)	18.84 (0.17)	4.91 (0.15)
	2080–2099	Low	30.66 (1.03)	8.28 (0.29)	6.95 (0.67)	18.73 (0.78)	7.53 (0.41)	21.55 (1.12)	17.20 (0.72)
	Medium	32.57 (0.96)	8.32 (0.30)	6.16 (0.55)	18.33 (0.79)	7.81 (0.58)	22.24 (1.32)	16.05 (0.97)	2.34 (0.50)

High	34.76	7.98	5.27	17.80	7.95	23.18	14.39	1.68
	(0.97)	(0.35)	(0.75)	(0.97)	(0.63)	(0.99)	(0.82)	(0.37)

Distribution of plant habitat

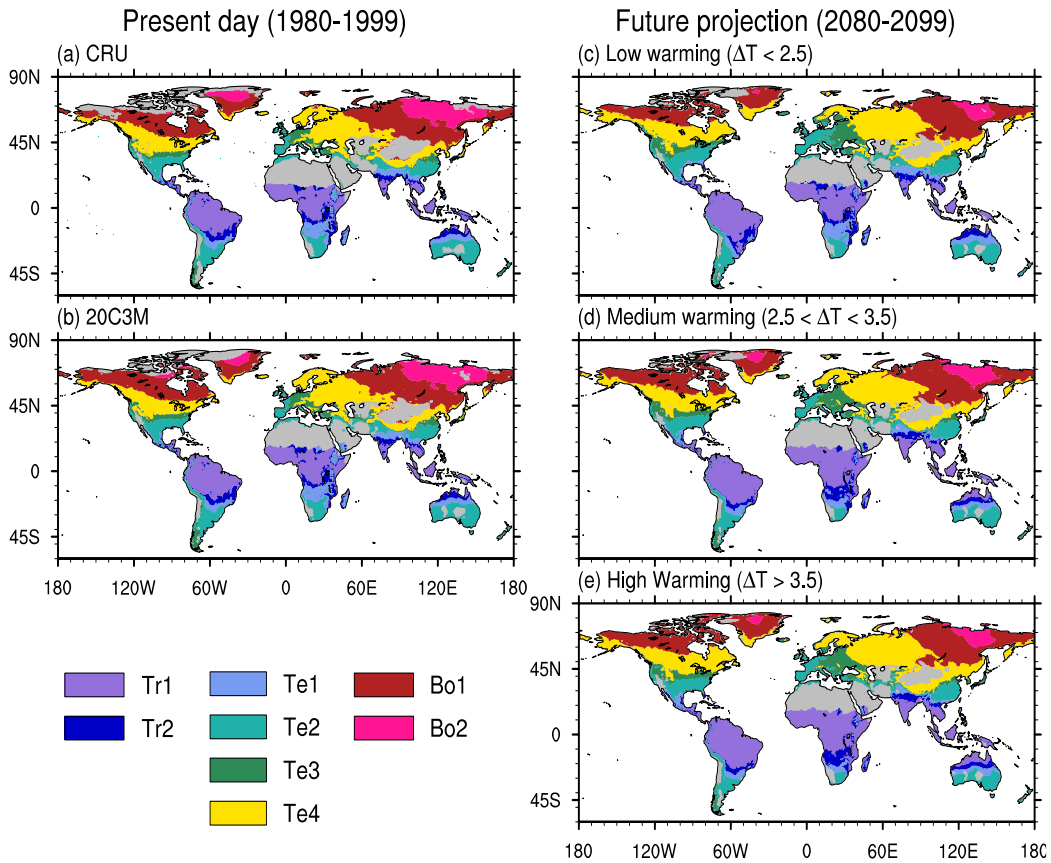


Figure 4.3. Spatial distribution of averaged plant habitat of present day (1980-1999) for (a) CRU and (b) ensemble of 20C3M simulations. Spatial distribution of averaged plant habitat of future projection (2080-2099) for (c) 12 models in low, (d) 18 models in medium, and (e) 18 models in high warming threshold. Regions with grey shading represent the desert areas.

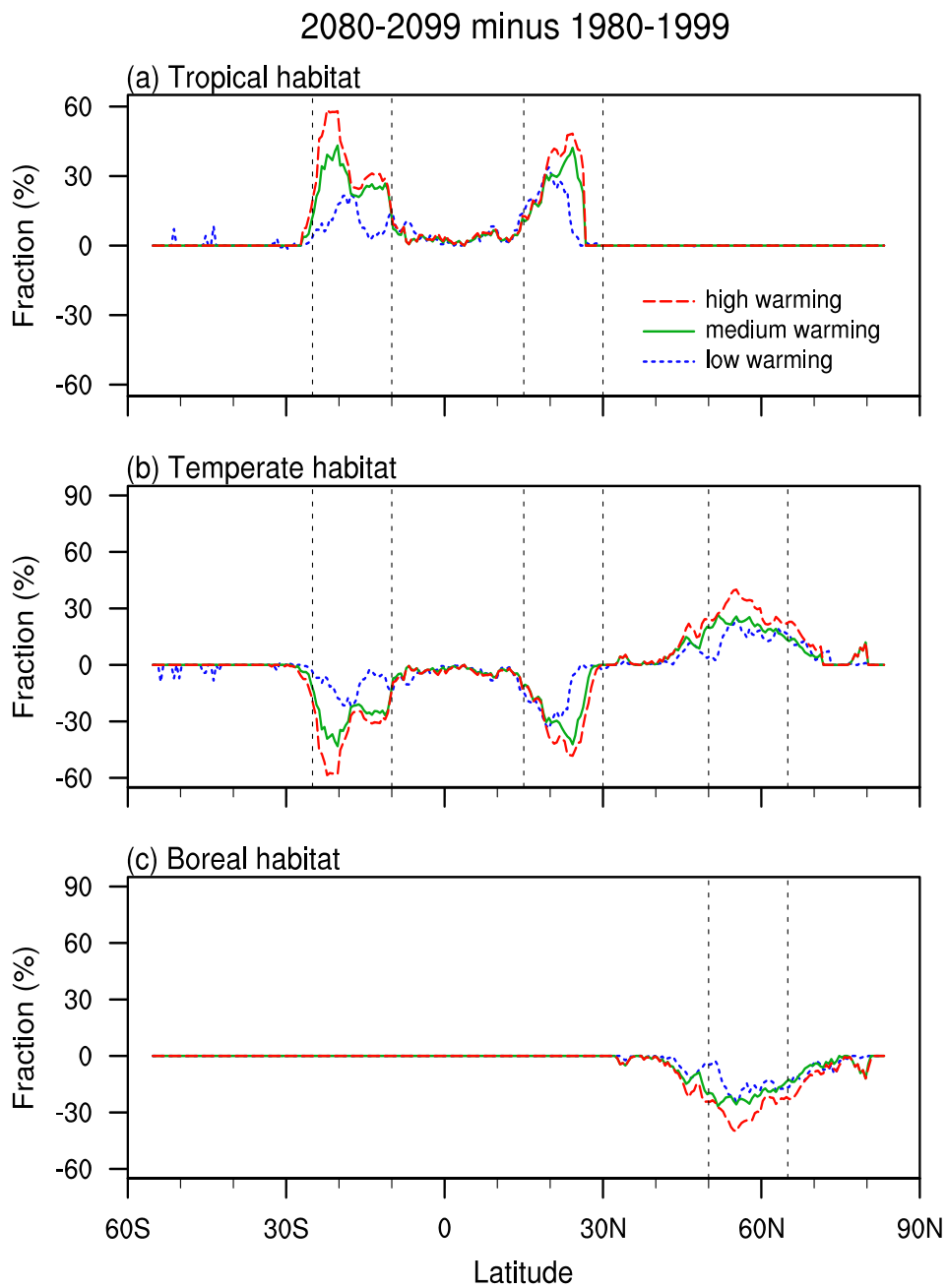


Figure 4.4. Difference of zonal-mean fractional change in plant habitat between the period of 2080–2099 and 1980–1999 for (a) tropical habitat, (b) temperate habitat, and (c) boreal habitat. Red dashed, green solid, and blue dotted line indicates high, medium, and low warming threshold.

4.3 Projected changes in the timing of plant habitat changes

4.3.1 Regional characteristics of timing of plant habitat change

Based on the changes in plant habitat for the three latitude bands, we further estimate the timing of the plant habitat change related to the three warming cases. Figure 4.5 plots the percentage of plant habitat change from the present-day (abscissa) against time (ordinate) for the three latitude bands. Due to the wide spread of the projected plant habitat changes induced by various climate model forcings, we focus on the ensemble mean of the plant habitat change between the projections (solid lines). In the regions 10°S–25°S, the ensemble mean exceeds 10% in 2032 for the high warming case (Fig. 4.5a and Table 4.4). This timing of the amount of habitat change precedes that of the low and medium warming cases by 11 and 5 years, respectively (Fig. 4.5a and Table 4.4). Increasing the threshold of fractional change to 20% and 30% also increases the difference in the timing between the high and other warming cases. The timing gap is 34 years between the low and high warming cases at 20% threshold, and 10 and 12 years between the medium and high warming cases at 20% and 30% threshold, respectively. In the regions 15°N–30°N, the mean habitat changes reach 10%, 20%, and 30% in the years 2046, 2070, and 2093, respectively in the high warming case (Fig. 4.5b and Table 4.4), earlier than those in the low warming

case by 12 years at the 10% threshold, and those of the medium warming case by 4 and 23 years at the 10% and 20% thresholds, respectively. In the latitudes 50°N–65°N, the plant habitat change also occurs earlier as the warming magnitude increases at the 20% and 30% thresholds (Fig. 4.5c and Table 4.4). For the 10% threshold, however, the timing of the low warming case precedes that of the medium warming case by 5 years (Table 4.4). This reversed relationship between the habitat-change timing and the warming magnitude is because of increase in averaged T_c of the latitudes 50°N–65°N is larger in the low warming case in the early 21st century (not shown). Despite this exception, overall patterns of projected plant habitat changes suggest that increased warming leads to faster habitat changes.

Due to the spatial heterogeneity of plant habitat changes, regional discrepancies in the timing of mean plant habitat changes are analyzed for the three latitudinal belts in each continent (Table 4.4). The most dominant features are found between southern Africa (0°–60°E) and central South America (30°W–90°W) in the latitudes 10°S–25°S. In the medium warming case, for example, the 20% habitat change occurs in 2052 for the southern Africa region, but in 2099 for the central South America region. This time gap in achieving the same amount of habitat change between these two regions indicates that southern Africa will experience larger and faster habitat change under the same global

warming. This regional variation is intensified as the warming increases. In southern Africa, the difference in the timing is 40 years for the 30% threshold between the low and high warming cases. However, central South America shows no change in the timing to achieve the 30% change for all three warming cases. Similar regional variations in the timing occur in the regions 15°N–30°N between East Asia (60°E–150°E) and northern North America (60°W–120°W) (Table 4.4); the same amount of plant habitat change occurs earlier in East Asia than in northern North America. The regional variation is amplified with increasing warming magnitudes.

For the region between 50°N–65°N, the difference between northern Eurasia (30°E–180°) and northern North America (50°W–170°W) is relatively small compared to other latitude bands (Table 4.4). The warming magnitude has only a small impact on the regional discrepancy in the timing of plant habitat change. Instead, the threshold value for the fractional habitat change is more important in examining the regional variations in the temporal changes in plant habitat. For the 10% threshold, the timing in northern Eurasia is earlier than that in northern North America, whereas this change is reversed at the 30% threshold (Table 4.4). In the high warming case, the timing is faster in northern Eurasia than in northern North America by 22 years for the 10% threshold; whereas, the timing only appears in northern North America for the 30% threshold (Table 4.4).

The ensemble mean of the timing of the plant habitat changes is analyzed by considering large variations of climate projections among model simulations. Nevertheless, the uncertainty in climate projections still exists. In figure 4.5, colored bars show the range of projected timings of plant habitat change. Upper and lower limit of the spread of timings provided as exact year for each colored bars. If upper limit is larger than 2099, the upper limit is presented upper arrow. Larger range with wider spread of projections represents larger uncertainty of projected timing. The ranges of projected timings in low warming case are generally larger than those in medium and high warming case for the 10% and 20% thresholds (Fig. 4.5). In regions of 10°N–25°N, for example, the range of projected timing is 48, 36, and 29 years for low, medium, and high warming cases at 10% thresholds. The ranges of projected timing also vary in difference latitudinal zones. The latitudes of 50°N–65°N shows broader range of projected timing than other latitudinal belts, especially at 10% thresholds of fractional change. These wide ranges of projected timings of the regions of 50°N–65°N are closely related to high uncertainty in temperature projection in high-latitudes (Meehl et al. 2007b).

Due to the ranges of projected timings, the relationship between the warming magnitude and the timing of plant habitat change is revised by changing the standard from the ensemble mean to the 90% proportion among all

models (Table 4.5). Analysis based on the timing of the 90% proportion can increase confidence level because of the 90% proportion indicates that particular habitat changes are almost certain to occur at a certain time. The timing of the 90% proportion is later than that of the ensemble mean by several decades (Table 4.5). In the case of the 90% proportion, the timing of habitat change is reduced with increased warming for all cases. Also, the 90% proportion is notable in the high warming case rather than in the low- and medium warming cases. This implies that the timing in the higher warming case makes the habitat change sure to be earlier, regardless of the uncertainty of future projections.

Table 4.4. Estimated year that ensemble mean of projected habitat changes firstly exceed 10%, 20%, and 30% threshold for all warming groups in the three latitudes belts. En-dash means that the ensemble means does not reach the three thresholds until 2099.

	Low warming ($\Delta T < 2.5^\circ\text{K}$)			Medium warming ($2.5^\circ\text{K} < \Delta T < 3.5^\circ\text{K}$)			High warming ($\Delta T > 3.5^\circ\text{K}$)		
	10%	20%	30%	10%	20%	30%	10%	20%	30%
10°S–25°S	2047	2094	-	2040	2068	2096	2034	2057	2076
southern Africa	2028	2063	2094	2026	2053	2067	2020	2044	2057
entral South America	-	-	-	2070	-	-	2059	-	-
15°N–30°N	2056	-	-	2050	2095	-	2045	2075	-
East Asia	2056	-	-	2052	2089	-	2046	2071	-
southern North America	-	-	-	2077	-	-	2065	-	-
50°N–65°N	2056	-	-	2049	2085	-	2045	2069	2097

northern Eurasia	2047	-	-	2041	2086	-	2040	2070	-
northern North America	2050	2084	-	2047	2073	2093	2039	2060	2073

Table 4.5. Estimated year that 10% and 90% of model simulations of projected habitat changes firstly exceed 10%, 20%, and 30% threshold for all warming groups in the three latitudes belts. En-dash means that the ensemble means does not reach the three thresholds until 2099.

		Low warming ($\Delta T < 2.5^\circ\text{K}$)			Medium warming ($2.5^\circ\text{K} < \Delta T < 3.5^\circ\text{K}$)			High warming ($\Delta T > 3.5^\circ\text{K}$)		
		10%	20%	30%	10%	20%	30%	10%	20%	30%
10°S–25°S	10%	2035	2066	-	2028	2057	2079	2023	2049	2067
	90%	2066	-	-	2051	2088	-	2043	2068	2087
southern Africa	10%	2019	2054	2066	2016	2039	2058	2012	2035	2046
	90%	2045	2087	-	2045	2074	2093	2040	2064	2072
central South America	10%	2065	-	-	2050	-	-	2042	-	-
	90%	-	-	-	2079	-	-	2074	-	-
15°N–30°N	10%	2044	-	-	2036	2078	-	2038	2067	2097
	90%	2073	-	-	2066	-	-	2057	2083	-
East Asia	10%	2045	2078	-	2037	2062	-	2036	2058	2087
	90%	2085	-	-	2068	-	-	2063	2087	-

southern	10%	-	-	-	2065	-	-	2052	2087	-
North America	90%	-	-	-	-	-	-	2086	-	-
<hr/>										
	10%	2035	2070	-	2030	2059	2099	2031	2058	2084
50°N–65°N	90%	2092	-	-	2068	-	-	2055	2086	-
northern Eurasia	10%	2021	2076		2013	2055	-	2009	2050	2083
	90%	-	-		2062	-	-	2059	2082	-
northern North America	10%	2013	2054	2069	2029	2048	2061	2016	2041	2059
	90%	2099	-	-	2086	-	-	2061	2076	2091
<hr/>										

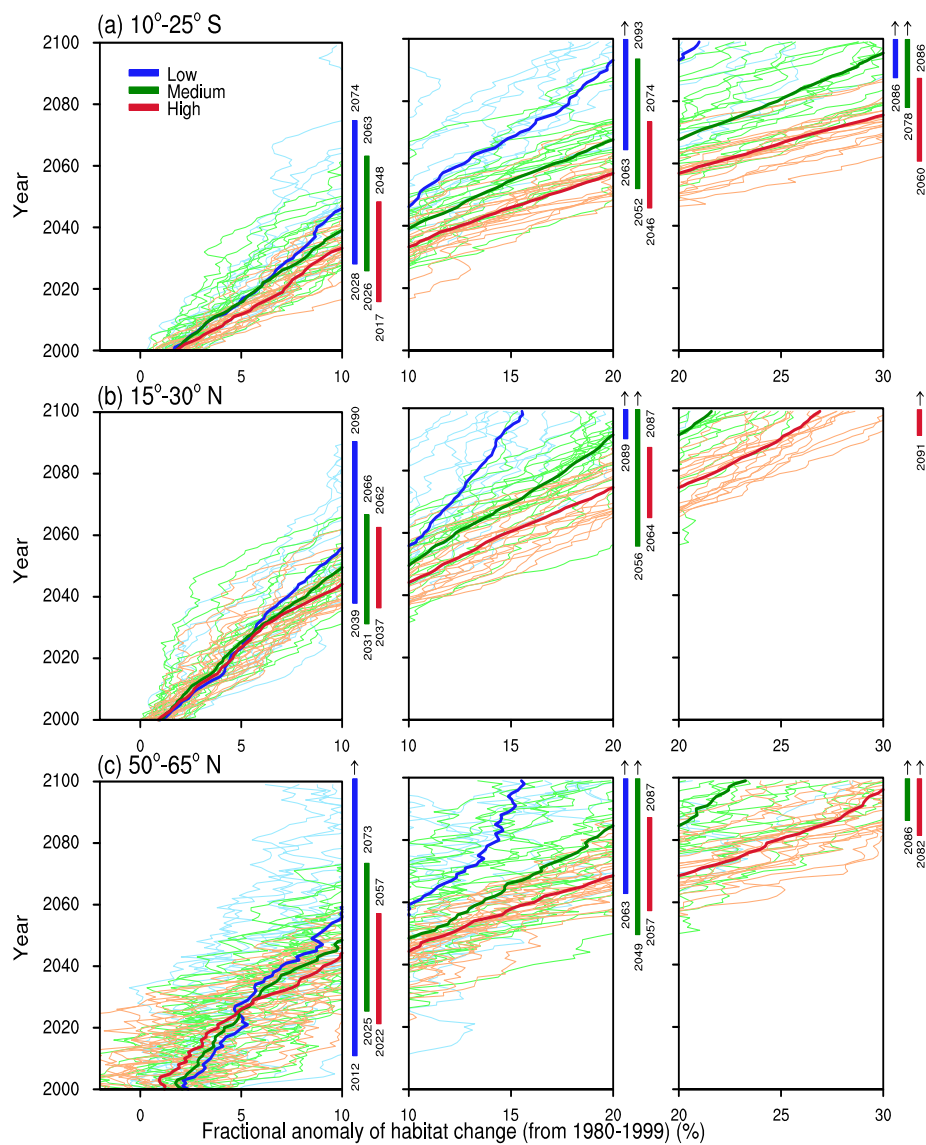


Figure 4.5. Regional mean fractional changes in plant habitats for (a) 10° – 25° S, (b) 15° – 30° N, and (c) 50° – 65° N. Each projection from the CMIP3 model simulation included in low-, medium-, and high- warming groups are shown in light blue, light green, and light orange. Blue, green, and red bars represent the range of timing when projected habitat changes might cross the 10%, 20%, and 30% thresholds of low-, medium-, and high- warming groups.

4.3.2 Relationship between national wealth and the timing of plant habitat change

Figure 4.6 shows the projected time (year) of the plant habitat change, along with the GDP values of the six nations for the three warming cases at three thresholds, respectively. For all thresholds and all warming cases, the timings of plant habitat change in Angola are overwhelmingly faster than the other countries by several decades (Figs. 4.6a and 4.6b). In particular, only Angola shows the timings of plant habitat change for the low and medium warming cases at the 30% threshold (Fig. 4.6c). The GDP of Angola is much lower than that of the other nations (Table 2.1). Thus, the vulnerability of plant habitat in Angola is amplified considering both the timing of plant habitat change and regional economic power.

The timing of the plant habitat change at all thresholds of fractional change is noticeably fast in Canada, Russia, and China (Fig. 4.6). However, these three nations have sufficiently large GDP: 1736.1, 1857.8, and 7318.5 billion US dollars for Canada, Russia, and China, respectively (Table 2.1). Thus, economic capability may allow these countries to alleviate the risk of plant habitat change. For Mexico and Brazil, the timings of plant habitat change are later than other regions by several decades in all warming cases at 10% and 20% threshold (Figs.

4.6a and 4.6b), indicating relatively low risk of plant habitat change (Figs. 4.6a and 4.6b). In addition, the large GDP values of the two nations (> 1000 billion US dollars) also decrease the adverse effects of plant habitat changes.

Timing of habitat change with GDP per Capita

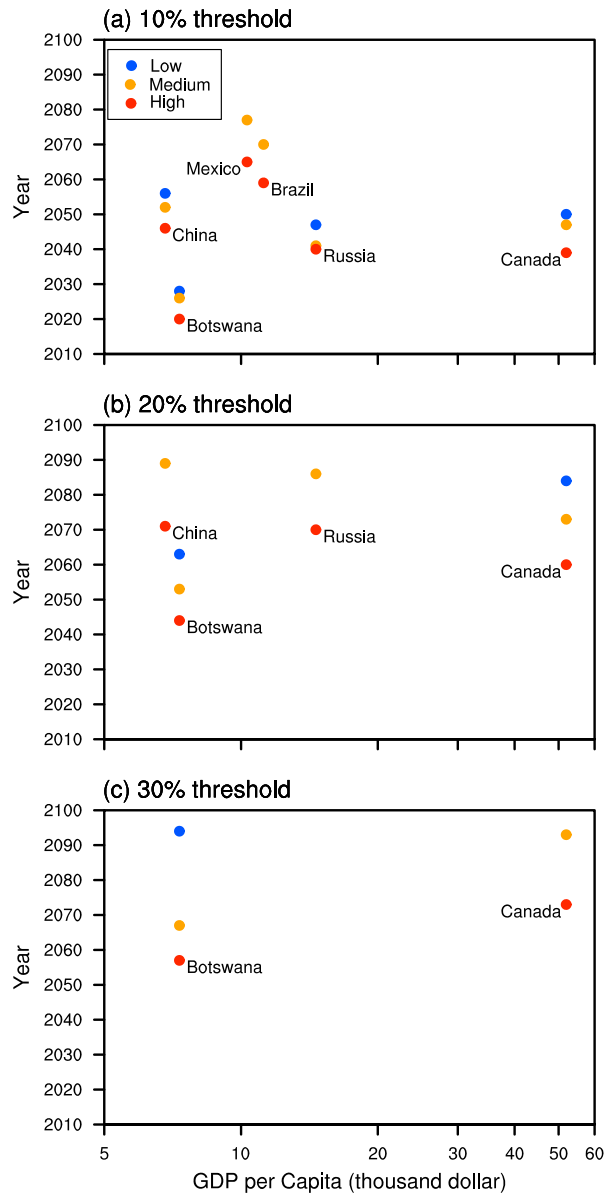


Figure 4.6. Timing of averaged plant habitat change reaches (a) 10%, (b) 20%, and (c) 30% threshold for GDP per Capita 2012 of Botswana, China, Mexico, Russia, and Canada. Blue, yellow, and red dots represent low, medium, and high warming threshold, respectively.

4.4 Summary and Discussion

Before evaluating the timing for specified plant habitat changes, the spatial patterns of plant habitat changes are analyzed in terms of global warming magnitudes. For the low warming case ($\Delta T < 2.5^\circ\text{K}$), the largest spatial changes in plant habitat are observed in the boundary regions between the tropical (10°S – 25°S), temperate (15°N – 30°N), and boreal (50°N – 65°N) habitats. With increasing magnitudes of global warming (medium case: $2.5^\circ\text{K} < \Delta T < 3.5^\circ\text{K}$ and high case: $\Delta T > 3.5^\circ\text{K}$), the fractional changes in plant habitat are increased in all three latitude zones. For example, in the regions 50°N – 65°N , boreal habitats are projected to decrease by 15.3%, 22.9%, and 32.3% in the low, medium, and high warming cases, respectively. These results are consistent with the spatial patterns of the simulated plant habitat changes in previous studies (Cramer et al. 2001; Lucht et al. 2006; Sitch et al. 2008; Gonzales et al. 2010; Jiang et al. 2012).

Estimating the timing of plant habitat changes due to global warming is one of the most important concerns that need to be improved upon from previous studies. Here the timing of plant habitat changes is firstly estimated using dominant spatial patterns of plant habitat changes over the globe. The timing of plant habitat changes is suggested for the three warming cases by specific years

when specified amounts of changes (10%, 20%, and 30%, respectively) will occur in the three latitudinal belts. Regardless of the warming magnitude, the fastest plant habitat changes appear in the regions 10°S–25°S. For the medium warming case, the plant habitat change in the latitude band 10°S–25°S exceeds 20% in 2066, faster than for the latitude bands 15°N–30°N and 50°N–65°N by 27 and 18 years, respectively (Table 4.4). In addition, the latitude band 10°S–25°S shows significant regional variations in the timing of plant habitat change. In the southern Africa region, the plant habitat change is projected to reach 30% in 2092 in the low warming case; in central South America, the projected plant habitat changes remain < 20% within the 21st century, even for the high warming case (Table 4.4). Furthermore, for all warming cases and thresholds of fractional habitat change, southern Africa shows the fastest plant habitat changes (Table 4.4). Thus, the estimated habitat-change timing indicates that the plant habitat in southern Africa is the most vulnerable to climate change.

Although the ensemble mean is used, the timing of plant habitat change still has uncertainties originated from various climate model simulations. The uncertainties in the projected timing of plant habitat change are represented by colored bars in Fig. 4.5. Due to the uncertainties the timing of plant habitat is re-estimated using both tolerant and strict standards: the 10% and 90% proportion of model projections. Comparing to the timing based on the ensemble means, the

timing of plant habitat change is advanced and delayed by several decades for the 10% and 90% proportion, respectively. This implies that the projected timing of the ensemble mean cannot guarantee that a specific amount of plant habitat change will happen at that timing. Nevertheless, there is consistency in the projected timing of plant habitat change regardless of the standards. Increasing the warming magnitude advances the timing. A specific amount of plant habitat change is appeared early in southern Africa and East Asia. Thus, the timing of plant habitat change can be a good indicator that representing regional vulnerability of ecosystem in response to climate change regardless of the uncertainty of future projections.

The estimated timing of plant habitat change presented in this study can help in planning mitigation policies, as many mitigation policies are developed for specific levels of climate change (UNFCCC 2009; Joshi et al. 2011). Nevertheless, implementation of these mitigation policies requires economic considerations (Naidoo and Ricketts 2006; IPCC 2007). Countries with weaker economic power are more vulnerable to plant habitat changes. We note that southern Africa has a low GDP and very fast timing of plant habitat change. In southern Africa, Angola shows the highest GDP of 104.3 billion dollars, which is only sixtieth in position among all nations in the world (World Bank 2012). Worse yet, the GDP of the other six nations in southern Africa is lower than 20

billion US dollars, less than one-fifth of Angola's (Table 2.1). Thus, nations in southern Africa are likely to experience greater economic hardships in coping with fast habitat changes and subsequent ecological problems, unless they achieve great economic development in a very short time. Support from the international community will be needed to mitigate the vulnerability of habitat change in southern Africa.

Information on the timing of plant habitat changes presented in this study will help to decide the optimum timing for implementing future ecosystem management policies. If plant habitat changes are reduced by timely management practice, many ecological advantages can be expected. For example, well-preserved plant habitats can protect terrestrial biodiversity from climate change due to the direct relationship between plant habitats and biodiversity (Fischlin and Midgley 2007; Giam et al. 2010; Bellard et al. 2012). Conservation of biodiversity can greatly benefit human society, as biodiversity is closely related to the ability of an ecosystem to supply goods and services (Cardinale et al. 2012), and is known to protect human society from the impact of climate change (Das and Vincent 2008; Turner et al. 2009; Nilsson and Persson 2012). In addition, regional impacts of global warming may be reduced through vegetation-climate feedback (Bonan 2008; Jackson et al. 2008). For instance, abrupt climate change and frequency of extreme weather may be prevented in

future climates by conserving plant habitat (Bounoua et al. 2010; Jeong et al. 2010).

The estimated timing of plant habitat change is limited in some aspects. Since the bio-climate rule is based only on surface temperature, the uncertainties of projected temperature are directly reflected on the projected plant habitat change, especially in high-latitudes. In addition, other important factors such as inter-species competition, physiological flexibility, and the effects of other climate variables are not included in the plant habitat changes projected in this study. Furthermore, eight types of plant habitats based on the bio-climate rule may be too simplistic for representing numerous types of plants in comparison to ecological niche models (Pearson and Dawson 2004; Morin and Thuiller 2009). Human-induced land-cover changes (or land use) can also play an important role in future changes in plant habitats (Foley et al. 2011; Lambin and Meyfroidt, 2011). Despite these limitations, which will be improved in future studies, the habitat changes projected in this study based on the bio-climate rule is generally consistent with previous studies (Cramer et al. 2001; Scholze et al. 2006; Sitch et al. 2008; Jiang et al. 2012), especially the latitudinal patterns in the plant habitats changes in previous studies on ecological responses to climate changes (Rosenzweig et al. 2008; Dillon et al. 2010). The three latitudinal zones, which are the main analysis domains in this study, also generally agree with regions

with high vulnerability to warming (Scholze et al. 2006; Williams et al. 2007; Gonzalez et al. 2010). From a global perspective, the projected timing of habitats changes is thus acceptable as one reference for designing policies for future forest management.

5. Significant drying trend over the humid area in continental East Asia by local warming

5.1 Trend in land surface dryness over continental East Asia

Figure 5.1 shows temporal variations in overall mean of annual PET/P, P, and PET over continental East Asia. For the whole period, PET/P is decreased by -2.30% decade⁻¹ due to both increase in P (2.44% decade⁻¹) and decrease in PET (-0.52% decade⁻¹). However, changes of the three variables are not monotonic. Changing point of long-term trends in PET/P is occurred in early 1980s (Methods). The trend of PET/P is negative (-1.81% decade⁻¹) and positive (1.66% decade⁻¹) for two periods of 1961-1983 and 1984-2010, respectively (Fig. 5.1a). Changes in both P and PET are consistent with the PET/P trend: increasing P and decreasing PET in former period, decreasing P and increasing PET in latter period (Figs. 5.1b, c). The decrease in PET/P before early 1980s is mainly caused by relatively large increase in P (4.56% decade⁻¹) rather than decrease in PET (-0.95% decade⁻¹). However, the increase in PET (1.22% decade⁻¹) contributes to the increase in PET/P largely in latter period.

The spatial distributions of PET/P, P, and PET trends are consistent with overall mean changes for both periods of 1961-1983 and 1984-2010 (Fig. 5.2). In

early period, about 60% of total stations shows decreasing trends of PET/P, particularly in arid (northwestern and northern China) and humid regions (southeastern China) (Fig. 5.2a). Increasing trends of PET/P are mainly shown over semi-arid region (northeastern and southwestern China), but the magnitudes are relatively small. The spatial pattern of P trends is very similar to that of P/PET trends with opposite sign, suggesting that changes in P are directly linked to those in PET/P regardless of the regional classification (Figs. 5.2a, b). PET is decreased over more than three quarters of the analysis domain with relatively small values (Fig. 5.2c). Changes in PET are meaningful on PET/P trends over the humid area only (Figs. 5.2a, c).

Spatial patterns of PET/P, P, and PET trends are drastically varied in latter period (Figs. 5.2d-f). PET/P is increased over most of analysis domain except for western part of the arid region ($< 100^{\circ}\text{E}$; northwestern China) (Fig. 5.2d). Notable shifts in PET/P trends from negative to positive values are observed in humid (southeastern China) and eastern part of arid regions (northern China) (Figs. 5.2a, d). The reversal of PET/P trends over those regions causes the increasing trend in overall mean PET/P from early 1980s considering relatively small changes in PET/P trends over other regions (Figs 5.1a, 5.2d). Spatial distribution of P trends also shows notable changes over arid and humid regions (Figs. 5.2b, e). Positive trends are reversed over eastern part of arid regions and

magnitude of increasing trends becomes smaller in humid regions. These regional patterns of P trends are consistent with PET/P trends over arid and semi-arid regions, but not in the humid area (Figs 5.2d, e). Significant increase in PET explains the inconsistency between changes in PET/P and P over the humid area (Figs. 5.2d, f). In other regions, positive trends of PET also contribute to increase PET/P.

Changes in both P and PET trends are consistent with regional pattern of climate changes appeared in continental East Asia. Trends in P over eastern part of analysis domain ($> 100^{\circ}\text{E}$) are closely related to variability of East Asian monsoon circulation. The weakening of monsoon circulation from late 1970s leads to both decreasing and increasing trends in P over arid and humid regions. However, increases in P over the humid area are much smaller than decreases over the arid regions (Fig. 5.2e). The asymmetry is come from decrease in monsoon rainfall over the humid region from early 1990s following the recovering of monsoon circulation. Notable shifts in other climate variables are connected to increasing trend in PET in latter period. For example, anthropogenic warming becomes severe in whole analysis domain after 1980s. The trend in absorbed solar radiation is changed from dimming to brightening, particularly in the humid area. Consequently, combined impacts of climate changes increase PET/P over both arid and humid regions since early 1980s.

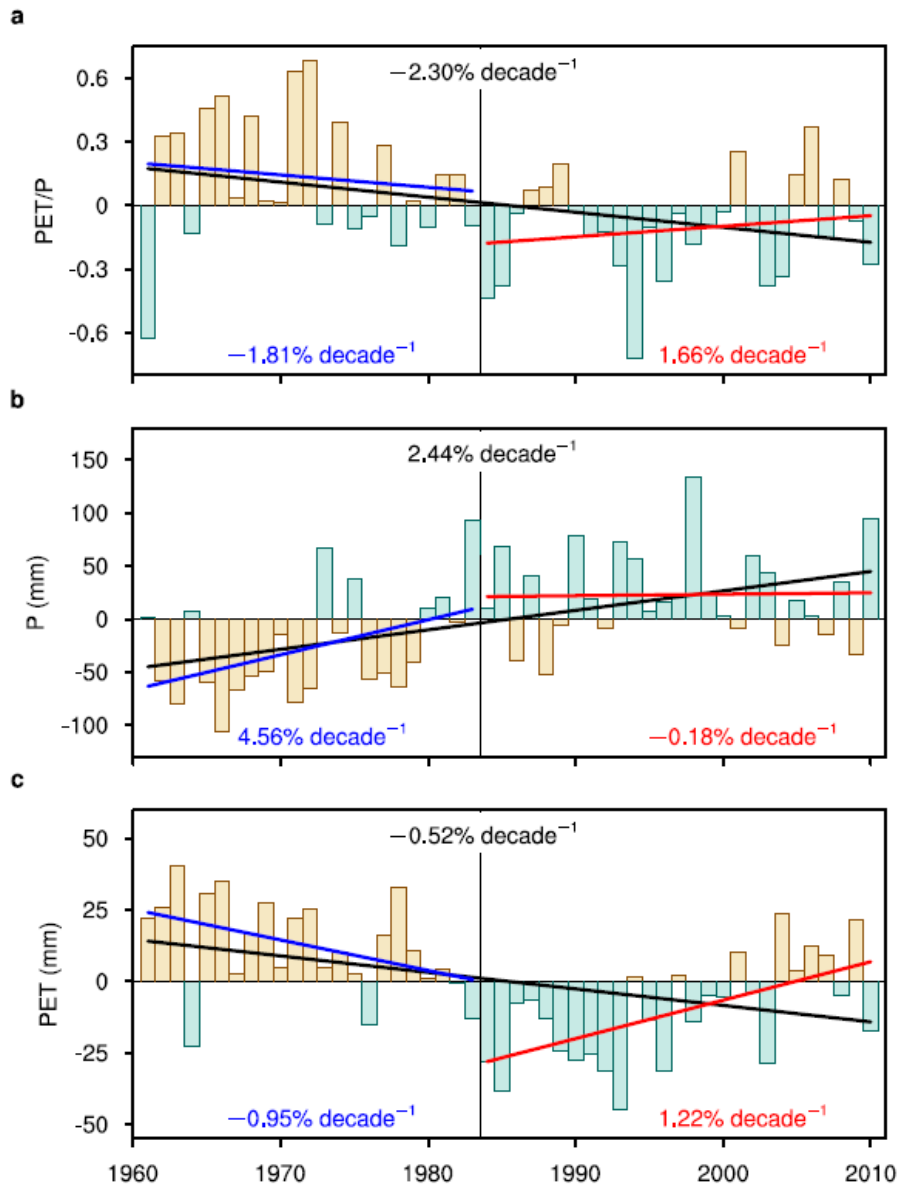


Figure 5.1. Temporal variations of annual mean PET/P, P, and PET in East Asia. a-c, PET/P (a), P (b), and PET (c). Yellow and blue bars indicate that positive and negative anomalies for PET/P and PET, but negative and positive anomalies for P. Black, blue, and red lines are linear regression lines (% decade⁻¹) for the period of 1961-2010, 1961-1983, 1984-2010, respectively.

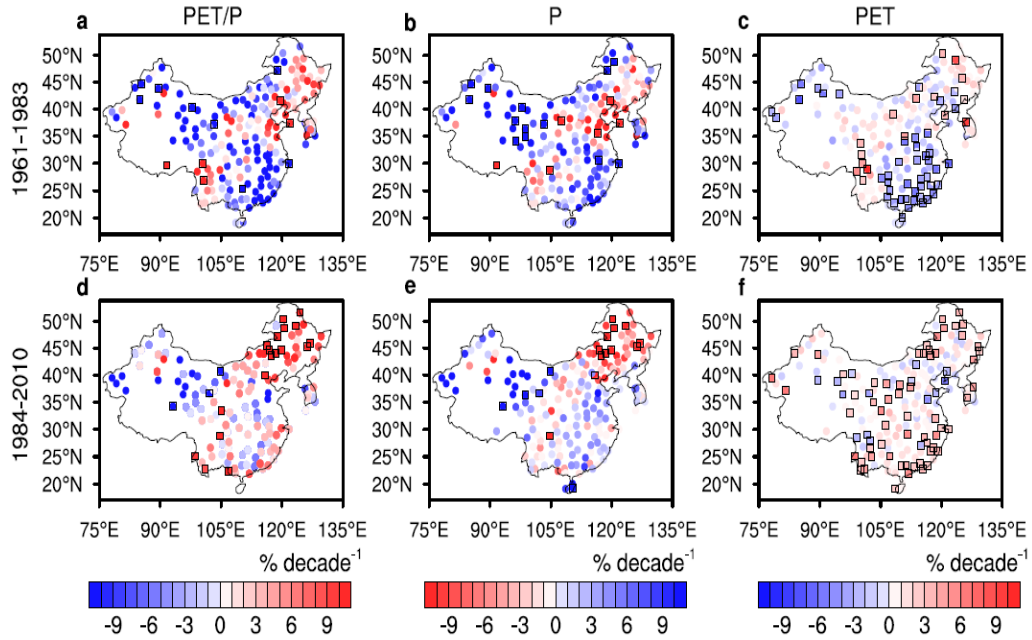


Figure 5.2. Spatial distributions of trends of PET/P, P, and PET in East Asia. a-c, The spatial distribution of trends in annual mean PET/P (a), P (b), and PET (c) for the period of 1961-1983. d-f, as a-c, but for the period of 1984-2010. The empty square indicates that the trend is significant at 95% level.

5.2 Causes of changes in land surface dryness

To determine exact causes of PET/P changes, we compute relative influences of changes in P, Rn, WS, Ta, and RH on trends in PET/P for two analysis periods (section 2.2.5). Figure 5.4 shows averaged influences of five climate parameters and their confidence intervals over three regimes for each period. Here, positive values of a particular variable indicate increasing rates of PET/P considering changes in that variable only and vice versa. Note that stations located on west of 100°E are excluded in averages. The mean climate of those regions is definitely different to other parts of continental East Asia, classified into monsoon climate region. Further, changes in land surface dryness mostly rely on variation of P rather than that of other climate variables for both analysis periods (Fig. 5.3).

Relative influences of each climate parameter are significantly different in according to both analysis periods and hydro-climate regimes, indicating that mechanisms of PET/P changes operate differently (Fig. 5.4). Over the arid region, negative impact of Rn (-1.47% decade⁻¹) looks to be offset by positive influences of P and Ta (0.83% and 0.75% decade⁻¹) before early 1980s (Fig. 5.4a). However, large confidence range of P indicates that substantial impact of P on PET/P changes locally (Fig. 5.3a). In latter period, changes in P shows the

largest influence ($3.17\% \text{ decade}^{-1}$), larger than that of other climate parameters by at least two times. These results mean that variation of P causes the significant increasing trend of PET/P over the arid region. Relative influences of climate variables over the semi-arid region are similar to those of the arid region in former period (Figs .5.4a, b). In 1984-2010, PET/P is increased by positive influences of P, Ta, and RH (1.81% , 0.90% , and $1.45\% \text{ decade}^{-1}$) despite of negative influence of WS ($-1.09\% \text{ decade}^{-1}$). Increasing trend of PET/P is contributed by both warming and decrease in P over the semi-arid area. Over the humid region, P and Rn are the primary and secondary important parameters for the PET/P decrease (-4.76% and $-2.11\% \text{ decade}^{-1}$) in early period (Fig. 5.4c). The contribution of other three variables is much smaller. In contrast, positive influences of Ta and RH (1.24% and $1.87\% \text{ decade}^{-1}$) are larger than negative influences of P and Rn (-0.95% and $-0.83\% \text{ decade}^{-1}$) in latter period. Thus, main reason for the increase in PET/P trends is warming and subsequent increase in atmospheric evaporative potential over the humid region.

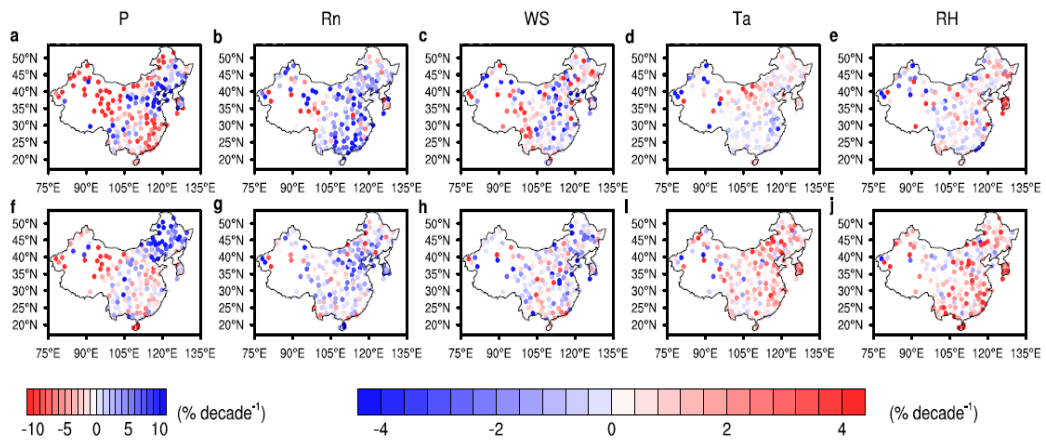


Figure 5.3. Spatial distributions of contributions of the five climate parameters on the PET/P trends in East Asia. a-e, The spatial distribution of the contribution of changes in P (a), Rn (b), WS (c), Ta (d), and RH (e) for the period of 1961-1983. f-j, as a-e, but for the period of 1984-2010.

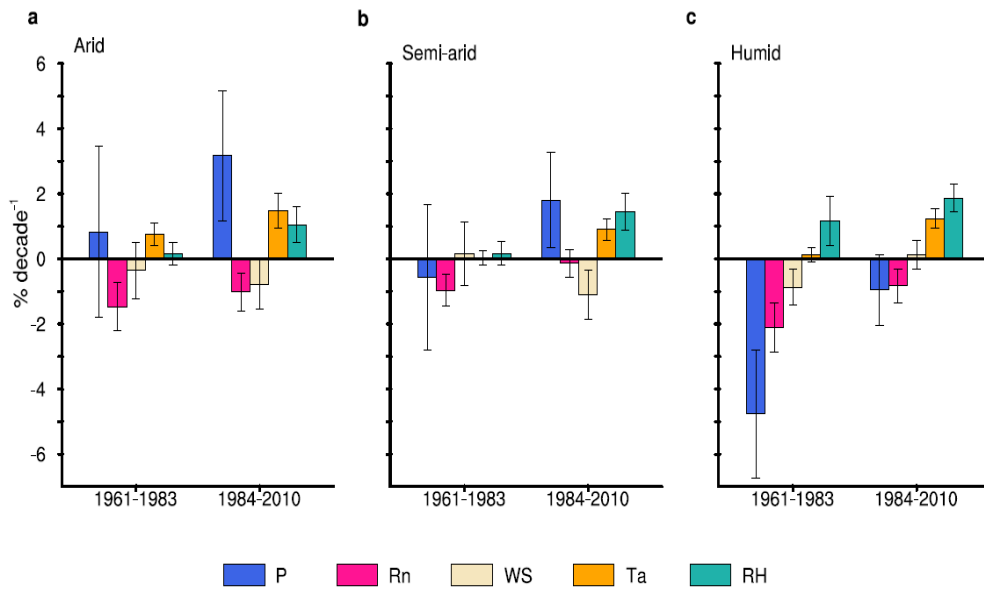


Figure 5.4. Averaged relative influences of five climate parameters on the PET/P changes. a-c, Relative influences (% decade⁻¹) of five climate parameters is averaged for the three hydro-climate regimes: arid (a), semi-arid (b), and humid (c). The averaged influences are computed for the two periods of 1961-1983 and 1984-2010. Blue, pink, beige, orange, and cyan bars represent averaged influence of P, Rn, WS, Ta, and RH, respectively. Error bars represent confidence intervals at 95% significance level.

5.3 Summary and Discussion

The above analysis clearly shows that P, Ta and RH are important three variables for increases in land surface dryness from early 1980s. Dominant influence of P on increases in PET/P in the arid region is contrast to causes of dryness increase over other water-limited regions. This contradictory comes from strong interdecadal variability of P, well known feature of East Asian monsoon region. In consistent with regional warming magnitude, the arid region shows the largest influence of Ta. However, the humid area shows the highest increasing rate of PET/P due to decrease in RH, related with increasing saturation vapor pressure (e_s) following the warming. Relationship between Ta and e_s according to Clausius-Clapeyron equation explains relatively small and large influence of RH in arid and humid regions, respectively (Fig. 5.5). Annual mean temperature is larger in the humid region than in the arid region by about 10°C (map in Fig. 5.5). Due to the difference in background air temperature, the humid region experiences steep increase in e_s and decrease in RH than the arid region despite small warming magnitude (graph in Fig. 5.5). Thus, influence of decrease in RH is relatively large in the humid region, but smaller in the arid region (bars in Fig. 5.5).

Influences of Ta and RH, always act to dry land surface, are significantly

increases in recent decades regardless of hydro-climate regions. These results could be observational evidences of the projected drying trend over the land surface during 21st century according to increase in greenhouse gas concentration. Also our results indicate that drying land surface due to warming is already in progress, not a risk of aftertime. Water management plans should consider the increased water demands due to warming to mitigate water scarcity particularly in humid areas.

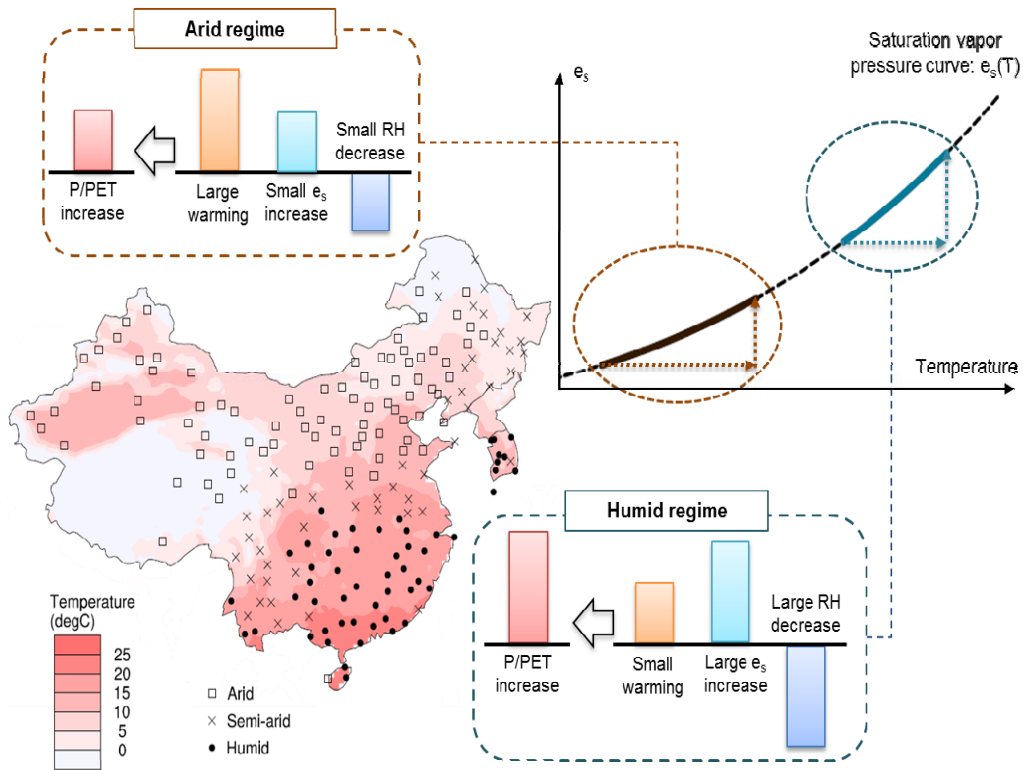


Figure 5.5. Schematic diagram explaining the small and large influence of RH on the PET/P trends in the arid and humid regions. The map shows the spatial distributions of annual mean temperature for the period of 1961-2010 (degree C). Empty squares, cross marks, and filled circles are stations that classified by arid, semi-arid, and humid regions, respectively. The map clearly shows that the arid and humid region of continental East Asia has the cold and warm climate, respectively. In the arid region, warming magnitude is large, but decrease in RH is small following the Clousius-Clapeyron relationship between the saturation vapor pressure (e_s) and T_a (brown line in the graph). In contrast, the increase in the e_s is relatively large in the humid region despite the small warming magnitude (blue line in the graph). The difference in the increment of e_s between two regions causes much larger decrease in RH, further large influence of RH on PET/P trends in the humid region.

6. Conclusions

The present thesis includes three studies about the change in vegetation and its feedback influence, and causes of changes in land surface dryness as followings:

- 1) Examination of potential impact of vegetation feedback on climate aridity over the United States in a condition of doubling CO₂ concentration
- 2) Investigation of regional plant habitat changes in according to three different warming scenarios using various future projections of fully-coupled GCMs
- 3) Emphasizing the impact of local warming on changes in land surface dryness over continental East Asia in recent decades

In chapter 3, first, increased climate aridity in according to doubled atmospheric CO₂ concentration is significantly decreased by vegetation feedback over the contiguous United States, particularly in hydrological transitional region

such as semi-arid and subhumid regions. Thornthwaite moisture index I_m is used as a represent of degree of climate aridity as well as standard of classification of hydrological climate regimes. The CAM3-DGVM model simulates the response of vegetation to climate changes due to doubled CO₂ concentration. For fixed vegetation cover and growth, warm and dry atmospheric conditions resulting from doubling CO₂ increase climate aridity over most of the US. When the vegetation actively responses to the increased CO₂ concentration and climate change, strong increases in I_m (reduced aridity) and subsequent alterations in climate types in the northwestern, midwestern, and southern contiguous US. In addition, strong impact of vegetation feedback appears in regions of subhumid climate types where large increases in aridity may occur due to CO₂-induced warming. Analysis shows that the density of vegetation is notably increased over the northwestern, midwestern, and southern contiguous US in response to doubled CO₂ centration. most part of the US. Increased evapotranspiration of dense vegetation is the key change of the decrease in climate aridity. Rich moisture amount of atmosphere according to the increase in ET is favorable condition for precipitation, indicating the increase in water supply. In addition, enhanced latent heat release due to the enhanced ET reduces water demands of atmosphere through decreasing air temperature. These results indicate that the impact of vegetation feedback on temperature and precipitation, further affects

climate aridity and climate types in future climate, particularly in intermediate climate zones.

Considering remarkable influence of vegetation feedback on future climate, accurate understanding of vegetation changes in response to climate change is important for national agencies to make various mitigation plans about agriculture, energy and water management. In chapter 4, future changes in vegetation are examined deeply using the definition of 8 plant habitat changes based on surface temperature and 64 sets of present and future projections based on 16 different fully-coupled GCMs. Spatial distributions of plant habitats in present climate are highly consistent with satellite-observed vegetation cover. In 21st century, GCMs simulate increase in global mean temperature and precipitation as rising GHGs. Changes in plant habitat changes are significant in three latitudinal zones, 10°-25°S, 15°-30°N, and 50°-65°N which are transitional regions of ecotone. In both 10°-25°S and 15°-30°N, tropical habitats are expanded accompanying poleward shift in temperature habitats. Fraction of boreal habitats is significantly decreased in latitudes 50°-65°N due to northward propagation of temperate habitats. Projected plant habitat changes are amplified with the magnitude of increase in global mean temperature.

In addition to spatial changes, the temporal side of plant habitat changes is clarified the timing of particular amounts of plant habitat change. The timing of plant habitat change is estimated on 6 continents located in latitudes 10°-25°S, 15°-30°N, and 50°-65°N to evaluate regional variability. In mid-latitude, plant habitat changes are relatively fast in Asia and Africa than America, but regional difference is small in high latitudes. Among 6 regions, the southern Africa shows the fastest changes in plant habitat. In worse, nations of weak economic power are concentrated in the southern Africa, thus the vulnerability of plant habitats in southern Africa will increase with continued warming, with potentially terrible economic and ecological consequences. The southern Africa will need the combined efforts of other nations to help mitigate the sudden plant habitat change and its impact on ecosystem and climate.

In chapter 5, lastly, concern of this thesis is returned on changes in land surface dryness. Contrasting to projected increase in land surface dryness in future due to increasing atmospheric water demands, various observations and model results show complex spatial variability of changes in land surface dryness during 20th century, but mechanisms of dryness changes are poorly understood. Thus, investigation of mechanisms of changes in land surface dryness is decided as next target. Land surface dryness is measured by the value of the ratio of PET, computed by Penman-Monteith method to P (PET/P). Over

continental East Asia, trend in overall mean PET/P shows significant changes from decrease to increase around early 1980s with consistent shift in P and PET at that timing. The shift in PET/P is noticeable in the northern and southeastern China, but mechanisms of dryness changes differ over those two regions. In arid northern China, decrease in monsoon rainfall after early 1980s mainly drives the shift in land surface dryness trend, whereas, exponentially increasing saturation vapor pressure due to atmospheric warming shows the largest impact on changes in PET/P over humid southeastern China. Results indicate that the humid area will experiences higher water need in warmer climate, may induce water scarcity.

In this thesis, both variation of precipitation and warming trend are main reason for changes in land surface dryness. Also influence of vegetation feedback could modulate the surface temperature and precipitation, further land surface dryness through changes in evapotranspiration.

Continental East Asia, target region of last study in the present thesis, experiences notable changes in composition of land surface due to urbanization and agricultural needs. The impact of land use/land cover changes (LULCC) on climate is already proved in both observations and model experiments. For example, contribution of urbanization on surface temperature increase is estimated by up to $0.2^{\circ}\text{C decade}^{-1}$ in China. Influences of LULCC may be also considered for examining historical changes in land surface dryness. Actually,

trends in atmospheric water demand show significant difference between urban and rural regions over China during 20th century. The observational evidence indicates that LULCC could be another reason for complexity of spatial changes in land surface dryness in many regions. Thus, quantification of the impact of LULCC on trend in land surface dryness can be a good topic of next study. Also this kind of study will be very helpful to establish a policy for problems associated with water availability in future.

The present thesis used CAM3-DGVM to simulate the response of vegetation in a CO₂ doubled condition and feedback influences of the changes in vegetation. Recently, next version of CAM3-DGVM, Community Earth System Model version 1, is released with new dynamic core and improved physical and chemical parameterizations. The most notable improvement in land surface model is prognostic biogeochemical cycle. Both carbon and nitrogen (CN) cycle is calculated in same time step with other physical processes in Community Land Model version 4 (CLM4). The prognostic CN cycle allows model to simulate vegetation growth adapt to immediately changed conditions of atmosphere and soil. In previous model, the speed of vegetation growth is fixed for each plant habitat changes using satellite-based phenology. Simultaneous vegetation growth shows possibility of new study to examine the impact of each climate variable on vegetation phenology. Lengthening of vegetation phenology due to climate

changes is reported by numerous assessments in globally and locally. Thus, it is valuable work to quantify the impact of various climate parameters on vegetation phenology.

References

- ACIA, 2005: *Arctic Climate Impact Assessment*. Cambridge University Press, 1042 pp.
- Adam, J. C., and D. P. Lettenmaier, 2003: Adjustment of global gridded precipitation for systematic bias. *J. Geophys. Res.*, **108**, 1–14.
- Adger, W. N., and Coauthors, 2007: Assessment of adaptation practices, options, constraints and capacity. *Climate Change 2007: Impacts, adaptation and vulnerability*, M. L. Parry et al., Eds., Cambridge University Press, 717-743.
- Allen, R.G., L.S. Pereira, D. Raes, and M. Smith, 1998: *Crop evapotranspiration – guidelines for computing crop water requirements – FAO Irrigation and drainage Paper 56*.
- Alo, C. A., and G. L. Wang, 2008: Potential future changes of the terrestrial ecosystem based on climate projections by eight general circulation models. *J. Geophys. Res-Biogeoe.*, **113**, G01004, doi:10.1029/2007JG000528.
- Barber, V.A., G.P. Juday, B.P. Finney, 2000: Reduced growth of Alaska white spruce in the twentieth century from temperature-induced drought stress, *Nature*, **405**, 668-672
- Bellard, C., C. Bertelsmeier, P. Leadley, W. Thuiller, and F. Courchamp, 2012: Impacts of climate change on the future of biodiversity. *Ecol. Lett.*, **15**, 365–377.

- Bonan, G. B., Coauthors, 2002: The land surface climatology of the Community Land Model coupled to the NCAR Community Climate Model, *J. Clim.*, **15**, 3123-3149.
- Bonan, G.B., S. Levis, S. Sitch, M. Vertenstein, K.W. Oleson, 2003: A dynamic global vegetation model for use with climate models: Concepts and description of simulated vegetation dynamics. *Glob. Change. Biol.*, **9(11)**, 1543–1566.
- Bonan, G.B., S. Levis, 2006: Evaluating aspects of the Community Land and Atmosphere Models (CLM3 and CAM3) using a dynamic global vegetation model. *J. Clim.*, **19**, 2290-2301.
- Bonan, G. B., 2008: Forests and climate change: Forcings, feedbacks, and the climate benefits of forests. *Science*, **320**, 1444–1449.
- Bounoua, L., and Coauthors, 2010: Quantifying the negative feedback of vegetation to greenhouse warming: A modeling approach. *Geophys. Res. Lett.*, **37**, L23701 doi:10.1029/2010gl045338.
- Burke, E.J., S.J. Brown, 2008: Evaluating uncertainties in the projection of future drought. *J. Hydrometeorol.*, **9**, 292–299.
- Cardinale, B. J., and Coauthors, 2012: Biodiversity loss and its impact on humanity. *Nature*, **486**, 59–67, doi:10.1038/Nature11148.
- Chan, M. A. K., L. Hoshizaki, and B. Klinkenberg, 2011: Ecosystem services in

- conservation planning: Targeted benefits vs. co-benefits or costs? *PLoS One*, **6**, doi:10.1371/journal.pone.0024378.
- Chapin, F. S., and Coauthors, 2005: Role of land-surface changes in Arctic summer warming. *Science*, **310**, 657–660.
- Chen, M., P. Xie, J. Janowiak, P.A. Arkin, 2002: Global land precipitation: A50-yr monthly analysis based on gauge observation. *J. Hydrometeorol.*, **3**, 249–266.
- Chou, C., and Coauthors, 2013: Increase in the range between wet and dry season precipitation. *Nature Geosci.* **6**, 263-267.
- Christensen, J.H., B. Hewitson, A. Busuioc, A. Chen, X. Gao, I. Held, R. Jones, R.K. Killi, W.-T. Kwon, R. Laprise, V.M. Rueda, L. Mearns, C.G. Menendez, J. Raisanen, A. Rinke, A. Sarr, P. Whetton, 2007: Regional climate projections. In: Solomon S., D. Qin, M. Manning, Z. Chen, M. Marquis, K.B. Averyt, M. Tignor, H.L. Miller (eds) *Climate change 2007: The physical science basis. Contribution of Working Group I to the fourth assessment report of the intergovernmental panel on climate change.* Cambridge University Press, Cambridge.
- Collins, W.D., coauthors, 2004: Description of the NCAR Community Atmosphere Model (CAM 3.0). Technical Note NCAR/TN-464+STR, National Center for Atmospheric Research, Boulder, CO, 214pp.

- Collins, W.D., coauthors, 2006: The Community Climate System Model Version 3 (CCSM3). *J. Clim.*, **19**, 2122-2243
- Cowling, S.A., C.D. Jones, P.M. Cox, 2009: Greening the terrestrial biosphere: simulated feedbacks on atmospheric heat and energy circulation, *Clim. Dyn.*, **32**, 287-299.
- Cramer, W., and Coauthors, 2001: Global responses of terrestrial ecosystem structure and function to CO₂ and climate change: Results from six dynamic global vegetation models. *Global Change Biol.*, **7**, 357–374. doi:10.1046/j.1365-2486.2001.00383.x.
- Dai, A., 2012: Increasing drought under global warming in observations and models. *Nature Clim. Change*. **3**, 52-28.
- Das, S., and J. R. Vincent, 2009: Mangroves protected villages and reduced death toll during Indian super cyclone. *P. Natl. Acad. Sci. USA*, **106**, 7357–7360, 0027-8424, doi:10.1073/pnas.0810440106.
- Denman, K.L., G. Brasseur, A. Chidthaisong, P. Ciais, P.M. Cox, R.E. Dickinson, D. Hauglustaine, C. Heinze, E. Holland, D. Jacob, U. Lohmann, S. Ramachandran, P.L. da Silva Dias, S.C. Wofsy and X. Zhang (2007) Couplings Between Changes in the Climate System and Biogeochemistry. In Solomon, S., D. Qin, M. Manning, Z. Chen, M. Marquis, K.B. Averyt, M.Tignor and H.L. Miller (eds) *Climate change 2007: The Physical Science*

- Basis. Contribution of Working Group I to the Fourth Assessment Report of the Intergovernmental Panel on Climate Change. Cambridge University Press, Cambridge.
- Diffenbaugh, N.S., 2009: Influence of modern land cover on the climate of the United States. *Clim. Dyn.*, **33**, 945–958.
- Dillon, M. E., G. Wang, and R. B. Huey, 2010: Global metabolic impacts of recent climate warming. *Nature*, **467**, 704–707.
- Ding, Y., Z. Wang, and Y. Sun, 2008: Inter-decadal variation of the summer precipitation in East China and its association with decreasing Asian summer monsoon. Part I: Observed evidences. *Int. J. Climatol.* **28**, 1139-1161.
- Edmonds J.A., N.J. Rosenberg, 2005: Climate change impacts for the conterminous USA: An integrated assessment summary. *Clim. Change*, **69**, 151–162.
- Fan, Y., H. van den Dool (2008) A global monthly land surface air temperature analysis for 1948-present. *J. Geophys. Res.*, 113:D01103 doi:10.1029/2007JD008470.
- Feddema, J.J. (2005a) A revised Thornthwaite-type global climate classification. *Physical Geography* 26: 442–466.
- Feng, S., R.J. Oglesby, C.M. Rowe, D.B. Loope, Q. Hu (2008) Atlantic and

- Pacific SST influences on Medieval drought in North America simulated by the Community Atmospheric Model. *J. Geophys. Res.*, 113, D11101,doi:10.1029/2007JD009347.
- Feng, S., Q. Fu, 2013: Expansion of global drylands under a warming climate. *Atmos. Chem. Phys.* **13**, 10081-10094.
- Field, C.B., L.D. Mortsch, M. Brklacich, D.L. Forbes, P. Kovacs, J.A. Patz, S.W. Running, M.J. Scott (2007) North America. In Parry, M., O. Canziani, J. Palutikof, P. Linden, C. Hansen (eds) *Climate change 2007: Impacts, adaptation and vulnerability. Contribution of Working Group II to the fourth assessment report of the Intergovernmental Panel on Climate Change.* Cambridge University Press, Cambridge.
- Fischlin, A., and Coauthors, 2007: Ecosystems, their properties, goods and services. *Climate Change 2007: Impacts, adaptation and vulnerability*, M. L. Parry et al., Eds., Cambridge University Press, 211-272.
- Foley, J. A., and Coauthors, 2011: Solutions for a cultivated planet. *Nature*, **478**, 337–342.
- Forbes, B. C., M. M. Fauria, and P. Zetterberg, P., 2010: Russian Arctic warming and ‘greening’ are closely tracked by tundra shrub willows. *Global Change Biol.*, **16**, 1542–1554.
- Friedl, M. A., and Coauthors, 2002: Global land cover mapping from MODIS:

- Algorithms and early results. *Remote Sens. Environ.*, **83**, 287–302.
- Friedl, M. A., and Coauthors, 2010: MODIS collection 5 global land cover: Algorithm refinements and characterization of new datasets. *Remote Sens. Environ.*, **114**, 168-182.
- Ge, Q., F. Wang, F., and J. Luterbacher, 2013: Improved estimation of average warming trend of China from 1951-2010 based on satellite observed land-use data. *Clim. Change* **121**, 365-379.
- Geng, Q.L., and Coauthors, 2014: Dry/wet climate zoning and delimitation of arid areas of Northwest China based on a data-driven fashion. *J. Arid. Land.* **6**, 287-299.
- Gong, D.-Y., and C.-H. Ho, 2004: Detection of large-scale climate signals in spring vegetation index (normalized difference vegetation index) over the Northern Hemisphere, *J. Geophys. Res.*, **108**, 4498, doi:10.1029/2002JG002300
- Giam, X., C. J. A. Bradshaw, H. T. W. Tan, and N. S. Sodhi, 2010: Future habitat loss and the conservation of plant biodiversity. *Biol. Conserv.*, **143**, 1594–1602.
- Gonzalez, P., R. P. Neilson, J. M. Lenihan, and R. J. Drapek, 2010: Global patterns in the vulnerability of ecosystems to vegetation shifts due to climate change. *Global Ecol. Biogeogr.*, **19**, 755–768.

- Greve, P., and Coauthors, 2014: Global assessment of trends in wetting and drying over land. *Nature Geosci.* **7**, 716-721.
- Han, S., D. Xu, and S. Wang, 2012: Decreasing potential evaporation trends in China from 1956 to 2005: Accelerated in regions with significant agricultural influence? *Agric. Forest Meteorol.* **154-155**, 44-56.
- Harris, I., P. D. Jones, T. J. Osborn, and D. H. Lister, 2012: Updated high-resolution grids of monthly climatic observations—the CRU TS3.10 dataset. *Int. J. Climatol.* (submitted).
- Hartley, I. P., and Coauthors, 2012: A potential loss of carbon associated with greater plant growth in the European Arctic. *Nature Climate Change*, **2**, 875–879.
- Hegerl, G.C., F.W. Zwiers, N.P. Braconnot, N.P. Gillett, Luo Y, J.A. Marengo Orsini, N. Nicholls, J.E. Penner, P.A. Stott, 2007: Understanding and attributing climate change. In: Solomon S., D. Qin, M. Manning, Z. Chen, M. Marquis, K.B. Averyt, M. Tignor, H.L. Miller (eds) *Climate change 2007: the physical science basis. Contribution of Working Group I to the fourth assessment report of the Intergovernmental Panel on Climate Change.* Cambridge University Press, Cambridge.
- Hegerl, G.C., and Coauthors, 2015: Challenges in quantifying changes in the global water cycle. *Bull. Amer. Meteor. Soc.* **96**, 1097-1115.

- Held, I.M., and B.J. Soden, 2006: Robust responses of the hydrological cycle to global warming. *J. Clim.* **19**, 5686-5699.
- Hightower, M., S.A. Pierce, 2008: The energy challenge. *Nature*, **452**, 285–286.
- Hoekstra, A.Y., and M.M. Mekonnen, 2012: The water footprint of humanity. *Proc. Natl Acad. Sci.* **109**, 3232-3237.
- Huo, Z., and Coauthors, 2013: Effect of climate change on reference evapotranspiration and aridity index in arid region of China. *J. Hydrol.* **492**, 24-34.
- IPCC, 2007: Summary for policymakers. *Climate Change 2007: Impacts, adaptation and vulnerability*, M. L. Parry et al., Eds., Cambridge University Press, 7-22.
- Jackson, R.B., Coauthors, 2008: Protecting climate with forests. *Environ. Res. Lett.*, doi:10.1088/1748-9326/3/4/044006.
- Jeong, S.-J., C.-H. Ho, K.-Y. Kim, J.-H. Jeong, 2009: Reduction of spring warming over East Asia associated with vegetation feedback. *Geophys. Res. Lett.*, **36**, L18705, doi: 10.1029/2009GL039114.
- Jeong, S.-J., C.-H. Ho, T.-W. Park, J. Kim, and S. Levis, 2011a: Impact of vegetation feedback on the temperature and its diurnal range over the Northern Hemisphere during summer in a $2 \times \text{CO}_2$ climate. *Clim. Dynam.*, **37**, 821–833.

- Jeong, S.-J., C.-H. Ho, M. E. Brown, J.-S. Kug, S. Piao, 2011b, Browning in desert boundaries in Asia in recent decades. *J. Geophys. Res.*, **116**, doi:10.1029/2010JD014633.
- Jia, G. J., H. E. Epstein, and D. A. Walker, 2009: Vegetation greening in the Canadian arctic related to decadal warming. *J. Environ. Monitor.*, **11**, 2231–2238.
- Jiang, Y., and Coauthors, 2012: Uncertainty analysis of vegetation distribution in the northern high latitudes during the 21st century with a dynamic vegetation model. *Ecol. Evol.*, **2**, 593–614.
- Joshi, M., E. Hawkins, R. Sutton, J. Lowe, and D. Frame, 2011: Projections of when temperature change will exceed 2°C above pre-industrial levels. *Nature Climate Change*, **1**, 407–412.
- Kundzewicz, Z.W., L.J. Mata, N.W. Arnell, P. Doll, P. Kabat, B. Jimenez, K.A. Miller, T. Oki, Z. Sen, I.A. Shiklomanov, 2007: Freshwater resources and their management. In Parry, M., O. Canziani, J. Palutikof, P. Linden, C. Hansen (eds) *Climate change 2007: Impacts, adaptation and vulnerability. Contribution of Working Group II to the fourth assessment report of the Intergovernmental Panel on Climate Change*. Cambridge University Press, Cambridge.
- Lambin, E. F., and P. Meyfroidt, 2011: Global land use change, economic

- globalization, and the looming land scarcity. *P. Natl. Acad. Sci. USA*, **108**, 3465–3472.
- Le Houerou, H.N., 1996: Climate change, drought and desertification. *J. Arid. Env.*, **34(2)**, 133–185.
- Levis, S., J.A. Foley, D. Pollard, 2000: Large-scale vegetation feedbacks on doubled CO₂ climate. *J. Clim.*, **13**, 1313–1325.
- Levis, S., G.B. Bonan, M. Vertenstein, K.W. Oleson, 2004: The Community Land Model's Dynamic Global Vegetation Model (CLM-DGVM): Technical description and user's guide. Technical Note NCAR/TN-459+IA, National Center for Atmospheric Research, Boulder, Colorado, 50 pp.
- Liu, Z., M. Notaro, J. Kutzbach, N. Liu, 2006: Assessing global vegetation-climate feedbacks from observations. *J. Clim.*, **19**, 787–814.
- Liu, M., Y. Shen, Y. Zeng, and C. Liu, 2010: Trends of pan evaporation in China in recent 50 years in China. *J. Geogr. Sci.* **20**, 557-568.
- Liu, H.W., T.J. Zhou, Y.X. Zhu, and Y.H. Lin, 2012: The strengthening East Asia summer monsoon since the early 1990s. *Chinese Sci. Bull.* **57**, 1553-1558.
- Liu, X., D. Zhang, Y. Luo, and C. Liu, 2013: Spatial and temporal changes in aridity index in northwest China: 1960 to 2010. *Theor. Appl. Climatol.* **112**, 307-316.
- Lucht, W., S. Schaphoff, T. Erbrecht, U. Heyder, and W. Cramer, 2006:

- Terrestrial vegetation redistribution and carbon balance under climate change. *Carbon Balance and Management*, **1**, doi:10.1186/1750-0680-1-6.
- Mather, J.R., J.J. Feddema, 1986: Hydrologic consequences of increases in trace gases and CO₂ in the atmosphere. In: James GT Effects of changes in stratospheric ozone and global climate volume 3: climate change, U.S. Environmental Protection Agency, Washington D.C.
- Maurer, E. P., J. C. Adam, and A. W. Wood, 2009: Climate model based consensus on the hydrologic impacts of climate change to the Rio Lempa basin of Central America. *Hydrology and Earth System Sciences*, **13**, 183–194.
- McCabe, G.J., D.M. Wolock, L.E. Hay, M.A. Ayers, 1990: Effects of climate change on the Thornthwaite moisture index. *Journal of the American Water Resources Association*, **26**, 633–643.
- McCabe, G.J., D.M. Wolock, 1992: Effects of climatic change and climatic variability on the Thornthwaite moisture index in the Delaware River basin. *Clim. Change*, **20**, 143–153.
- McKee, T.B., N. J. Doesken, J. Kleist, 1993: The relationship of drought frequency and duration to time scales. In Proceedings of the 8th Conference of Applied Climatology, 17-22 January 1993, Anaheim, CA. American Meteorological Society. pp.179-184.

- Meehl, G. A., and Coauthors, 2007a: The WCRP CMIP3 multi-model dataset: A new era in climate change research. *Bull. Amer. Meteor. Soc.*, **88**, 1383–1394.
- Meehl, G.A., and Coauthors, 200b: Global climate projection. *Climate Change 2007: The Physical Science Basis*, S. Solomon et al., Eds., Cambridge University Press, 747-846.
- Menzel, A., P. Fabian, 2000: Growing season extended in Europe. *Nature*. **397**, 659.
- Morin, X., and W. Thuiller, 2009: Comparing niche- and process-based models to reduce prediction uncertainty in species range shifts under climate change. *Ecology*, **90**, 1301–1313.
- Myneni, R.B., C.D. Keeling, C.J. Tucker, G. Asrar, R.R. Nemani, 1997: Increased plant growth in the northern high latitudes from 1981 to 1991, *Nature*, **386**, 698-702.
- Naidoo, R., and Coauthors, 2006: Integrating economic costs into conservation planning. *Trend in Ecology and Evolution*, **21**, 681–687.
- Naidoo, R., and T. H. Ricketts, 2006: Mapping the economic costs and benefits of conservation. *PLoS Biology*, **4**, e360, doi:10.1371/journal.pbio.0040360.
- Neale, R.B., Coauthors, 2010: Description of the NCAR Community Atmosphere Model (CAM 4.0). Technical Note NCAR/TN-???+STR,

- National Center for Atmospheric Research, Boulder, CO, 206pp.
- Nilsson, M., and A. Persson 2012: Reprint of “Can Earth system interactions be governed? Governance functions for linking climate change mitigation with land use, freshwater and biodiversity protection”. *Ecological Economics*, **75**, 61–71.
- Notaro, M., Z. Liu, J.W. Williams, 2006: Observed vegetation-climate feedbacks in the United States. *J. Clim.*, **19**, 763–785.
- Oleson, K.W., Coauthors, 2010: Technical Description of version 4.0 of the Community Land Model (CLM). Technical Note NCAR/TN-478+STR, National Center for Atmospheric Research, Boulder, CO, 257pp.
- Park, C.-E., C.-H. Ho, S.-J. Jeong, J. Kim, and S. Feng, 2012: Impact of vegetation on feedback to alleviate climate aridity over the United States associated with a $2 \times \text{CO}_2$ climate condition, *Clim. Dynam.*, **38**, 1489-1500, doi:10.1008/s00382-011-1150-x.
- Parmesan, C., and G. Yohe, 2003: A globally coherent fingerprint of climate change impacts across natural systems. *Nature*, **421**, 37–42.
- Pearson, R. G., and T. P. Dawson, 2003: Predicting the impacts of climate change on the distribution of species: are bioclimate envelope models useful? *Global Ecol. Biogeogr.*, **12**, 361–374.
- Penman, H.L., 1948: Natural evaporation from open water, bare soil and grass.

- Proc. Roy. Soc. Lond.* **193**, 120-145.
- Piao, S., A. Mohammat, J. Fang, Q. Cai, J. Feng, 2005: NDVI-based increase in growth of temperate grasslands and its responses to climate changes in China. *Glob. Env. Change*, **16**, 340-348.
- Piao, S., and Coauthors, 2010: The impacts of climate change on water resources and agriculture in China. *Nature* **467**, 43-51.
- Rosenzweig, C., and Coauthors, 2007: Assessment of observed changes and responses in natural and managed systems. *Climate Change 2007: Impacts, adaptation and vulnerability*, M. L. Parry et al., Eds., Cambridge University Press, 79-131.
- Rosenzweig, C., and Coauthors, 2008: Attributing physical and biological impacts to anthropogenic climate change. *Nature*, **453**, 353–358.
- Sala, O., 2005: Biodiversity across scenarios. *Millenium Ecosystem Assessment, volume 2: Scenarios*. Island Press, 375-408.
- Scholze, M., W. Knorr, N. W. Arnell, and I. C. Prentice, 2006: A climate-change risk analysis for world ecosystems. *P. Natl. Acad. Sci. USA*, **103**, 13116–13120.
- Seager, R., A. Tzanova, J. Nakamura, 2009: Drought in the southeastern United States: Causes, variability over the last millennium, and the potential for future hydroclimate change. *J. Clim.*, **22(19)**, 5021–5045.

- Sheffield, J., G. Goteti, E.F. Wood, 2006: Development of a 50-Year High-Resolution Global Dataset of Meteorological Forcings for Land Surface Modeling. *J. Clim.*, **19**, 3088-3111
- Sheffield, J., E.F. Wood, 2008: Projected changes in drought occurrence under future global warming from multi-model, multi-scenario, IPCC AR4 simulations. *Clim. Dyn.*, **31**, 79–105.
- Sherwood, S., and Q. Fu, 2014: A Drier Future? *Science* **343**, 737-739.
- Shi, Y., and Coauthors, 2007: Recent and future climate change in northwestern China. *Clim. Change* **80**, 379-393.
- Sitch, S., and Coauthors, 2003: Evaluation of ecosystem dynamics, plant geography and terrestrial carbon cycling in the LPJ dynamic global vegetation model. *Global Change Biol.*, **9**, 161–185.
- Sitch, S., and Coauthors, 2008: Evaluation of the terrestrial carbon cycle, future plant geography and climate-carbon cycle feedbacks using five dynamic global vegetation models (DGVMs). *Global Change Biol.*, **14**, 2015–2039.
- Song, S., L. Li, X. Chen, and J. Bai, 2015: The dominant role of heavy precipitation in precipitation change despite opposite trends in west and east of northern China. *Int. J. Climatol.* doi:10.1002/joc.4290.
- Sturm, M., C. Racine, and K. Tape, 2001: Climate change–increasing shrub abundance in the Arctic. *Nature*, **411**, 546–547.

- Sulla-Menashe, D., and Coauthors, 2011: Hierarchical mapping of Northern Eurasian land cover using MODIS data. *Remote Sens. Environ.*, **115**, 392-403
- Tang, W.-J., and Coauthors, 2011: Solar radiation trend across China in recent decades: a revisit with quality-controlled data. *Atmos. Chem. Phys.* **11**, 393-406.
- Thomas, J. A., and R. T. Clarke, 2004: Extinction risk from climate change. *Nature*, **427**, 145–148.
- Thornthwaite, C.W., 1948: An approach toward a rational classification of climate. *Geogr. Rev.*, **38**, 55–94.
- Trenberth, K.E., P.D. Jones, P. Ambenje, R. Bojariu, D. Easterling, A.K. Tank, D. Parker, F.Rahimzadeh, J.A. Renwich, M. Rusticucci, B. Soden, P. Zhai, 2007: Observations: Surface and atmospheric climate change. In: Solomon S., D. Qin, M. Manning, Z. Chen, M. Marquis, K.B. Averyt, M. Tignor, H.L. Miller (eds) *Climate change 2007: the physical science basis. Contribution of Working Group I to the fourth assessment report of the Intergovernmental Panel on Climate Change*. Cambridge University Press, Cambridge.
- Turner, W. R., M. Oppenheimer, D. S., Wilcove, 2009: A force to fight global warming. *Nature*, **462**, 278–279.

- van Mantgem, P.J., Coauthors, 2009: Widespread increase of tree mortality rates in the western United States. *Science*, **323(5913)**, 521–524.
- United Nations Environment Programme (UNEP), 2009: *Global Deserts Outlooks*. Eds. Ezcurra, Nairobi, 164pp.
- United Nations Framework Convention on Climate Change (UNFCCC), 2007: Investment and financial flows to address climate change. UNFCCC, 273pp.
- Wang, G., 2005: Agricultural drought in a future climate: results from 15 global climate models participating in the IPCC 4th assessment. *Clim. Dyn.*, **25**, 739–753.
- Wang, B., and Q. Ding, 2006: Changes in global monsoon precipitation over the past 56 years. *Geophys. Res. Lett.* **33**, L06711.
- Wang, L., and W. Chen, 2014: A CMIP5 multimodel projection of future temperature, precipitation, and climatological drought in China. *Int. J. Climatol.* **34**, 2059-2078.
- Williams, J. W., S. T. Jackson, and J. E. Kutzbach, 2007: Projected distributions of novel and disappearing climates by 2100 AD. *P. Natl. Acad. Sci. USA*, **104**, 5738–5742.
- Williamson, D.L., 2002: Time-split versus process-split coupling of parameterizations and dynamical core. *Mon. Wea. Rev.*, **130**, 2024-2041
- Wilmking, M., Juday, G.P., Barber, V.A., Zald, H.S., 2004: Recent climate

- warming forces contrasting growth responses of white spruce at treeline in Alaska through temperature thresholds, *Glob. Change Biol.*, **10**, 1724–1736, 2004.
- Wood, A. W., L. R. Leung, V. Sridhar, and D. P. Lettenmaier, 2004: Hydrologic implications of dynamical and statistical approaches to downscaling climate model outputs. *Climatic Change*, **62**, 189–216.
- Wu, S., Y. Yin, D. Zheng, and Q. Yang, 2006: Moisture conditions and climate trends in China during the period 1971-2000. *Int. J. Climatol.* **26**, 193-206.
- The World Bank, 2012: *Gross domestic production 2011 included in World development indicators*.
<http://databank.worldbank.org/databank/download/GDP.pdf>.
- Xu, L., and Coauthors, 2013: Temperature and vegetation seasonality diminishment over northern lands. *Nature Climate Change*, **3**, 581–586, doi::10.1038/nclimate1836.
- Yin, Y., D. Ma, S. Wu, and T. Pan, 2015: Projections of aridity and its regional variability over China in the mid-21st century. *Int. J. Climatol.* doi:10.1002/joc.4295.
- Yohe, G.W., R.D. Lasco, Q.K. Ahmad, N.W. Arnell, S.J. Cohen, C. Hope, A.C. Janetos, R.T. Perez, 2007: Perspectives on climate changes and sustainability. In Parry, M., O. Canziani, J. Palutikof, P. Linden, C. Hansen

- (eds) Climate change 2007: Impacts, adaptation and vulnerability. Contribution of Working Group II to the fourth assessment report of the Intergovernmental Panel on Climate Change. Cambridge University Press, Cambridge.
- Yue, T.-X., and Coauthors, 2013: Climate change trend in China, with improved accuracy. *Clim. Change* **120**, 137-151.
- Zhang, J., J.E. Walsh, 2006: Thermodynamic and hydrological impacts of increasing greenness in northern high latitudes. *J. Hydrometeorol.*, **7**, 1147–1163.
- Zhang, L.X., and T.J. Zhou, 2011: An assessment of monsoon precipitation changes during 1901-2001. *Clim. Dyn.* **37**, 279-296.
- Zhou, L.M., C.J. Tucker, R.K. Kaufmann, D. Slayback, N.V. Shabanov, and R.B. Myneni, 2001: Variations in northern vegetation activity inferred from satellite data of vegetation index during 1981-1999, *J. Geophys. Res.*, **106**, 20,069-20,083.
- Zhu, C., B. Wang, W. Qian, and B. Zhang, 2012: Recent weakening of northern East Asian summer monsoon: A possible response to global warming. *Geophys. Res. Lett.* **39**, doi:10.1029/2012GL051155.

국문 초록

기후 변화에 따라 지속적으로 변화하는 지면의 특성 중, 식생과 지표 건조도의 변화는 지면의 반응들 중에서도 가장 중요한 두 가지라 할 수 있다. 식생은 지면의 70%를 차지할 뿐 아니라 지면의 물리, 화학 과정에 지대한 영향을 끼치는 요소로서 식생 변화 및 그에 따른 되먹임 효과에 대한 연구는 현재 기후 변화에 대한 이해 및 미래 기후 예측에 있어 매우 중요한 요소이다. 또한 지표 건조도 변화는 지면 물 순환 변화와 밀접하게 관련되어 있으며 농업과 물 관리의 측면에서 매우 중요하게 다루어지고 있다. 식생 및 지표 건조도 변화는 기후뿐 아니라 사회, 경제적으로도 큰 영향을 끼치며 이에 따라 관련 연구들은 기후 변화 적응 및 완화에 있어 매우 중요하다. 본 학위 논문은 식생 및 지표 건조도에 대한 세 가지 연구 내용으로 이루어져 있다.

첫 번째로 미국 지역에서 이산화탄소 배증에 의한 식생 증가의 효과가 여름철 지표 건조도를 감소시키는 것을 식생 역학 모델이 접합된 전구기후모델 실험을 통해 밝혀내었다. 지표 건조도는 Thornthwaite의 습윤 지수(Thornthwaite's moisture index)를 이용하여 측정하였으며 습윤 지수의 변화를 통해 미국 지역의 건조도가 증가 혹은 감소하는 것을 보였다. 이산화탄소 배증 시 미국 지역의 지표 건조도가 증가하며 이는 늘어난 강수량보다 온도 증가에 따른 잠재증발량(potential evapotranspiration)의 증가량이 더 크기 때문이다. 이 때, 식생 변화가 고려될 경우, 이산화탄소 및 온도 증가에 따른 식생 밀도의 증가는 지표면에서의 증발량 및 이에 따른 잠열 방출을 활발하게 하여 기온 증가를 완화하는 효과가 있고, 이는 결국 지표 건조도를 낮추는 것으로 나타난다. 이와 같은 효과는 특히 식생 밀도 증가가 뚜렷한 미국 동부 및 동남부, 북서부에서 뚜렷하게 나타나고 있다.

두 번째 연구는 온난화에 따른 21세기의 식생 서식지 변화 시기를 세 개의 온난화 강도에 따라 측정하였다. 식생 서식지의 정의는 현재 식생 역학

모델에서 식생 구분을 위해 쓰는 생물기후학적 규칙 (bio-climate rule)을 이용하였으며 실제 식생 구분 및 식생 변화 시기 예측을 위한 현재 및 미래 기후 자료는 IPCC 4차 보고서에 쓰인 16개의 전구 기후 모형을 이용하여 생산되었다. 식생 변화 시기는 각 식생 서식지의 변화 비율이 처음으로 10%, 20%, 30%가 되는 시기로 정의하였다. 또한 식생 변화 시기와 온난화 강도와와의 관계를 알기 위하여 전구 평균 지면 온도 변화 (ΔT)를 이용, 미래 예측 자료를 약한 온난화 ($\Delta T < 2.5K$), 중간 온난화 ($2.5K < \Delta T < 3.5K$), 강한 온난화 ($\Delta T > 3.5K$)의 세 가지로 나누어 식생 변화 시기를 추정하였다. 분석 결과, 21세기 식생 변화는 온난화 강도와 관계 없이 다른 종의 식생이 같이 분포하는 지역에서 뚜렷하게 나타나는 것을 확인하였다. 식생 변화 시기는 온난화가 심할수록 빨라졌으며 남부 아프리카 및 아시아 지역에서의 식생 변화 시기가 같은 위도의 다른 지역에 비해 매우 빠른 것으로 나타났다. 특히 남부 아프리카 지역에서의 식생 변화가 가장 빠르게 나타났는데, 온난화가 약한 경우에도 식생이 10%만큼 변화하는 시기가 아메리카 대륙에 비해 약 70년이나 빠른 것을 확인하였다. 이에 더해 식생 변화가 빠르게 나타나는 아프리카 및 아시아 지역은 경제력이 낮은 국가가 밀집되어 있어 식생 변화에 의한 피해가 더욱 크게 나타날 가능성이 있는 것으로 분석되었다.

마지막으로 최근 동아시아 지역에서 나타나는 지표 건조도 변화에 대한 5가지 주요 기후 요소들의 영향을 정량적으로 측정하여 지표 건조도 변화의 원인을 제시하였다. 위의 분석을 위해 동아시아의 189개 기상 관측 지점에서 제공하는 1961년부터 2010년까지 50년 동안의 일별 기후 자료를 이용하였으며 해당 지역을 수문학적으로 습윤, 반건조, 건조의 세 가지 지역으로 나누어 분석하였다. 동아시아는 전체 기간에 대해서는 습윤해지는 것처럼 보이나 실제로는 1980년대 초반부터 건조해지는 것을 알 수 있다. 이는 몬순의 영향을 받는 동경 100° 동쪽 지역에서 나타나며 건조 지역과 습윤 지역에서 뚜렷하게 나타나고 있다. 건조 지역의 건조화 경향은 강수량 감소가 주요 원

인이나 습윤 지역의 경우, 온도 증가에 따른 상대 습도 감소가 가장 중요한 원인인 것으로 나타났다.

본 학위 논문의 연구 결과들이 시사하는 점은 다음과 같이 세 가지가 있다. 첫 번째로 증가한 식생의 되먹임 효과에 따른 지표 건조도 감소 결과는 기후 변화에 취약한 지역에서 뚜렷하기 때문에 건조화에 대한 완화 대책에 중요할 것이다. 두 번째로 경제력이 약한 아시아 및 아프리카 지역의 빠른 식생 변화 및 이에 따른 피해를 줄이기 위한 국제적인 공조가 필요하다는 것을 알려준다. 마지막으로 온난화에 의한 지표 건조도 상승은 매우 급격하게 나타나고 있으므로 미래의 물 부족을 피하기 위해서는 이를 고려한 물 관리 정책이 필요하다는 것이다.

주요어: 기후 변화, 식생 변화, 지표 건조도, 식생 되먹임, 건조 지수,
대기의 물 요구량

학 번: 2010-30105